

Advances in Civil Engineering

Multiobjective Optimization Techniques in Civil Engineering Problems

Lead Guest Editor: Tayfun Dede

Guest Editors: Murat Kankal, Ali R. Vosoughi, Maksym Grzywinski, and
Moacir Kripka





Multiobjective Optimization Techniques in Civil Engineering Problems

Advances in Civil Engineering

**Multiobjective Optimization
Techniques in Civil Engineering
Problems**

Lead Guest Editor: Tayfun Dede

Guest Editors: Murat Kankal, Ali R. Vosoughi,
Maksym Grzywinski, and Moacir Kripka



Copyright © 2020 Hindawi Limited. All rights reserved.

This is a special issue published in "Advances in Civil Engineering." All articles are open access articles distributed under the Creative Commons Attribution License, which permits unrestricted use, distribution, and reproduction in any medium, provided the original work is properly cited.

Chief Editor

Cumaraswamy Vipulanandan, USA

Associate Editors

Chiara Bedon , Italy
Constantin Chalioris , Greece
Ghassan Chehab , Lebanon
Ottavia Corbi, Italy
Mohamed ElGawady , USA
Husnain Haider , Saudi Arabia
Jian Ji , China
Jiang Jin , China
Shazim A. Memon , Kazakhstan
Hossein Moayedi , Vietnam
Sanjay Nimbalkar, Australia
Giuseppe Oliveto , Italy
Alessandro Palmeri , United Kingdom
Arnaud Perrot , France
Hugo Rodrigues , Portugal
Victor Yepes , Spain
Xianbo Zhao , Australia

Academic Editors

José A.F.O. Correia, Portugal
Glenda Abate, Italy
Khalid Abdel-Rahman , Germany
Ali Mardani Aghabaglou, Turkey
José Aguiar , Portugal
Afaq Ahmad , Pakistan
Muhammad Riaz Ahmad , Hong Kong
Hashim M.N. Al-Madani , Bahrain
Luigi Aldieri , Italy
Angelo Aloisio , Italy
Maria Cruz Alonso, Spain
Filipe Amarante dos Santos , Portugal
Serji N. Amirkhania, USA
Eleftherios K. Anastasiou , Greece
Panagiotis Ch. Anastasopoulos , USA
Mohamed Moafak Arbili , Iraq
Farhad Aslani , Australia
Siva Avudaiappan , Chile
Ozgur BASKAN , Turkey
Adewumi Babafemi, Nigeria
Morteza Bagherpour, Turkey
Qingsheng Bai , Germany
Nicola Baldo , Italy
Daniele Baraldi , Italy

Eva Barreira , Portugal
Emilio Bastidas-Arteaga , France
Rita Bento, Portugal
Rafael Bergillos , Spain
Han-bing Bian , China
Xia Bian , China
Huseyin Bilgin , Albania
Giovanni Biondi , Italy
Hugo C. Biscaia , Portugal
Rahul Biswas , India
Edén Bojórquez , Mexico
Giosuè Boscato , Italy
Melina Bosco , Italy
Jorge Branco , Portugal
Bruno Briseghella , China
Brian M. Broderick, Ireland
Emanuele Brunesi , Italy
Quoc-Bao Bui , Vietnam
Tan-Trung Bui , France
Nicola Buratti, Italy
Gaochuang Cai, France
Gladis Camarini , Brazil
Alberto Campisano , Italy
Qi Cao, China
Qixin Cao, China
Iacopo Carnacina , Italy
Alessio Cascardi, Italy
Paolo Castaldo , Italy
Nicola Cavalagli , Italy
Liborio Cavaleri , Italy
Anush Chandrappa , United Kingdom
Wen-Shao Chang , United Kingdom
Muhammad Tariq Amin Chaudhary, Kuwait
Po-Han Chen , Taiwan
Qian Chen , China
Wei Tong Chen , Taiwan
Qixiu Cheng, Hong Kong
Zhanbo Cheng, United Kingdom
Nicholas Chileshe, Australia
Prinya Chindaprasirt , Thailand
Corrado Chisari , United Kingdom
Se Jin Choi , Republic of Korea
Heap-Yih Chong , Australia
S.H. Chu , USA
Ting-Xiang Chu , China

Zhaofei Chu , China
Wonseok Chung , Republic of Korea
Donato Ciampa , Italy
Gian Paolo Cimellaro, Italy
Francesco Colangelo, Italy
Romulus Costache , Romania
Liviu-Adrian Cotfas , Romania
Antonio Maria D'Altri, Italy
Bruno Dal Lago , Italy
Amos Darko , Hong Kong
Arka Jyoti Das , India
Dario De Domenico , Italy
Gianmarco De Felice , Italy
Stefano De Miranda , Italy
Maria T. De Risi , Italy
Tayfun Dede, Turkey
Sadik O. Degertekin , Turkey
Camelia Delcea , Romania
Cristoforo Demartino, China
Giuseppe Di Filippo , Italy
Luigi Di Sarno, Italy
Fabio Di Trapani , Italy
Aboelkasim Diab , Egypt
Thi My Dung Do, Vietnam
Giulio Dondi , Italy
Jiangfeng Dong , China
Chao Dou , China
Mario D'Aniello , Italy
Jingtao Du , China
Ahmed Elghazouli, United Kingdom
Francesco Fabbrocino , Italy
Flora Faleschini , Italy
Dingqiang Fan, Hong Kong
Xueping Fan, China
Qian Fang , China
Salar Farahmand-Tabar , Iran
Ilenia Farina, Italy
Roberto Fedele, Italy
Guang-Liang Feng , China
Luigi Fenu , Italy
Tiago Ferreira , Portugal
Marco Filippo Ferrotto, Italy
Antonio Formisano , Italy
Guoyang Fu, Australia
Stefano Galassi , Italy

Junfeng Gao , China
Meng Gao , China
Giovanni Garcea , Italy
Enrique García-Macías, Spain
Emilio García-Taengua , United Kingdom
DongDong Ge , USA
Khaled Ghaedi, Malaysia
Khaled Ghaedi , Malaysia
Gian Felice Giaccu, Italy
Agathoklis Giaralis , United Kingdom
Ravindran Gobinath, India
Rodrigo Gonçalves, Portugal
Peilin Gong , China
Belén González-Fonteboa , Spain
Salvatore Grasso , Italy
Fan Gu, USA
Erhan Güneyisi , Turkey
Esra Mete Güneyisi, Turkey
Pingye Guo , China
Ankit Gupta , India
Federico Gusella , Italy
Kemal Hacıfendioglu, Turkey
Jianyong Han , China
Song Han , China
Asad Hanif , Macau
Hadi Hasanzadehshooiili , Canada
Mostafa Fahmi Hassanein, Egypt
Amir Ahmad Hedayat , Iran
Khandaker Hossain , Canada
Zahid Hossain , USA
Chao Hou, China
Biao Hu, China
Jiang Hu , China
Xiaodong Hu, China
Lei Huang , China
Cun Hui , China
Bon-Gang Hwang, Singapore
Jijo James , India
Abbas Fadhil Jasim , Iraq
Ahad Javanmardi , China
Krishnan Prabhakan Jaya, India
Dong-Sheng Jeng , Australia
Han-Yong Jeon, Republic of Korea
Pengjiao Jia, China
Shaohua Jiang , China

MOUSTAFA KASSEM , Malaysia
Mosbeh Kaloop , Egypt
Shankar Karuppannan , Ethiopia
John Kechagias , Greece
Mohammad Khajehzadeh , Iran
Afzal Husain Khan , Saudi Arabia
Mehran Khan , Hong Kong
Manoj Khandelwal, Australia
Jin Kook Kim , Republic of Korea
Woosuk Kim , Republic of Korea
Vaclav Koci , Czech Republic
Loke Kok Foong, Vietnam
Hailing Kong , China
Leonidas Alexandros Kouris , Greece
Kyriakos Kourousis , Ireland
Moacir Kripka , Brazil
Anupam Kumar, The Netherlands
Emma La Malfa Ribolla, Czech Republic
Ali Lakirouhani , Iran
Angus C. C. Lam, China
Thanh Quang Khai Lam , Vietnam
Luciano Lamberti, Italy
Andreas Lampropoulos , United Kingdom
Raffaele Landolfo, Italy
Massimo Latour , Italy
Bang Yeon Lee , Republic of Korea
Eul-Bum Lee , Republic of Korea
Zhen Lei , Canada
Leonardo Leonetti , Italy
Chun-Qing Li , Australia
Dongsheng Li , China
Gen Li, China
Jiale Li , China
Minghui Li, China
Qingchao Li , China
Shuang Yang Li , China
Sunwei Li , Hong Kong
Yajun Li , China
Shun Liang , China
Francesco Liguori , Italy
Jae-Han Lim , Republic of Korea
Jia-Rui Lin , China
Kun Lin , China
Shibin Lin, China

Tzu-Kang Lin , Taiwan
Yu-Cheng Lin , Taiwan
Hexu Liu, USA
Jian Lin Liu , China
Xiaoli Liu , China
Xuemei Liu , Australia
Zaobao Liu , China
Zhuang-Zhuang Liu, China
Diego Lopez-Garcia , Chile
Cristiano Loss , Canada
Lyan-Ywan Lu , Taiwan
Jin Luo , USA
Yanbin Luo , China
Jianjun Ma , China
Junwei Ma , China
Tian-Shou Ma, China
Zhongguo John Ma , USA
Maria Macchiaroli, Italy
Domenico Magisano, Italy
Reza Mahinroosta, Australia
Yann Malecot , France
Prabhat Kumar Mandal , India
John Mander, USA
Iman Mansouri, Iran
André Dias Martins, Portugal
Domagoj Matesan , Croatia
Jose Matos, Portugal
Vasant Matsagar , India
Claudio Mazzotti , Italy
Ahmed Mebarki , France
Gang Mei , China
Kasim Mermerdas, Turkey
Giovanni Minafò , Italy
Masoomah Mirrashid , Iran
Abbas Mohajerani , Australia
Fadzli Mohamed Nazri , Malaysia
Fabrizio Mollaioli , Italy
Rosario Montuori , Italy
H. Naderpour , Iran
Hassan Nasir , Pakistan
Hossein Nassiraei , Iran
Satheeskumar Navaratnam , Australia
Ignacio J. Navarro , Spain
Ashish Kumar Nayak , India
Behzad Nematollahi , Australia

Chayut Ngamkhanong , Thailand
Trung Ngo, Australia
Tengfei Nian, China
Mehdi Nikoo , Canada
Youjun Ning , China
Olugbenga Timo Oladinrin , United Kingdom
Oladimeji Benedict Olalusi, South Africa
Timothy O. Olawumi , Hong Kong
Alejandro Orfila , Spain
Maurizio Orlando , Italy
Siti Aminah Osman, Malaysia
Walid Oueslati , Tunisia
SUVASH PAUL , Bangladesh
John-Paris Pantouvakis , Greece
Fabrizio Paolacci , Italy
Giuseppina Pappalardo , Italy
Fulvio Parisi , Italy
Dimitrios G. Pavlou , Norway
Daniele Pellegrini , Italy
Gatheeshgar Perampalam , United Kingdom
Daniele Perrone , Italy
Giuseppe Piccardo , Italy
Vagelis Plevris , Qatar
Andrea Pranno , Italy
Adolfo Preciado , Mexico
Chongchong Qi , China
Yu Qian, USA
Ying Qin , China
Giuseppe Quaranta , Italy
Krishanu ROY , New Zealand
Vlastimir Radonjanin, Serbia
Carlo Rainieri , Italy
Rahul V. Ralegaonkar, India
Raizal Saifulnaz Muhammad Rashid, Malaysia
Alessandro Rasulo , Italy
Chonghong Ren , China
Qing-Xin Ren, China
Dimitris Rizos , USA
Geoffrey W. Rodgers , New Zealand
Pier Paolo Rossi, Italy
Nicola Ruggieri , Italy
JUNLONG SHANG, Singapore

Nikhil Saboo, India
Anna Saetta, Italy
Juan Sagaseta , United Kingdom
Timo Saksala, Finland
Mostafa Salari, Canada
Ginevra Salerno , Italy
Evangelos J. Sapountzakis , Greece
Vassilis Sarhosis , United Kingdom
Navaratnarajah Sathiparan , Sri Lanka
Fabrizio Scozzese , Italy
Halil Sezen , USA
Payam Shafigh , Malaysia
M. Shahria Alam, Canada
Yi Shan, China
Hussein Sharaf, Iraq
Mostafa Sharifzadeh, Australia
Sanjay Kumar Shukla, Australia
Amir Si Larbi , France
Okan Sirin , Qatar
Piotr Smarzewski , Poland
Francesca Sollecito , Italy
Rui Song , China
Tian-Yi Song, Australia
Flavio Stochino , Italy
Mayank Sukhija , USA
Piti Sukontasukkul , Thailand
Jianping Sun, Singapore
Xiao Sun , China
T. Tafsirojjan , Australia
Fujiao Tang , China
Patrick W.C. Tang , Australia
Zhi Cheng Tang , China
Weerachart Tangchirapat , Thailand
Xiabin Tao, China
Piergiorgio Tataranni , Italy
Elisabete Teixeira , Portugal
Jorge Iván Tobón , Colombia
Jing-Zhong Tong, China
Francesco Trentadue , Italy
Antonello Troncone, Italy
Majbah Uddin , USA
Tariq Umar , United Kingdom
Muahmmad Usman, United Kingdom
Muhammad Usman , Pakistan
Mucteba Uysal , Turkey

Ilaria Venanzi , Italy
Castorina S. Vieira , Portugal
Valeria Vignali , Italy
Claudia Vitone , Italy
Liwei WEN , China
Chunfeng Wan , China
Hua-Ping Wan, China
Roman Wan-Wendner , Austria
Chaohui Wang , China
Hao Wang , USA
Shiming Wang , China
Wayne Yu Wang , United Kingdom
Wen-Da Wang, China
Xing Wang , China
Xiuling Wang , China
Zhenjun Wang , China
Xin-Jiang Wei , China
Tao Wen , China
Weiping Wen , China
Lei Weng , China
Chao Wu , United Kingdom
Jiangyu Wu, China
Wangjie Wu , China
Wenbing Wu , China
Zhixing Xiao, China
Gang Xu, China
Jian Xu , China
Panpan , China
Rongchao Xu , China
HE YONGLIANG, China
Michael Yam, Hong Kong
Hailu Yang , China
Xu-Xu Yang , China
Hui Yao , China
Xinyu Ye , China
Zhoujing Ye, China
Gürol Yildirim , Turkey
Dawei Yin , China
Doo-Yeol Yoo , Republic of Korea
Zhanping You , USA
Afshar A. Yousefi , Iran
Xinbao Yu , USA
Dongdong Yuan , China
Geun Y. Yun , Republic of Korea

Hyun-Do Yun , Republic of Korea
Cemal YİĞİT , Turkey
Paolo Zampieri, Italy
Giulio Zani , Italy
Mariano Angelo Zanini , Italy
Zhixiong Zeng , Hong Kong
Mustafa Zeybek, Turkey
Henglong Zhang , China
Jiupeng Zhang, China
Tingting Zhang , China
Zengping Zhang, China
Zetian Zhang , China
Zhigang Zhang , China
Zhipeng Zhao , Japan
Jun Zhao , China
Annan Zhou , Australia
Jia-wen Zhou , China
Hai-Tao Zhu , China
Peng Zhu , China
QuanJie Zhu , China
Wenjun Zhu , China
Marco Zucca, Italy
Haoran Zuo, Australia
Junqing Zuo , China
Robert Černý , Czech Republic
Süleyman İpek , Turkey

Contents

Corrigendum to “Prediction of Concrete Compressive Strength and Slump by Machine Learning Methods”

M. Timur Cihan 

Corrigendum (1 page), Article ID 8201734, Volume 2020 (2020)

Development of a Nonlinear Integer Optimization Model for Tenant Mix Layout in a Shopping Centre

Hongyue Lv and Ting-Kwei Wang 

Research Article (15 pages), Article ID 2787351, Volume 2020 (2020)

Prediction of Concrete Compressive Strength and Slump by Machine Learning Methods

M. Timur Cihan 

Research Article (11 pages), Article ID 3069046, Volume 2019 (2019)

Fuzzy Multicriteria Decision-Making Model for Time-Cost-Risk Trade-Off Optimization in Construction Projects

M. Ammar Alzarrad , Gary P. Moynihan, Muhammad T. Hatamleh, and Siyuan Song

Research Article (7 pages), Article ID 7852301, Volume 2019 (2019)

A Multiobjective Bilevel Programming Model for Environmentally Friendly Traffic Signal Timings

Ozgur Baskan 

Research Article (13 pages), Article ID 1638618, Volume 2019 (2019)

Multiobjective Optimization Design for Structural Parameters of TBM Disc Cutter Rings Based on FAHP and SAMPGA

Laikuang Lin , Yimin Xia , and Dun Wu

Research Article (13 pages), Article ID 8438639, Volume 2019 (2019)

Multiobjective Construction Optimization Model Based on Quantum Genetic Algorithm

Wei He  and Yichao Shi 

Research Article (8 pages), Article ID 5153082, Volume 2019 (2019)

Corrigendum

Corrigendum to “Prediction of Concrete Compressive Strength and Slump by Machine Learning Methods”

M. Timur Cihan 

Civil Engineering, Tekirdağ Namık Kemal University, Çorlu Faculty of Engineering, Tekirdağ 59860, Turkey

Correspondence should be addressed to M. Timur Cihan; mehmetcihan@nku.edu.tr

Received 20 July 2020; Accepted 20 July 2020; Published 30 August 2020

Copyright © 2020 M. Timur Cihan. This is an open access article distributed under the Creative Commons Attribution License, which permits unrestricted use, distribution, and reproduction in any medium, provided the original work is properly cited.

In the article titled “Prediction of Concrete Compressive Strength and Slump by Machine Learning Methods” [1], there was an error in equation (1), which should be corrected as follows:

$$\text{MAE} = \frac{1}{n} \sum_{i=1}^N |\text{predicted}_i - \text{actual}_i|. \quad (1)$$

References

- [1] M. Timur Cihan, “Prediction of concrete compressive strength and slump by machine learning methods,” *Advances in Civil Engineering*, vol. 2019, p. 11, Article ID 3069046, 2019.

Research Article

Development of a Nonlinear Integer Optimization Model for Tenant Mix Layout in a Shopping Centre

Hongyue Lv and Ting-Kwei Wang 

BIM Research Centre, School of Management Science and Real Estate, Chongqing University, Chongqing 400045, China

Correspondence should be addressed to Ting-Kwei Wang; tingkwei@cqu.edu.cn

Received 13 September 2019; Revised 3 February 2020; Accepted 10 February 2020; Published 19 March 2020

Guest Editor: Maksym Grzywinski

Copyright © 2020 Hongyue Lv and Ting-Kwei Wang. This is an open access article distributed under the Creative Commons Attribution License, which permits unrestricted use, distribution, and reproduction in any medium, provided the original work is properly cited.

The tenant mix layout of shopping malls affects shopper consumption behaviour and the performance of malls. The main function of the tenant mix layout is to increase store sales by increasing footfall. However, although existing studies have shown the importance of the spatial clustering effect and the physical information about tenants, the authors of those studies did not properly consider both the spatial clustering effect and the physical information about tenants at the meantime. Through this study, we aimed to maximize the spillover effect of the stores in the shopping centre while considering both the spatial clustering effect and physical information about tenants. Therefore, we present a problem called *the tenant mix problem*, which is to determine the optimal tenant configuration scheme for existing shopping centre space segmentation to maximize the rental income of a shopping centre. To solve this problem, a nonlinear integer optimization model with defined characteristics was proposed and solved using a genetic algorithm. A shopping centre case study is also presented to verify the performance of the model.

1. Introduction

The retail industry is facing great challenges and transformation opportunities [1]. Traditional retailers are facing difficulties as retail spending shifts from offline to online shopping, and a large proportion of retail spending is covered by service spending. Online retailing increased by 10% a year from 2009 to 2014 while spending at big box and department stores declined by about 4% a year [2], followed by a spate of retail property closures in China and the United States [3].

Shopping centres are faced with escalating retail challenges, forcing owners to optimize rental pricing, store layout, tenant mix, and product selection and continuously utilize other strategies [4]. A shopping centre's lease form gives the owner enough motivation to create and improve the retail environment for retailers during the operating period [5, 6]. Previous studies have shown that tenant mix is one of the determinants of the success of shopping centres [7–11]. The physical environment of a store is a trigger that can significantly affect the shopping attitudes and behaviours of consumers. The reasonable

distribution of anchor stores and nonanchor stores in a mall, as well as the accumulation of homogeneous and heterogeneous retail types, enables each area of the shopping centre to have a specific dynamic atmosphere and guide the flow of customers, thus reducing gross shopping time and increasing the frequency at which shops on both sides are patronized [12, 13]. An excellent tenant mix layout can make the customer flow in a shopping centre orderly, strengthen customers' impressions of the stores, encourage shopping behaviour, improve shopping efficiency, and benefit both retailers and developers. Therefore, both scientific researchers and retail practitioners have a great interest in the mix of tenants in a shopping centre, the effective use of shopping space, and the optimization of a retail layout [14].

Researchers have summarized many general rules for the spatial arrangement and selection of tenants in shopping centres [15]. In practice, however, those theories are generally single stores and lack practicability and effectiveness in the whole mall. Hence, developers and owners have to come up with preliminary tenant mix layouts based on experience or existing shopping centre layouts. The searching for an

optimal tenant mix layout is a complex decision problem called the tenant mix problem (TMP) [16]. Different from the classic facility layout problem (FLP) and location allocation problem (LAP) in the field of spatial layout, first, the goal of the TMP is to maximize the benefits of shopping centre owners rather than minimizing the travel time of customers or maximizing area utilization. Second, although consumer paths are guided by their shopping purposes and shopping mall movement lanes, they still choose random routes instead of flowing among certain facilities. Third, the spatial layout of tenants needs to involve taking the competition and cooperation between different retail stores into account. The relationship between material flow and fixed facilities is often not complex.

Unfortunately, there exists limited research on the TMP. Early TMP researchers only calculated the rental income of specific shopping centres under the constraints of several indicators, including total leasable area, the upper and lower limits of each type of business area, the upper and lower limits of each size of a shop, and the maximum amount of interior decoration allowance [16]. Nevertheless, in shopping centre retail theories, the layout of tenant mix is also affected by the interaction between shops, namely, the agglomeration of the same retail types and the retail externality of the anchor store. The reason for these influences is the consumer's psychology during shopping, which means the tenant mix is not determined based on the physical constraints of the shopping centre. Yim Yiu and Xu [17] compare a shopping centre to an ecosystem, so the tenant mix of a mature and stable shopping centre can be regarded as the product of evolution after the selection of consumers. Shopping centre operators often take consumer psychology into consideration as much as possible at the beginning of considering tenant layout to balance the proportion and spatial layout among various retail types. However, due to the dilemma of quantifying interstore interaction, it is difficult to solve this problem using qualitative analysis and empirical rules alone. Therefore, the problem of how to arrange tenants for each floor of a shopping centre so that merchants can get the maximum patronage from consumers remains to be solved.

Aimed at solving this problem, we propose a tenant mix layout model. This model is a solution to the TMP that involves determining the optimal tenant spatial layout scheme for each floor of a shopping centre to maximize customer flow past shops. In this way, scattered customers can be converted into actual sales to maximize the rent of the shopping centre. Considering the complexity involved in solving an integer nonlinear programming model, we adopted a genetic algorithm (GA). We also analysed the sensitivity of the layout generated by the GA by changing parameters representing different consumer types.

In Section 2, we present the existing tenant mix layout literature. Then, in Section 3, we propose the tenant composite space layout model, and, in Section 4, we define the model parameters and procedures for a GA. In Section 5, a case study is presented and the program execution results are discussed. Finally, in Section 6, we present the conclusions and prospects of our research.

2. Literature Review

The idea of optimizing a shopping centre space has existed for a long time. Scholars have conducted many empirical studies on the tenant allocation of retail space, but the literature on the TMP is very limited. According to Nie, generally, the TMP includes three levels of decisions, namely, the division of physical space [18–20], the selection of retail types, and the brand level of stores [18]. In the development process of shopping malls, tenants are arranged into empty shops through these three procedures. Spatial division was the common subject of literature research on retail layout in the past. However, spatial allocation was calculated without considering the retail type and brand level of stores. Therefore, if researchers only consider the division of physical space in the TMP problem, the estimated value of shopping centre obtained from the conclusion is biased. However, the actual mall development process is one in which the operations team only needs to decide quickly how to allocate retail types and brand levels to vacant stores so that owners can negotiate with potential tenants rather than partition the mall's interior. In other words, operators are more concerned about matching suitable tenants to existing empty spaces than designing the interior of the mall. The concerns of our research are consistent with those of operators. However, the literature on tenant mix layout is insufficient. We refer to the limited related literature [6, 16, 21–24] to explain how we selected variables in the proposed model.

The tenant mix describes the number, size, sales, or service categories of stores, as well as their locations in a shopping centre [11, 25]. It plays an important role in gross rental income, retail sales income, tourist attraction, shopping centre image, and user experience of the shopping centre [26]. It is an internal factor that determines the attractiveness of the shopping centre [15, 27] and one of the decisive factors in the success of a shopping centre [5, 11, 28]. In shopping centres, retail leases usually include both basic and excess rents, also known as percentage rents, which take effect when store sales reach a certain threshold [29, 30]. Rent paid by stores is often affected by brand level, retail type, location, size, and other factors [11, 31, 32]. Therefore, rent is adjusted for each store according to these influencing factors in our model.

Seagle [33] first tried to model the layout for commercial real estate tenants. He established a linear programming model to allocate an area for each tenant to maximize the present value of shopping malls. This model took into account the limitations of usable area, investment, and other developer resources. Jensen and Arthur [34] proposed a mixed integer programming model for the TMP, which solved the problems of space segmentation and the number of tenants in different size classes. Bean et al.'s nonlinear programming model [16] inspired our research. Bean's team planned the number of tenants of each tenant type for a new shopping centre and arranged the size and location of each tenant. They tried to give a simple description of the interaction effects among each tenant class, but, due to the complexity of computing, the final model simplified the

interaction. In summary, past models have involved too little consideration of customer behaviour in shopping centres. The interaction between the same and different types of retail stores has not been taken into account, and the roles of specific retail stores in a shopping centre have not been defined.

In other cases, the tenant mix layout uses a set of general rules. For example, (1) the classic “barbell” shopping centre model advocates placing anchor shops and dining areas at both ends and setting smaller tenants on both sides of the corridor connecting the two ends; (2) nonanchor stores should not be clustered together but scattered in the mall; (3) the layout of a shopping centre should enable consumers to pass through as many stores as possible [35, 36]. Scholars help architects envision possible layouts through surveys and questionnaires [27]. Borgers et al. [11] used a virtual reality tool to generate a virtual shopping centre that enabled respondents to select the major categories, subcategories and specific stores to measure their preferences and help owners select optimal layout strategies.

Consumer behaviour in a shopping centre can create retail externalities in stores due to shopping attitudes, such as multipurpose shopping, comparison shopping, and reducing search costs, and those externalities have been widely identified [6, 21, 22]. These externalities have been widely observed; for example, when customers make multipurpose purchases, they require shopping malls to have rich retail types. In addition, the presence of the anchor stores creates customer spillover effect for other stores. At the same time, the external economy is reflected in the gathering of stores. Clustering retail stores of the same type reduces search times and uncertainty for customers, which benefits stores while generating competition [37, 38]. Yuo and Lizieri [39] focused on the decentralization and agglomeration strategies of stores in a multilayer shopping centre and considered the search cost of consumers to achieve the purpose of shopping. They believe that the dispersion of low-floor nonanchor stores can minimize total search distances for shoppers and enhance retail externality, while in a shopping centre with a large crowd flow or vertical structure, the same type of clustering enables consumers to identify their destinations, creating spillover effects and increasing flow effectiveness.

Peter et al. [23] linked store sales to whether the store can be seen. In other words, products that repeatedly appear in consumers’ sight will prompt consumers to buy them on impulse. Sorensen [24] proposed a visibility-based attractiveness evaluation, believing that the size of a store and the distance between a store and a shopper affect a shopper’s attention. Lu and Seo [40] measured visibility and exposure based on a GIS and confirmed the two-way influence between store layout and shoppers through a set of experiments in bookstores. In a shopping centre, the degrees of exposure of the stores are complicated and related to the vision of consumers, the floor space of the store, the distance of the store from consumers, and other indoor things, such as elevators and toilets.

Some researchers simulate consumer behaviour to layout the tenant mix. Hirsch et al. [41] analysed the customer density and retail type concentration in a

shopping centre with a GIS. They coupled the retail cluster using category aggregation and variable agglomeration methods and then visualized the passenger flow of the shopping centre through the core density estimator (KDE), thus reflecting retail agglomeration externalities more clearly through customer trajectories. In the exploration of retail correlation, GIS has incomparable advantages, but the clustering method in GIS can only tell us which tenants are related. Because the customer trajectories simulated by GIS are affected by each different tenant layout, it is difficult to determine how to optimize tenant placement. In addition, the tenant mix layout obtained from the above research does not involve consideration of the maximum profit of the owner; that is, the researchers did not attempt to maximize the size of stores in the eyes of customers in their search paths. However, if customers are aware of the larger size of the store, tenants can get more sales, which is the purpose of mall operators.

Based on the research gaps in the TMP, our contribution focuses on proposing a nonlinear programming model that takes into account both the spatial clustering effect and physical information about tenants. The model describes the impacts of consumer behaviour on store externalities which were not presented in previous TMP models. Then we use a GA to solve this complex problem. Finally, a case study of a realistic shopping centre is used to verify the model.

3. Nonlinear Integer Optimization Model for the TMP

3.1. Assumptions. Early versions of the TMP were similar to the FLP, which was designed to arrange rectangular objects (empty stores, machines, or departments) in a defined entire space without overlapping.

The TMP discussed in this paper is similar to the LAP, whose purpose is to explore how to best arrange the retail type and brand level of each empty shop in a vacant shopping centre to maximize the exposure of the shops on the floor to customers, increase the sales of the shops, and maximize the total rental income of a shopping centre.

We made the following assumptions when developing our optimization model:

- (i) Customers go shopping for multiple purposes, so one customer can be a potential consumer for various types of business.
- (ii) The attraction of a store is directly proportional to its size.
- (iii) Anchor store generates retail externalities but is not affected by the externalities of other stores. Because of the large size of the anchor store, customers need to spend a lot of time shopping in it. To save time, customers will not wander in without the intention to buy products in the anchor store [42].
- (iv) Each floor has a main type of retail; for example, the 3rd floor of a shopping mall mainly sells clothes, and the 4th floor mainly sells electrical appliances. This

main type of retail is called floor theme, and floor theme retail stores are only distributed on this floor.

- (v) To simplify the problem, the potential relationship between business types is not considered (e.g., the potential relationship between beer and diapers is not considered).

Table 1 lists the coefficients and decision variables. To improve tenant mix layout, we propose the use of the following optimization model.

3.2. The Objective Function for Calculating Rent. Our rental estimation equation is based on the widely accepted shopping centre lease framework [5, 42–44]. That is, total rent usually consists of basic rent and percentage rent:

$$\text{Rent} = \text{Basic rent} + \text{Excess rent.} \quad (1)$$

First, basic rent is the fixed rent per square meter of the leasable area of a shopping centre. It constitutes the fixed income of the owner. Excess rent is also called percentage rent. When the sales of the shop reach the agreed threshold, the percentage will take effect, and the tenants need to pay the excess rent.

$$c_{po} = \frac{1}{\sum_{\text{entr}} \sqrt{(x_{\text{store}} - x_{\text{entr}})^2 + (y_{\text{store}} - y_{\text{entr}})^2} + \sum_{\text{elev}} \sqrt{(x_{\text{store}} - x_{\text{elev}})^2 + (y_{\text{store}} - y_{\text{elev}})^2}} \quad (3)$$

That means the further away the store is from the entrance or elevator, the less likely it is to be seen by customers and, thus, the lower the basic rent that those tenants must pay.

To eliminate the problems of dimensional inconsistency and numerical incomparability between different coefficients, the adjustment coefficients were normalized. Thus, the basic rental equation of the store located on the f floor with the central coordinate of (x, y) :

$$\text{Basic rent} = S_{(f,x,y)} r_B c_f c_h c_{po}. \quad (4)$$

Excess Rent. Sales above the threshold generate excess rent, contributing to total rent. There is a significantly positive correlation between the rent paid by a single store and its retail sales. Therefore, when discussing the influencing factors of excess rent, we tend to pay attention to factors that affect store sales.

Obviously, the sales of a store are directly related to its type of retail and brand level, as well as the customer flow that the store can get. In our previous Assumptions, the number of customers in each location is equal at the initial state of the mall. However, this situation is not realistic. To make it more realistic, we revised the original customer distribution. Shopping centre customers tend to be concentrated at the elevator entrance. In addition, due to retail externalities, customer flow is affected by the concentration of anchor stores and similar retail types.

Basic rent. The authors of many empirical studies have proved that, among the micro factors that affect shopping central rent, the basic rent discrimination of stores mainly comes from the influence of store area (AREA), the brand rank of the store tenant (LEVEL), store floor (FLOOR), and location on the floor (POSITION). Then we use the functional form of equation (2) to describe the basic rent:

$$\text{Basic rent} = f(\text{AREA, FLOOR, LEVEL, POSITION, TYPE}). \quad (2)$$

In equation (2), AREA is determined in a given shopping centre, and LEVEL is generated by a GA. Moreover, the coefficient c_f was used to quantify FLOOR's impact on rent. We used empirical data in this case.

When measuring the coefficient c_{po} of POSITION, in addition to considering how the distribution of customers is attracted by different types of stores, the necessary entrance and elevator on the floor also lead to their uneven distribution in space. Because the shopping mall is convex, we can use the Euclidean distance equation to measure the distance between the centre point of each store and the entrance or elevator centre point and define the store position adjustment coefficient c_{po} as follows:

Generally, consumers come to a shopping centre for two reasons, to hang out or to buy certain items, or a combination of the two.

As a general rule for tenant layout, the owner usually sets the anchor stores at both ends of the shopping central corridor to guide consumers to pass other shops on both sides of the corridor. The anchor store is regarded as the most important tenant that guides customer flow. The closer a store is to the anchor store, the more likely that store is to be exposed to the view of consumers. Secondly, to save time, consumers are inclined to conduct shopping in areas with many similar retail stores. The externalities of the anchor store and similar agglomeration externalities are referred to as retail externalities. Based on the above analysis, we propose the function of retail sales per unit area of the store as

$$\text{SALES} = f(\text{TYPE, LEVEL, EXTERNALITY, POSITION}). \quad (5)$$

According to the second assumption, we use the store area to represent the attraction of the store. We defined the externality of the anchor store as w_1 and adopted the gravity model to calculate the attraction level of the anchor store in relation to the other stores around it:

$$w_1 = \frac{S_{\text{anchor}} S_{(f,x,y)}}{d_{\text{anchor}}^2}. \quad (6)$$

TABLE 1: Parameters used in the model.

Notation	Definition
r_B	Basic rent for the first floor (US\$/m ²)
c_{f_i}	Adjustment coefficient of shop grade (for basic rent)
c_f	Adjustment coefficient of the floor (for basic rent)
F	The floor number
f_1	Floor threshold coefficient
c_{po}	Regulation coefficient of the entrance and exit and elevator (for basic rent)
(x_{store}, y_{store})	The (x, y) coordinates of the centre of the store
(x_{entr}, y_{entr})	The (x, y) coordinates of the centre of entry and exit
(x_{elev}, y_{elev})	The (x, y) coordinates of the centre of the elevator
S_{anchor}	The size of the anchor store (m ²)
$S_{(f,x,y)}$	The store's area of coordinates (f, x, y) ; f is the floor of the store
d_{anchor}	European distance between other stores and the anchor store
w_1	Externality coefficient of the anchor store
n_i	The number of potential consumers of retail type i
$cost_i$	The annual consumption capacity of consumers for goods of type i
S_i	The total area of stores with retail type i
p_i	Unit area sales when the total area of the retail type i store is S_i
$S_{trav(i)}$	The maximum size of a retail type, which potential consumers are willing to search to find products that meet their needs
$S_{(f,i)}$	The total area of the i retail type stores on floor f
α	The proportion of customers entering other stores of the same type of retail for the purpose of comparison shopping
β	The proportion of real consumers that individual stores lose in competition
$S_{thre(i)}$	The total area of a store with retail type i when the retail sales of per unit area reach the maximum
p_m	The threshold that stores with retail type i should pay a percentage rent
$S_{max(i)}, S_{min(i)}$	The total area of stores with retail type i when the sales are p_m (two possibilities)

Compared to the retail externalities of anchor stores, similar agglomeration externalities are more complex. Clustering stores of the same retail type can effectively increase customers by enabling comparison shopping, thus improving the sales of stores [22]. In practice, owners are also aware of this externality and enhance the shopping experience by setting a specific retail theme for each floor. However, it is difficult to control the limits of store agglomeration, and the competition caused by the increase in the number of stores of the same type will reduce the sales of stores. Therefore, under the premise of a fixed number of potential consumers in the shopping centre, economies of scale gradually shift to diseconomies of scale as the area of stores increases [13]. In our model, a floor theme control matrix is built-in, and the theme of each floor is set by the owner. On each floor, more tenants will be arranged in the corresponding theme retail type, so as to realize the spatial agglomeration of theme retail type.

Next, we deduced the mathematical expression of the agglomeration externality of the same type of retail stores in shopping malls.

Suppose the following:

- (i) The number of potential consumers in a shopping centre with retail type i is n_i
- (ii) The annual consumption capacity of consumers for commodities with type i is $cost_i$
- (iii) The total area of retail type i in a shopping centre is S_i
- (iv) The sales of unit area is p_i when the total area of type i shops is S_i

Then

$$S_i p_i \leq n_i \text{ cost}_i, \quad (7)$$

S_i and p_i are both variables, and p_i can be written as a function of S_i . Due to the influence of agglomeration and competition, the relationship between p_i and S_i is not simply linear. This relationship is typical of scale effects, and Henderson [45] made a similar point in his model of urban systems. With the continuous expansion of the city scale, the utility generated by diseconomy will gradually offset the scale benefit of industrial concentration within the city. Therefore, the synergy between the external economy and diseconomy determines the optimal size of a city. There is an inverted U-shaped relationship between the size of a city and the utility of a typical resident. Based on the above analysis, we assume that there is an inverted U-shaped relationship between the sales per unit area of a typical store in a shopping centre and the sum area of the same type of retail stores, as shown in Figure 1.

In Figure 1, S_{thre} is the total area of a typical retail store of type i with the largest retail sales per unit area in the shopping centre. S_{max} and S_{min} are the maximum total area and minimum area of the stores that do not need to pay percentage rent, respectively. S_{thre} , S_{max} , and S_{min} are all variables affected by typical stores.

The constant S_{trav} is defined as the maximum i -type store area that potential consumers are willing to search for to find desired goods. When the store area of this type reaches S_{trav} , it can meet the needs of consumers for comparison shopping and control the time consumers spend on shopping.

Therefore, in the theme floor, we built a sales function for a typical theme store:

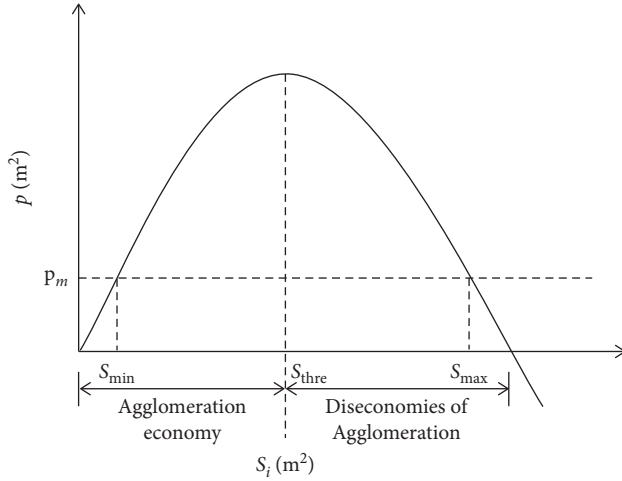


FIGURE 1: The relationship between p_i and S_i .

$$g = \frac{S_i}{S_{trav}} \cdot \frac{S_{(f,i)}}{S_i} \cdot n_i \cdot \frac{S_{(f,x,y)} + \alpha(S_{(f,i)} - S_{(f,x,y)}) - \beta(S_{(f,i)} - S_{(f,x,y)})}{S_{trav}} \quad (8)$$

In equation (8), S_i is the total area of shops of type i in the shopping centre, $S_{(f,i)}$ is the total store area of type i on floor f , α refers to the proportion of customers entering a store (f, x, y) from other stores of the same retail type on the same floor for the purpose of comparison shopping, and β is the proportion of real consumers lost by store (f, x, y) due to competition.

Under the assumption that all shops of type i in the shopping centre are clustered on floor f , namely, $S_{(f,i)} = S_i$, we differentiate the variable S_i of function g :

$$\frac{dg}{d(S_i)} = \frac{2(\alpha - \beta)S_i + (1 - \alpha + \beta)S_{(f,x,y)}}{S_{trav}^2} n_i \text{cost}_i = 0. \quad (9)$$

Hence,

$$S_i = \frac{(1 - \alpha + \beta)S_{(f,x,y)}}{2(\beta - \alpha)} = S_{thre}. \quad (10)$$

It is easy to know that, for any single store in the shopping centre, when the sales per unit area reaches the maximum, the corresponding S has nothing to do with the purchasing ability of potential customers and the store area that customers are willing to search for but does have to do with the demand for comparison shopping and store competition. Given that $\beta - \alpha \neq 0$ and $\alpha - \beta \neq 1$, the agglomeration area that a store can afford is related to its size. Compared to a small store, a large store needs a larger agglomeration to obtain the maximum sales per unit area. After the agglomeration area exceeds S_{thre} , the sales per unit area of a single store decreases as competition gradually becomes dominant in synergy (see Figure 2).

Total rental income is the combination of excess rent and basic rent, and the opportunity cost is the basic rent of the

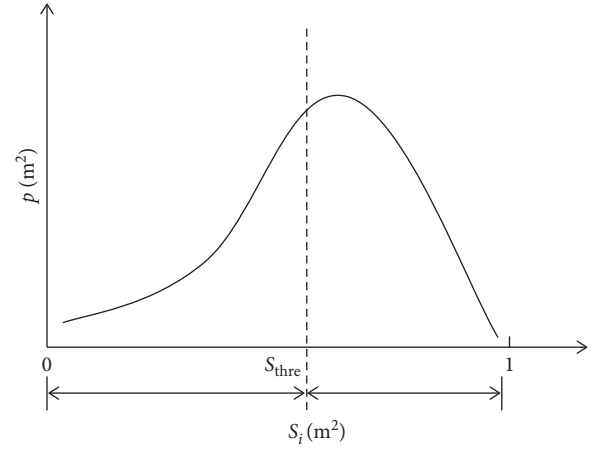


FIGURE 2: The relationship between the total store area of type i and the total sales of one store of this type.

occupied area. When the income equals the opportunity cost, the maximum S_i can be obtained:

$$S_{max} p_i \cdot a\% + S_{max} r_B c_f c_h c_{po} = S_{max} r_B c_f c_h c_{po}. \quad (11)$$

Therefore, $S_{max} p_i \cdot a\% = 0$

At this point, p_i equals p_m of threshold sales, and the rental income of a store of type i is the basic rent.

$$\frac{S_i}{S_{trav}} n_i \text{cost}_i \frac{S_{(f,x,y)} + (\alpha - \beta)(S_i - S_{(f,x,y)})}{S_{trav}} = p_m, \quad (12)$$

$$\frac{(\alpha - \beta)S_i^2 + (1 - \alpha + \beta)S_{(f,x,y)}S_i}{S_{trav}^2} n_i \text{cost}_i = p_m. \quad (13)$$

According to the above equation, S_{max} and S_{min} of a typical theme store in a shopping centre can be obtained.

For the nonthemed retail shops on themed floors, according to the third assumption, the spillover effect of retail externalities is spread from the dominant shop in a shopping centre to nondominant shops. The anchor store is not affected by the externalities of other shops in a shopping centre, and its customers are only attracted by its own gathering ability. Hence, similarly, due to the multiobjective shopping demand of consumers, the nontheme store is affected by the spillover effect of theme store aggregation, increasing visitor flow. Therefore, the sales function of a typical nontheme store on the floor is calculated as follows:

$$u = \frac{S_j}{S_{trav}} \cdot \frac{S_{(f,j)}}{j} \cdot n_j \cdot \frac{S_{(f,m,n)} + (\alpha - \beta)(S_{(f,j)} - S_{(f,m,n)}) + \varphi S_{(f,j)}}{S_{trav}} \text{cost}_j, \quad (14)$$

where φ is the spillover effect coefficient of the theme retail type to the nontheme retail type. Thus, the sales of nontheme retail type stores are restricted by the ability of theme stores to gather customers.

3.3. *Model for the TMP.* Based on the above analysis, for a particular floor, the function of sales per unit area of a single store with a thematic retail type is calculated:

$$P_{(f,x,y)} = \begin{cases} 0, S \notin U, \\ \frac{S_i}{S_{\text{trav}}} \cdot \frac{S_{(f,i)}}{S_i} \cdot n_i \cdot \frac{S_{(f,x,y)} + (\alpha - \beta)(S_{(f,i)} - S_{(f,x,y)})}{S_{\text{trav}}} \text{cost}_i c_f c_{p0}, & S_i \in U. \end{cases} \quad U = [S_{\min}, S_{\max}], \quad (15)$$

The function of sales per unit area of a store with nonthematic retail type is calculated as follows:

$$P_{(f,m,n)} = \begin{cases} 0, S \notin U, \\ \frac{S_i}{S_{\text{trav}}} \cdot \frac{S_{(f,i)}}{S_i} \cdot n_i \cdot \frac{S_{(f,m,n)} + (\alpha - \beta)(S_{(f,i)} - S_{(f,m,n)}) + \varphi S_{(f,i)}}{S_{\text{trav}}} \text{cost}_i c_f c_{p0}, & S_i \in U. \end{cases} \quad U = [S_{\min}, S_{\max}], \quad (16)$$

The form of excess rent for a single store is as follows, where $a\%$ is the payment ratio when the store reaches the sales threshold:

$$\text{Excess rent} = f(\text{AREA}, \text{SALE}, \text{PERCENT}), \quad (17)$$

$$\text{Excess rent} = \begin{cases} P_{(f,x,y)} S_{(f,x,y)} w_1 a_{\text{type}} \%, & \text{type} = i, \\ P_{(f,m,n)} S_{(f,m,n)} w_1 a_{\text{type}} \%, & \text{type} \neq i. \end{cases} \quad (18)$$

Meanwhile, according to the actual business conditions of shops in a shopping centre, there are two stages of rent:

$$\text{rent} = \begin{cases} \text{Basic rent}, & P_{(f,x,y)} \leq P_m, \\ \text{Basic rent} + \text{Excess rent}, & P_{(f,x,y)} > P_m. \end{cases} \quad (19)$$

The complete model can be simply expressed as follows:

$$\text{Maximum grossrent} : \sum \text{Rent}, \quad (20)$$

S.t.

$$\sum_{f=\min}^{\max f} \sum_{x=x_1}^{x_n} \sum_{y=y_1}^{y_n} S_{(f,x,y)} \leq G, \quad (21)$$

$$\sum_{x=x_1}^{x_n} \sum_{y=y_1}^{y_n} S_{(F,x,y)} \in G_F, \quad F = \min f, \dots, 0, \dots, \max f, \quad (22)$$

$$S_{(F,i_F)} \geq 0.5G_F, \quad F = \min f, \dots, 0, \dots, \max f, \quad (23)$$

$$S_{\{(F,X,Y),i_F,h\}} = \max(s), \quad F = \min f, \dots, 0, \dots, \max f, \quad (24)$$

$$h \in \{1, 2\},$$

$$\begin{aligned} \beta - \alpha &\neq 0, \\ \alpha - \beta &\neq 1. \end{aligned} \quad (25)$$

The purpose of constraints (21) and (22) is to make full use of the leasable area in the shopping centre. Constraint (23) makes the floor area of theme shops dominant on the floor, constraint (24) indicates that the retail type of the largest store on each floor is the floor themed retail type, and constraint (25) guarantees the uniqueness of S_{thre} .

In addition, it is easy to be troubled by the following problem: according to the lease agreement of shopping centre, different retail types of stores pay different rent proportions ($a\%$); for example, the rent proportion of food stores is higher than that of movie theatres. If all stores are placed with a retail type requiring high rent, then the rent of the shopping centre will undoubtedly reach the maximum, but this obviously violates reality and the principle of shopping centre diversity. Therefore, there is a potential constraint between the tenant mix and the available space in the shopping centre. The general rules are detailed in Section 4.2.

4. Genetic Algorithm Optimization for the Objective Optimization Problem

A GA is an adaptive optimization technique based on a biological genetic and evolutionary mechanism first proposed by Holland [46]. It first generates a set of candidate populations, each of which represents a solution. Individual fitness is calculated by simulating adaptive conditions. According to the idea of natural selection, the algorithm automatically retains excellent individuals and eliminates others. Under the continuous evolution of the population, the surviving individuals gradually converge as the optimal solution to the problem.

To apply a GA to solve a model, we improve the original algorithm. The improved GA makes the population quickly

converge to the optimal solution through three key subroutines:

- (1) Layout generation: when initializing the tenant layout of shops on all floors of a shopping centre, the relationship between store level, retail type, and store area is stipulated to ensure that the randomly generated tenant mix is feasible and in line with the practical logic.
- (2) Rent calculation: by simulating the shopping behaviours of different types of consumers, the algorithm calculates the basic rent and excess rent for each store in the shopping centre.
- (3) Layout update: brand level and retail type in the same individual are updated simultaneously and correspondingly. The population is then updated for the next iteration. The algorithm structure is shown in Table 2.

Next, we discuss how to represent the spatial layout of the tenant mix in the GA and explain the key settings in the algorithm.

4.1. Representation of Tenant Mix Scheme in the GA. Aickelin and Dowsland [47] proposed the GA of direct coding and indirect coding for the problems of mall layout and tenant combination. In our experiment, a clear and straightforward coding method was adopted to determine the retail type and brand grade of stores. A single individual represents a solution in the search space and represents the tenant mix layout of a certain floor in a shopping centre. That means each individual's chromosome is represented by a row of an integer array, which is composed of $2N$ elements, where N is the number of shops on the floor, the first N elements correspond to the retail types, and the last N elements represent the brand level.

For example, if a shopping centre has five floors in total, then the final result of a feasible tenant mix scheme is a cell containing five arrays that represent the retail type and brand level of each tenant on one floor of a shopping centre.

4.2. Subroutine: Layout Generation and Layout Update. As mentioned above, because there are many shops in a shopping mall, the solution space is very complex. Most randomly generated sample populations are not feasible, and it is difficult for the algorithm to converge to the optimal feasible solution in the solution space without restricting the relationship between the vacant shop area, retail type, and brand level.

The following is the general logic of the tenant mix layout:

- (1) Brand level setting: the brand level is divided into five levels, the anchor store ($h = 1$), the secondary anchor store ($h = 2$), secondary anchor stores that contribute to increased rent ($h = 3$), nonanchor stores that make rental contributions ($h = 4$), and nonanchor stores that enrich the retail type of the shopping mall ($h = 5$).

TABLE 2: Algorithm flow.

Input information about the shopping centre to be laid out
Initialize the tenant layout population under logical constraints
Set parameters of the GA
Do
For each iteration
Calculate the fitness of all individuals in the population
Find and then save the best solution and elite individuals in this generation into the next generation population
Use the roulette method to select the individuals who can enter the next iteration
The selected individual genes are crossed and mutated under logical constraints
Update the population
End
Until default number of iterations

- (2) Area setting: the store is mainly divided into three levels. G represents the leasable area of the store floor, and $S_{(f,x,y)}$ represents the area of a store.

Small store, $S_{(f,x,y)} < 0.05G$.

Medium store, $0.05G \leq S(f, x, y) < 0.1G$.

Large stores are divided into three levels:

- (i) Third level: third class is a large area store that is not the largest store on a floor. That is, $S_{(f,x,y)} > 0.1G$ and $S_{(f,x,y)}$, and the store (f, x, y) is not the largest store on the floor.
- (ii) Second class: the store area is the largest on the floor, but it is not big enough to accommodate an anchor store; $0.1G \leq S(f, x, y) < 0.25G$.
- (iii) First class: it is a store that can accommodate the anchor store; $S(f, x, y) \geq 0.25G$.

- (3) Setting of brand level matching area: stores with brand levels of 3, 4, and 5 can be placed in small stores. Stores with brand levels of 2, 3, 4, and 5 can be placed in medium stores. The second class of large stores can arrange tenants with brand levels of 2, 3, and 4. The first class of large store can be placed in stores with brand levels of 1 and 2. Table 3 shows matching principles of area and level more clearly.

- (4) Agreement on the expression of retail types:

We classified and numbered the retail types of a shopping centre with the Guidance of the Shopping Centre Tenant Mix Strategy (SB/T 10813-2012), which is the business industry standard published by the ministry of commerce of China:

Beauty salon (1), photo studio (2), training and education (3), the cinema (4), the gym (5), children's park (6), KTV (7), skating rink or video games city (8), and desserts (9), beverages (10), Chinese/western fast food (11), Chinese style dinner (12), western food (13), gourmet street (14), supermarket (15), department store (16), women's clothing (17), men's clothing (18), children's clothing (19), sports equipment (20), personal daily (21), and jewelry (22).

TABLE 3: Matching principle of area and level.

Area setting	Area range	Brand level of store
Small stores	$S_{(f,x,y)} < 0.05G$	3, 4, 5
Medium stores	$0.05G \leq S_{(f,x,y)} < 0.1G$	2, 3, 4, 5
Large stores	$S_{(f,x,y)} \geq 0.1G$ and $S_{(f,x,y)} \neq \max(s)$	2, 3, 4
	$0.1G \leq S_{(f,x,y)} < 0.25G$ and $S_{(f,x,y)}$ is $\neq \max(s)$	2, 3, 4
	$S_{(f,x,y)} \geq 0.25G$ and $S_{(f,x,y)} = \max(s)$	1, 2

*S is the area vector of a single floor.

Particularly, when a store is vacant, its retail type shall be expressed as (0).

(5) Level and retail type matching setting:

The corresponding relationship between store area and brand level is shown in Table 4.

In layout design and update, the randomly generated scheme must strictly follow settings 3 and 5 to ensure that the scheme is feasible and complies with reality.

4.3. Subroutine: Rent Calculation. The second key subroutine is calculating the rental income of each feasible scheme according to the fitness function. In our program, the adaptability function is a nonclosed subroutine that is divided into a coefficient definition module, basic rent calculation module, excess rent calculation module, and fitness calculation module. In the program, the excess rent module includes the anchor store retail externality coefficient calculation module, the cluster externality coefficient calculation module, and the store sales per unit area calculation module. In the last module, to obtain the sales per unit area of the store, we simulate the shopping behaviour of consumers.

4.4. Population Regeneration. During each iteration, the new population will enter the next-generation population after crossover and mutation by the individuals selected from the previous population. To preserve the genes of excellent individuals from being destroyed and accelerate the rate of convergence, we skip the crossover and mutation operation to retain an elite individual with the best fitness from the previous generation for the new population.

4.5. Optimal Solution. Each individual (corresponding to a feasible tenant combination layout plan) can determine the optimal solution in the population according to the rent calculation module. Such an individual is called an elite individual.

In the GA, the approximate global optimum is determined based on whether the average fitness is close enough to the maximum fitness. When the average fitness of the population is close to the maximum fitness and tends to be stable, it is generally regarded that the algorithm has found an optimal solution, which is the termination condition of the whole algorithm. When solving high-dimensional optimization problems, GAs are prone to “prematurity”; that

TABLE 4: Matching principle of level and retail type.

Brand level	Area rules	Retail types
1	$S_{(f,x,y)} \geq 0.25G$ and $S_{(f,x,y)} = \max(s)$	15, 16
2	$S_{(f,x,y)} < 0.25G$ and $S_{(f,x,y)} = \max(s)$, or $S_{(f,x,y)} > 0.05G$ and $S_{(f,x,y)} \neq \max(s)$	5, 6, 7, 8, 9
	$S_{(f,x,y)} \geq 0.25G$ and $S_{(f,x,y)} = \max(s)$	4
3	$S_{(f,x,y)} > 0.1G$ and $S_{(f,x,y)} \neq \max(s)$, or $S_{(f,x,y)} < 0.25G$ and $S_{(f,x,y)} = \max(s)$	17, 19
	$S_{(f,x,y)} > 20$ and $S_{(f,x,y)} \leq 0.1G$	17, 18, 19
	$S_{(f,x,y)} < 0.1G$	20, 21
4	$S_{(f,x,y)} > 20$ and $S_{(f,x,y)} \neq \max(s)$, or $S_{(f,x,y)} < 0.25G$ and $S_{(f,x,y)} = \max(s)$	11, 12, 13, 14
	$S_{(f,x,y)} < 20$	10
5	$S_{(f,x,y)} < 0.1G$	1, 2, 3, 22

*S is the area vector of a single floor.

is, the algorithm does not reach the end conditions mentioned above and only finds a local optimum within a small search range. In this case, the results of each operation of the algorithm are different, showing the characteristics of instability. According to our test, the crossover and mutation operators in the algorithm will slow down the convergence rate of the population. Therefore, adding new individuals to the population and improving the probability of finding the global optimal solution are two methods to deal with premature convergence.

5. Case Study

We used the indoor map data of a shopping centre in Chongqing, China, to test the optimization model. The mall has six floors: five above ground and one below ground, and it also has 158 shops for rent. After a simple estimation, the feasible solution space was found to be large. Through multiple tests of the algorithm coefficients, we chose to randomly generate a population of 5000 individuals according to the constraints. A total of 400 iterations were carried out and repeated three times to observe the stability of the algorithm and obtain multiple feasible solutions. The crossover rate and mutation rate of the algorithm were 0.8 and 0.003, respectively.

5.1. Operation Results. Figure 3 shows three tenant layouts after the program runs three times (Figure 3 only shows the first floor plan, while the complete results are stored in the appendix), the three-tenant layout is expected to help operators to obtain rental income 5.025×10^4 , 5.007×10^4 , and 5.028×10^4 thousand USD, respectively, and the average total rental income is 5.021×10^4 thousand USD. According to the maximum and average fitness curves (see Figure 4), we find that the maximum rent fluctuates by 0.4%, thus confirming the stability of the algorithm.

Figure 5 shows the original tenant layout, and the calculated rental income is 2.191×10^4 thousand USD. In Table 5, the number of stores and the leasable area of each floor are shown.

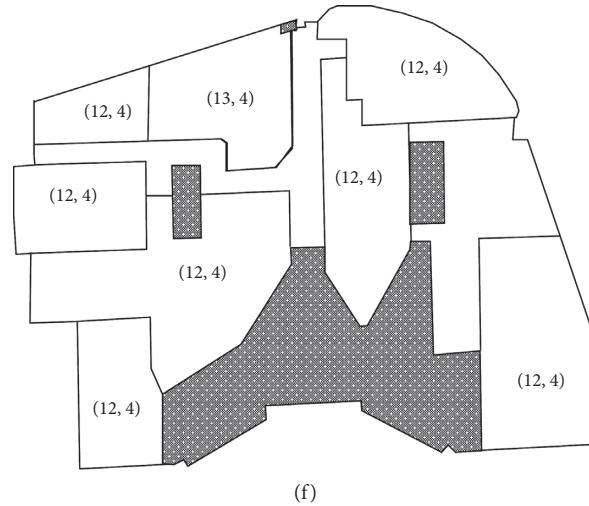


FIGURE 5: Original tenant mix layout. (a) Original tenant mix layout, B1. (b) Original tenant mix layout, F1. (c) Original tenant mix layout, F2. (d) Original tenant mix layout, F3. (e) Original tenant mix layout, F4. (f) Original tenant mix layout, F5. *In (i, h) , i represents the retail type of the tenant, and h represents the brand level of the store. The shaded area represents the nonrental area.

TABLE 5: Physical information.

Floor	Leasable area (m ²)	The number of stores
B1	8750.59	46
F1	2192.24	21
F2	2843.75	29
F3	2834.47	28
F4	2853.80	26
F5	2788.61	8

5.2. Model Stability Test. The fitness curve shows the stability of the improved algorithm. To verify whether the coefficients have an effect on the stability of the model results, we tested the effects of partial coefficients on the stability of model results. The coefficients in the model are mainly divided into three categories: (1) physical information coefficients of the shopping centre, such as the position coefficient (c_{po}) and floor coefficient (c_f); (2) coefficients of rental agreement, such as the deduction point ($a\%$) and store grade coefficient (c_h); and (3) assumptions coefficients obtained from the survey, such as the store area (S_{trav}) that customers are willing to search for, consumer consumption capacity ($n_i \cdot cost_i$), and consumer preference coefficient (α, β, φ).

According to the conclusion deduced using equation (10), S_{thre} , which leads to the largest sales per unit area of a store, is only related to the demand of comparison shopping and the competition among stores and has nothing to do with the purchasing capacity of potential consumers and the store area consumers are willing to search for products in. Therefore, we discuss the theme store through a simplified model.

In the simplified model, the consumer's consumption capacity, $n_i \cdot cost_i$, is a fixed value. We set a store with an initial area of 350 m² and gradually increase the area of the same type of retail stores in the shopping centre with a growth step of 1 m². To test whether the consumption preference coefficient will affect the results of the model, we tested four groups of different (α, β) combinations, $\beta -$

$\alpha \in \{0.2, 0.3, 0.4, 0.5\}$. The results are shown in Figure 6. Figure 6(a) shows the impact of the consumer preference coefficient on the sales of the store per unit area, and Figure 6(b) shows the impact of the consumer preference coefficient on the total sales of all stores in the retail type of shopping centre. Similarly, by fixing (α, β) and changing the consumption power $n_i \cdot cost_i \in \{2.4 \times 10^6, 3.4 \times 10^6, 4.4 \times 10^6\}$ (USD), which means the three groups of consumers, we discussed the influence of consumption power on the total sales of a single retail type. The conclusion is shown in Figure 7.

According to Figure 7, the consumption power is the same as the physical coefficient of the shopping centre, and its influence on the total sales does not change with the accumulation of similar stores. In the interview with the owner of the shopping centre, we compared the rent of the shopping centre calculated using the model to the actual rent, and the owner thought it could be used as an auxiliary tool for tenant layout. As shown in Figure 6, the difference in consumer preference coefficient causes the change in sales volume because it affects the store agglomeration of certain retail types in the shopping centre, so the difference in its value may have some impact on our conclusion. However, when we modify the consumer preference coefficient in the program's rent calculation module several times within a reasonable range, the rental performance of the optimized tenant mix is still better than that in the original tenant mix. Thus, the validity of the model is proved.

6. Conclusions

Tenant mix influences shopper behaviour and store performance. One of its essential purposes is to create a shopping environment that stimulates consumption and meets shoppers' preferences and needs to improve the overall sales of a shopping centre. The study on tenant mix layout has solved the problem of how to arrange the location,

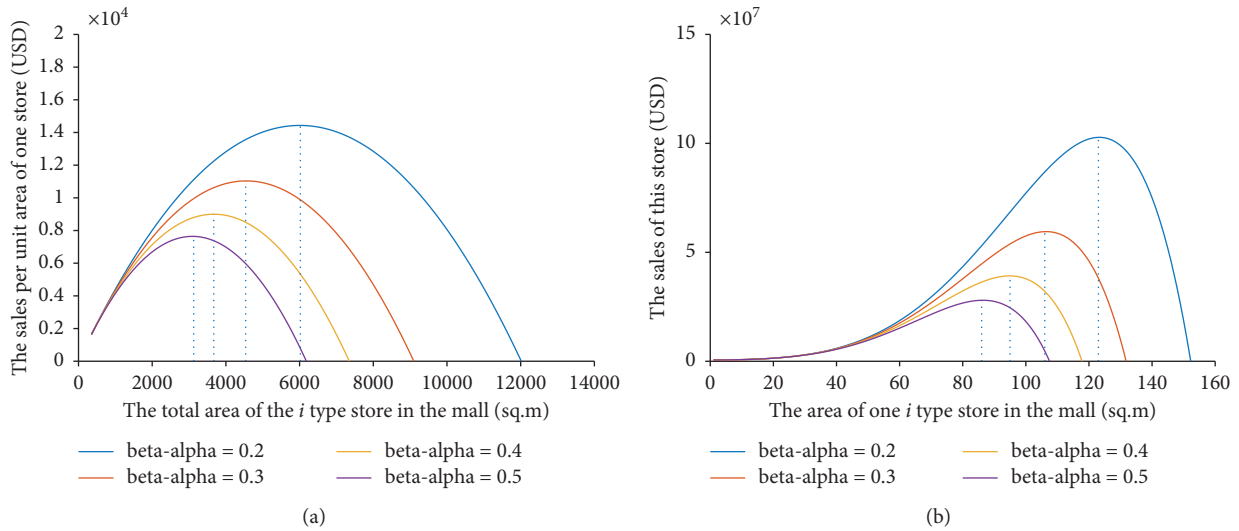


FIGURE 6: (a) Alternative preference coefficients' effect on sales of per unit area. (b) Alternative preference coefficients' effect on one store's total sales.

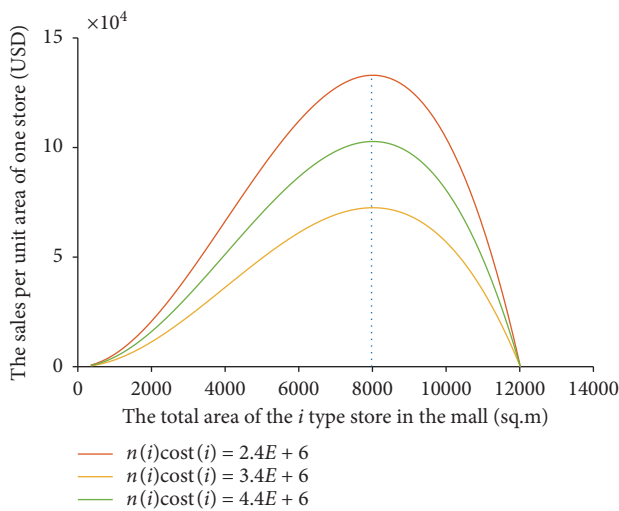


FIGURE 7: Alternative consumption ability.

retail type, and brand level of shops in shopping centre. The observation of the actual tenant mix of many local shopping centres shows that the owners used some previous research conclusions in their decisions about the placement of tenants, such as clustering certain types of retail shops on a certain floor and arranging many small shops near large supermarkets. However, the general rules they used are too complex and trivial to be applied to an entire shopping mall to determine the ideal tenant mix.

To solve this problem, the main contribution of our study is that it led to the development of a mathematical model that helps the owners of shopping centres optimize tenant mix layout and increase rental income. In the proposed model, we considered store externalities caused by consumer behaviour, which makes the operation results of the model closer to the actual needs. However, the proposed model is not intended to replace the decision-making

process of shopping centre management. It is a powerful tool that can be used to assist owners in quickly generating preliminary tenant mix layout plans, measuring the financial performance of the established tenant mix, and updating the layout plan according to the actual sales data in the operation process. We hope that the model proposed in this paper can be incorporated into software tools in the future to provide better decision-making information for shopping centre retail space planning.

This paper considers only the two main externalities that affect the layout of tenant mix, namely, the anchor store retail externalities and the similar agglomeration externalities. In future research, it is worth exploring to extend the model proposed in this paper. For example, researchers can discuss the agglomeration externalities of different types of retail in a mall, match shoppers' consumption habits with store impressions, or use more specific methods to simulate the exposure of the store in the vision.

Data Availability

The data of the real shopping centre used to support the findings of this study are included in the article, while other data and code are included within the supplementary information file(s).

Conflicts of Interest

The authors declare that they have no conflicts of interest.

Acknowledgments

This paper was vitally supported by Industry-University-Research Cooperation Project (no. 4418a4c49307416 78058b6cb12ca860c) of Ministry of Education of the People's Republic of China and Shenzhen THS Hi-Tech

Corporation. The authors greatly appreciate the support from these institutions.

Supplementary Materials

The data of the real shopping centre used to support the findings of this study are included in the article, while other data and code are included within the supplementary information file(s). (*Supplementary Materials*)

References

- [1] V. Couture, B. Faber, Y. Gu, and L. Liu, *E-Commerce Integration and Economic Development: Evidence from China*, CEPR, Washington, DC, USA, 2018.
- [2] POPAI, "Mass merchant shopper engagement study executive summary report," 2014, <http://www.shopassociation.org/a-re-popai-mass-merchant-shopper-study/>.
- [3] D. Zhang, P. Zhu, and Y. Ye, "The effects of E-commerce on the demand for commercial real estate," *Cities*, vol. 51, pp. 106–120, 2016.
- [4] V. Kumar, A. Anand, and H. Song, "Future of retailer profitability: an organizing framework," *Journal of Retailing*, vol. 93, no. 1, pp. 96–119, 2017.
- [5] W. C. Wheaton, "Percentage rent in retail leasing: the alignment of landlord-tenant interests," *Real Estate Economics*, vol. 28, no. 2, pp. 185–204, 2000.
- [6] J. K. Brueckner, "Inter-store externalities and space allocation in shopping centers," *The Journal of Real Estate Finance and Economics*, vol. 7, no. 1, pp. 5–16, 1993.
- [7] M. Gerbich, "Shopping center rentals: an empirical analysis of the retail tenant mix," *Journal of Real Estate Research*, vol. 15, no. 3, p. 283, 1998.
- [8] C. Teller, "Shopping streets versus shopping malls—determinants of agglomeration format attractiveness from the consumers' point of view," *The International Review of Retail, Distribution and Consumer Research*, vol. 18, no. 4, pp. 381–403, 2008.
- [9] J. Kunc, F. Križan, K. Bilková, P. Barlík, and J. Maryáš, "Are there differences in the attractiveness of shopping centres? Experiences from the Czech and Slovak Republics," *Moravian Geographical Reports*, vol. 24, no. 1, pp. 27–41, 2016.
- [10] J. D. Benjamin, *Megatrends in Retail Real Estate*, vol. 3, Springer, Dordrecht, Netherlands, 1996.
- [11] A. Borgers, M. Brouwer, T. Kunen, J. Jessurun, and I. Janssen, "A virtual reality tool to measure shoppers' tenant mix preferences," *Computers, Environment and Urban Systems*, vol. 34, no. 5, pp. 377–388, 2010.
- [12] V. Shankar, M. S. Yadav, M. Mantrala, E. Kelley, and R. Rizley, "Innovations in shopper marketing: current insights and future research issues," *Journal of Retailing*, vol. 87, no. 1, pp. S29–S42, 2011.
- [13] L. C. Mejia and M. J. Eppli, "Inter-center retail externalities," *The Journal of Real Estate Finance and Economics*, vol. 27, no. 3, pp. 321–333, 2003.
- [14] J. A. Dawson, *Shopping Center Development*, Longman Inc., New York, NY, USA, 1983.
- [15] S. Brown, "Tenant mix, tenant placement and shopper behaviour in a planned shopping centre," *The Service Industries Journal*, vol. 12, no. 3, pp. 384–403, 1992.
- [16] J. C. Bean, C. E. Noon, S. M. Ryan, and G. J. Salton, "Selecting tenants in a shopping mall," *Interfaces*, vol. 18, no. 2, pp. 1–9, 1988.
- [17] C. Yim Yiu and S. Y. S. Xu, "A tenant-mix model for shopping malls," *European Journal of Marketing*, vol. 46, no. 3/4, pp. 524–541, 2012.
- [18] N. Chong, *Empirical Study on Micro Determinants of Retail Rent and Tenant Mix in Shopping Center*, Economic Sciences Press, Cambridge, MA, USA, 2008.
- [19] M. A. Vitorino, "Empirical entry games with complementarities: an application to the shopping center industry," *Journal of Marketing Research*, vol. 49, no. 2, pp. 175–191, 2012.
- [20] H. Cho and J. D. Shilling, "Valuing retail shopping center lease contracts," *Real Estate Economics*, vol. 35, no. 4, pp. 623–649, 2007.
- [21] D. H. Gatzlaff, G. T. Sirmans, and B. A. Diskin, "The effect of anchor tenant loss on shopping center rents," *Journal of Real Estate Research*, vol. 9, no. 1, pp. 99–110, 1994.
- [22] M. J. Eppli and J. D. Shilling, "Changing economic perspectives on the theory of retail location," in *Megatrends in Retail Real Estate*, J. D. Benjamin, Ed., vol. 3, Berlin, Germany, Springer, 1996, Research Issues in Real Estate.
- [23] B. A. Peters, G.-A. Klutke, and A. R. Botsali, "Research issues in retail facility layout design progress," in *Progress in Material Handling Research*, R. D. Meller, Ed., pp. 399–414, Material Handling Institute, Charlotte, NC, USA, 2004.
- [24] H. Sorensen, "Long tail media in the store," *Journal of Advertising Research*, vol. 48, no. 3, pp. 329–338, 2008.
- [25] M. Kirkup and M. Rafiq, "Managing tenant mix in new shopping centres," *International Journal of Retail & Distribution Management*, vol. 22, no. 6, pp. 29–37, 1994.
- [26] H. Hamzah, "The tenant mix of shopping malls: a customers' perspective," in *Proceedings of the Pacific Rim Real Estate Society Conference*, Kuala Lumpur, Malaysia, January 2015.
- [27] C. Teller and T. Reutterer, "The evolving concept of retail attractiveness: what makes retail agglomerations attractive when customers shop at them?" *Journal of Retailing and Consumer Services*, vol. 15, no. 3, pp. 127–143, 2008.
- [28] C.-Y. Yiu, S. Y. Xu, and H. C. Ng, "Space allocation and tenant placement at high-rise shopping malls," *Journal of Retail & Leisure Property*, vol. 7, no. 4, pp. 315–324, 2008.
- [29] J. D. Benjamin, G. W. Boyle, and C. F. Sirmans, "Retail leasing: the determinants of shopping center rents," *Real Estate Economics*, vol. 18, no. 3, pp. 302–312, 1990.
- [30] M. J. Eppli and J. D. Shilling, "What's a shopping center worth?" in *Proceedings of the American Real Estate and Urban Economics Association Annual Meeting*, Key West, FL, USA, January 1993.
- [31] F. Rosiers, M. Thériault, and L. Ménétrier, "Spatial versus non-spatial determinants of shopping center rents: modeling location and neighborhood-related factors," *Journal of Real Estate Research*, vol. 27, no. 3, pp. 293–320, 2005.
- [32] C. C. Cater and K. D. Vandell, "Store location in shopping center: theory and estimates," *Journal of Real Estate Research*, vol. 27, no. 3, pp. 237–265, 2005.
- [33] J. P. Seagle, *An Allocation Model for Commercial Real Estate*, Graduate School of Business, Stanford University, Stanford, CA, USA, 1967.
- [34] Jensen and N. Arthur, *A Mixed Integer Programming Approach to Shopping Center Planning*, Arizona State University, Tempe, AZ, USA, 1980.
- [35] Urban Land Institute, *Shopping Center Development Handbook*, Urban Land Institute, Washington, DC, USA, 1985.
- [36] J. A. Dawson, *Shopping Centre Development*, Longman, London, UK, 1983.

- [37] J. J. Gabszewicz and J. F. Thisse, "On the nature of competition with differentiated products," *The Economic Journal*, vol. 96, no. 381, pp. 160–172, 1986.
- [38] B. P. Pashigian and E. D. Gould, "Internalizing externalities: the pricing of space in shopping malls," *The Journal of Law and Economics*, vol. 41, no. 1, pp. 115–142, 1998.
- [39] S. T. Yuo and C. Lizieri, "Tenant placement strategies within multi-level large-scale shopping centers," *Journal of Real Estate Research*, vol. 35, no. 1, pp. 25–51, 2013.
- [40] Y. Lu and H.-B. Seo, "Developing visibility analysis for a retail store: a pilot study in a bookstore," *Environment and Planning B: Planning and Design*, vol. 42, no. 1, pp. 95–109, 2015.
- [41] J. Hirsch, M. Segerer, K. Klein, and T. Wiegmann, "The analysis of customer density, tenant placement and coupling inside a shopping centre with GIS," *Journal of Property Research*, vol. 33, no. 1, pp. 37–63, 2016.
- [42] C. L. Mallows and R. D. Luce, "Individual choice behaviour," *Biometrika*, vol. 48, no. 1/2, p. 234, 1961.
- [43] T. J. Miceli and C. F. Sirmans, "Contracting with spatial externalities and agency problems the case of retail leases," *Regional Science and Urban Economics*, vol. 25, no. 3, pp. 355–372, 1995.
- [44] J. D. Benjamin and P. Chinloy, "The structure of a retail lease," *Journal of Real Estate Research*, vol. 26, no. 2, pp. 223–236, 2004.
- [45] J. V. Henderson, "The sizes and types of cities," *American Economic Review*, vol. 64, no. 4, pp. 640–656, 1974.
- [46] J. H. Holland, "Genetic algorithms and the optimal allocation of trials," *SIAM Journal on Computing*, vol. 2, no. 2, pp. 88–105, 1973.
- [47] U. Aickelin and K. A. Dowsland, "Enhanced direct and indirect genetic algorithm approaches for a mall layout and tenant selection problem," *Journal of Heuristics*, vol. 8, no. 5, pp. 503–514, 2002.

Research Article

Prediction of Concrete Compressive Strength and Slump by Machine Learning Methods

M. Timur Cihan 

Civil Engineering, Tekirdağ Namık Kemal University, Çorlu Faculty of Engineering, Tekirdağ 59860, Turkey

Correspondence should be addressed to M. Timur Cihan; mehmetcihan@nku.edu.tr

Received 26 July 2019; Revised 10 October 2019; Accepted 8 November 2019; Published 29 November 2019

Guest Editor: Murat Kankal

Copyright © 2019 M. Timur Cihan. This is an open access article distributed under the Creative Commons Attribution License, which permits unrestricted use, distribution, and reproduction in any medium, provided the original work is properly cited.

Machine learning methods have been successfully applied to many engineering disciplines. Prediction of the concrete compressive strength (f_c) and slump (S) is important in terms of the desirability of concrete and its sustainability. The goals of this study were (i) to determine the most successful normalization technique for the datasets, (ii) to select the prime regression method to predict the f_c and S outputs, (iii) to obtain the best subset with the ReliefF feature selection method, and (iv) to compare the regression results for the original and selected subsets. Experimental results demonstrate that the decimal scaling and min-max normalization techniques are the most successful methods for predicting the compressive strength and slump outputs, respectively. According to the evaluation metrics, such as the correlation coefficient, root mean squared error, and mean absolute error, the fuzzy logic method makes better predictions than any other regression method. Moreover, when the input variable was reduced from seven to four by the ReliefF feature selection method, the predicted accuracy was within the acceptable error rate.

1. Introduction

Concrete is a complex composite material. The predictability of concrete properties is extremely low. Therefore, it is challenging to model the concrete properties according to the effect variables. The biggest challenge of experimental designs is a high number of effect variables affecting the response variables. Multiple effect variables increase the number of trials. The higher amount of uncontrollable variables makes it difficult to obtain the real response function.

Generally, the one-factor-at-a-time method is used in experimental designs to determine the concrete properties. The major disadvantage of this approach is that it does not consider the interaction between the factors (interaction terms). The higher the number of the controlled and uncontrolled effect variables that influence the concrete properties, the lesser the predicted accuracy. Despite this, a few experimental designs have been suggested by considering the controllable effect variables and interaction terms between them [1].

Machine learning (ML) is a highly multidisciplinary field and consists of various methods for obtaining new

information [2]. ML is most often used for prediction. Predicting the categorical variable values is called classification, whereas predicting the numerical variable values is called regression. Regression is the process of analyzing the relationship between one or more independent variables and a dependent variable [3].

In recent years, the ML methods have become popular as they allow researchers to improve the prediction accuracy of concrete properties [4] and are used for various engineering applications [5, 6]. The ML methods have been used to increase the prediction accuracy of concrete properties [7–15], and the data derived from the literature sources were used. However, Chopra et al. [16, 17] applied the data generated under the controlled laboratory conditions.

Regression models tend to be used for the prediction of the compressive strength of high-strength concrete [18, 19]. These models also demonstrate how the concrete compressive strength depends on the mixing ratios [20]. Topçu and Sarıdemir [21] and Başıyigit et al. [22] developed models using the neural network (NN) and fuzzy logic (FL) methods to improve the prediction accuracy of the compressive strength of the mineral-additive (fly ash) concrete and

heavy-weight concrete. Both studies concluded that the compressive strength could be predicted by using the models that were developed with the NN and FL methods without any further experiments. NN is more successful than the data mining methods and does not enhance the prediction accuracy of the concrete compressive strength [15, 17, 23–26]. Khademi et al. [27] compared the multiple linear regression, neural network, and adaptive neuro-fuzzy inference system (ANFIS) methods to estimate the concrete compressive strength for 28 days and reported that the NN and ANFIS models provide reliable results.

Previous studies evaluated the amount of the concrete component materials and compared their results to the published data. In this study, the ML regression methods were compared to predict the compressive strength and slump values of the cube samples. The samples were prepared by accounting for seven simultaneously controllable effect variables in the laboratory. The study aimed to determine the most successful regression method by comparing the decision tree (DT), random forest (RF), support vector machine (SVM), partial least squares (PLS), artificial neural networks (ANN), bootstrap aggregation (bagging), and FL models for the prediction of the concrete compressive strength and slump values. The R , RMSE, and MAE metrics were used to compare the prediction accuracy of the developed models. Finally, feature reduction was accomplished by the feature selection method. Then, the model's success rates were compared to predict the compressive strength and slump value using fewer variables.

2. Materials and Methods

2.1. Experimental Datasets. Datasets used for this study comprised seven input variables (i.e., W/C , C , f_{cc} , FA , k_k , CA , and TA) and two output (response) variables (i.e., f_c and S) for two different maximum aggregate sizes $D_{max} = 22.4$ mm (D_{224}) and $D_{max} = 11.2$ mm (D_{112}). The input variables were selected considering the simultaneously controllable effect variables [28–30]. D-optimal design obtained by the augmentation of the fractional factorial design (2^{7-3}) was used as the experimental design. In the D-optimal design, 58 and 56 test results were employed for D_{112} and D_{224} , respectively. Each experimental result was calculated as an average of three sample results that are produced under laboratory conditions [28–30]. Properties of the constituents are given in Table 1 [28–30]. Abbreviations of the effect and response variables and the basic statistic of the datasets are presented in Table 2.

3. Methods

In this study, the concrete compressive strength and slump values were predicted using the ML regression models, namely, the regression tree, RF, support vector machines, artificial neural network, partial least square, bagging, and FL. Datasets were randomly split into 70% for the training set and 30% for the independent test set. The training data were used to train the ML model. The independent test data

were applied for the evaluation of the model's performance. The 10-fold cross-validation procedure helped in the estimation of the ML model skills.

The ML preprocessing steps were applied to the raw datasets before they could be utilized for the regression method training. The datasets were not normally distributed according to the Shapiro–Wilk normality test [31] results. Many normalization methods have been previously developed to normalize the dataset [32]. In this study, four different normalization methods (i.e., min-max, decimal, sigmoid, and z-score) were applied to derive the most successful normalization method for the raw dataset. Then, the K-nearest neighbor (KNN) regression method was applied to the normalized datasets. The prediction results were compared to determine the most suitable normalization method. Later, the raw datasets were normalized with the determined normalization technique.

The ML regression models were trained to predict the f_c and S values. The correlation coefficient (R), root mean squared error (RMSE), and mean absolute error (MAE) metrics were employed to compare the models' prediction performance. According to these statistical results, the most successful regression method was determined to predict the f_c and S values. Afterward, the feature selection method was used to obtain the subset with fewer features, and the prediction accuracy was examined. All regression methods and computations were performed using the R programming language [33]. The prediction process is illustrated in Figure 1 in the form of a flow diagram.

3.1. Normalization Methods. Normalization is the preprocessing step in ML. The normalization methods are used where the variation intervals of the variables in the dataset differ. When the mean and variance of the variables differ significantly, the variables with a large mean and variance increase the impact on the other variables. This may result in the loss of important variables due to the low variation intervals. It can also affect the success of the ML models [34, 35]. Therefore, regression models are normalized by the numerical data normalization methods to standardize the effect of each variable on the results. In this study, the dataset was normalized by the min-max, decimal, sigmoid, and z-score normalization techniques, and then their performances were compared.

3.2. Machine Learning Methods. The ML regression method estimates the output value using the input samples of the dataset. Such a procedure is also termed as the training set. The purpose of the regression method is to minimize the error between the predicted and actual outputs [36]. Herein, seven different regression methods (i.e., DT, RF, support vector machine, partial least squares, artificial neural networks, bootstrap aggregation (bagging), and FL) were used to predict the concrete compressive strength and slump values. Additionally, the K-nearest neighbor method was

TABLE 1: Properties of the constituents.

		Fineness modulus, k (-)	Particle density, ρ (kg/m ³)	Water absorption, μ (kg/kg)	Compressive strength, f_{cc} (MPa)	Blaine specific surface, σ (m ² /kg)
<i>Aggregate</i>						
Basalt	Crushed stone II	10.456	2872	0.0100	—	—
	Crushed stone I	9.129	2878	0.0130	—	—
	Crushed stone sand	5.198	2845	0.0220	—	—
Limestone	Crushed stone II	10.181	2600	0.0120	—	—
	Crushed stone I	7.107	2590	0.0170	—	—
	Crushed stone sand	4.791	2550	0.0260	—	—
	Sand	3.770	2600	0.0140	—	—
<i>Binding material</i>						
Cement	CEM V/A (S-P) 32.5 N	—	2990	0.0000	34.4	416.0
	SDC 32.5 R	—	3160	0.0000	44.75	339.0
	CEM I 42.5 R	—	3140	0.0000	55.1	379.0
<i>Admixture</i>						
Super plasticizer	—	—	1100	0.0000	—	—

TABLE 2: Basic statistic of used datasets.

Data	Attribute	Abbreviation	Unit	Min	Max	μ	σ	σ^2
D_{112}	Water/cement	W/C	%	54.95	59.88	57.38	2.07	4.29
	Cement content	C	Kg	330.00	345.00	337.72	6.31	39.76
	Compressive strength of cement	f_{cc}	MPa	34.40	55.10	44.75	9.09	82.69
	Fine aggregate	FA	%	65.00	68.00	66.47	1.27	1.62
	Fineness module	k_k	—	5.60	5.80	5.70	0.07	0.01
	Chemical admixture	CA	%	1.20	1.40	1.30	0.08	0.01
	Concrete compressive strength	f_c	MPa	19.86	44.19	33.30	6.91	47.81
	Slump value	S	cm	1.20	23.20	12.35	7.06	49.85
	Type of aggregate	TA	—	0: limestone, 1: basalt				
D_{224}	Water/cement	W/C	%	50.00	54.95	52.60	2.11	4.46
	Cement content	C	kg	330.00	345.00	337.63	6.49	42.14
	Compressive strength of cement	f_{cc}	MPa	34.40	55.10	45.12	9.25	85.56
	Fine aggregate	FA	%	48.00	54.00	51.00	2.36	5.56
	Fineness module	k_k	—	6.60	6.80	6.70	0.09	0.01
	Chemical admixture	CA	%	1.20	1.40	1.230	0.09	0.01
	Concrete compressive strength	f_c	MPa	26.59	53.87	40.38	8.12	65.92
	Slump value	S	cm	2.60	21.70	13.33	6.56	43.00
	Type of aggregate	TA	—	0: limestone, 1: basalt				

μ : mean, σ : standard deviation, and σ^2 : variance.

applied to determine the suitable normalization method for the dataset. These methods are briefly described below.

Decision tree (DT) [37] is a supervised ML algorithm. It can be used for both regression and classification. The aim of the DT algorithm is to divide the dataset into smaller, meaningful pieces, where each input has its own class label (tag) or value. Different measurements are used for the DT splitting, such as Gini and information gain. Regression tree is a type of a DT and a hierarchical model for the supervised learning. Classification and regression trees (CART), ID3, and C4.5 methods are the most important learning algorithms mentioned in the literature. In this study, the CART [38] model is used for the regression.

Random forest (RF) [39] is an ensemble method that combines many DTs. It can be used for both regression and classification. Each DT in the forest is created by the selection of different samples from the original dataset by the bootstrap technique. These samples are then trained using a set of attributes selected by the bagging mechanism. Subsequently, the decisions made by a large number of individual trees are subjected to voting. As such, the most voted class is presented as the class estimate of the community.

Support vector machine (SVM) has been developed by Vapnik [40]. It is applied both for regression and classification. The SVM method is based on finding an optimal hyperplane that maximizes the margin between the classes.

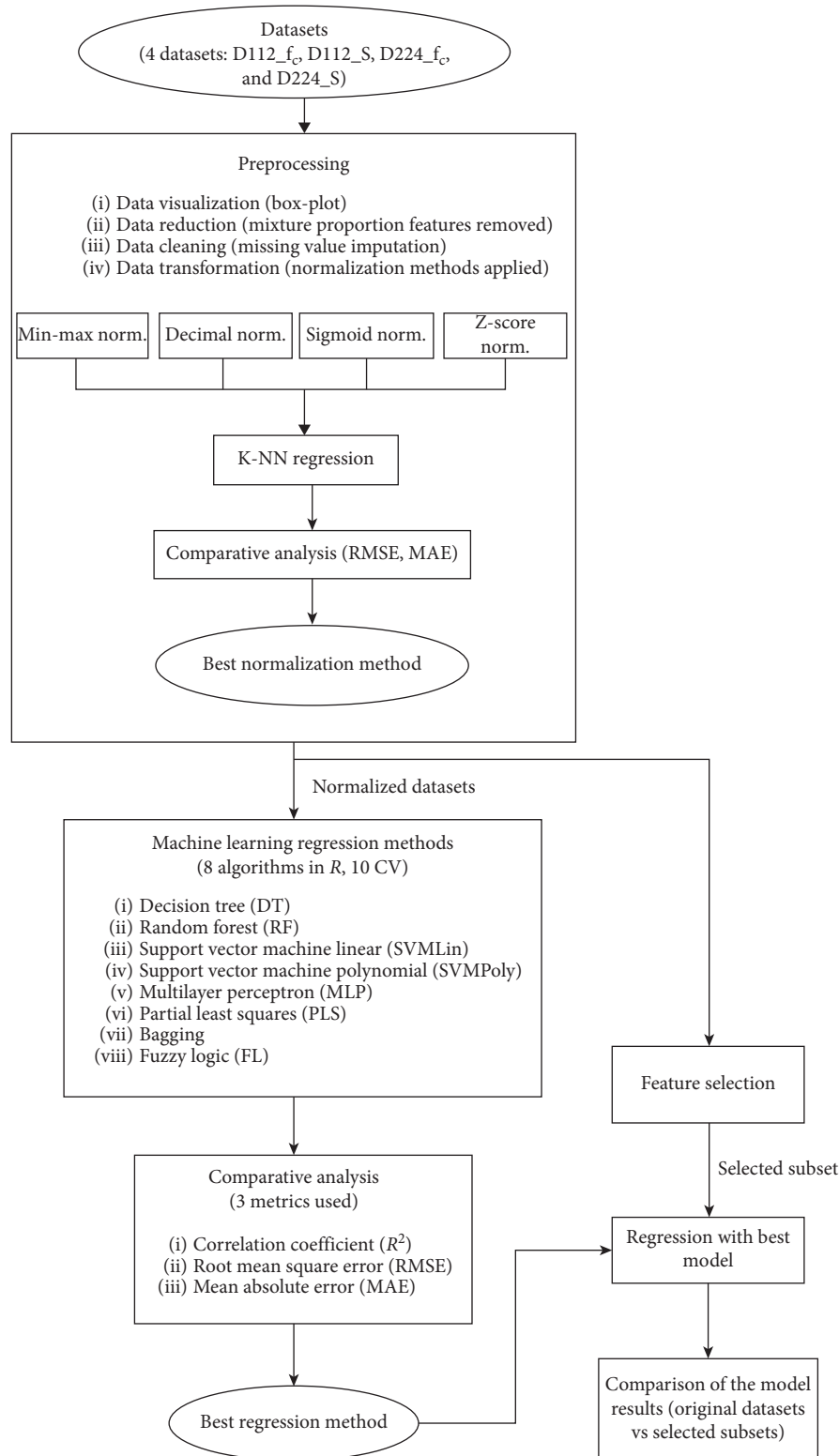


FIGURE 1: Flow diagram of the prediction process.

Partial least squares (PLS) [41] regression generalizes and combines the attributes from the principal component analysis and multiple regression. The most important characteristic of the PLS method is its ability to obtain a

simple model with a few components, even when the variables are highly correlated or linearly independent.

Artificial neural networks (ANN) [42] involve a system of many interconnected neurons. The neurons are connected

by the weighted links. The ANN architecture consists of the input, hidden, and output layers. The multilayer perceptron neural network (MLP) is a fully connected, feedforward type of network. It is mostly used in network architecture. The output of all the neurons in the input layer is scaled by the related connection weights. Then, the input of the neurons is feedforwarded to the output layer. Activation functions are used for the sum of the input neuron signals in the output layer.

Bootstrap aggregation (bagging) was introduced by Breiman [43] and can be utilized for both regression and classification. Bagging is performed by aggregating the resulting prediction rules using the bootstrap samples from the training sample.

Fuzzy logic (FL) is an ML method and was introduced by Zadeh [44]. FL is a mathematical-based method used to analyze the systems in a manner similar to how people do. As many problems could not be expressed by the exact mathematical definitions, a new method was developed. In the classical approach, an element is a member or non-member of the cluster, making the result equal to zero or one. However, in the FL, the situation is expressed by the membership degrees, which indicate the element's involvement in the cluster. The membership function is used to map each element into a continuous interval from zero to one. In other words, the membership degree of the element can vary as an infinite number from zero to one. A typical fuzzy system consists of a rule base, membership functions, and inference procedure. In this study, Wang and Mendel's technique (WM) was employed to generate the fuzzy rule.

K-nearest neighbor (KNN) [45] is an instance-based algorithm and can be applied for both regression and classification. The KNN method searches for the k-data points closest to the test object and uses the features of these neighbors to classify the new object. For this, a distance is measured between each instance in the training dataset and the test instance. Herein, $k = 3, 5,$ and 7 were chosen. The Euclidean distance was deployed as a distance measure. The "knn.reg" function was used in the "FNN" package [46]. The detailed information regarding the ML regression methods applied in this study is presented in Table 3.

3.3. Evaluation Metrics. To evaluate the predicted values of the regression methods, the actual and predicted values were compared. In this study, the R , RMSE, and MAE metrics were used to evaluate the prediction accuracy [47]. The model parameters were optimized for the highest R , lowest RMSE, and lowest MAE. All of them were calculated according to the following equations:

$$R = \frac{\sum_i^N (\text{actual}_i - \overline{\text{actual}})(\text{predicted}_i - \overline{\text{predicted}})}{\sqrt{\sum_{i=1}^N (\text{actual}_i - \overline{\text{actual}})^2 \sum_{i=1}^N (\text{predicted}_i - \overline{\text{predicted}})^2}}, \quad (1)$$

$$\text{RMSE} = \sqrt{\frac{1}{N} \sum_{i=1}^N (\text{predicted}_i - \text{actual}_i)^2}, \quad (2)$$

$$\text{MAE} = \sqrt{\frac{1}{N} \sum_{i=1}^N |\text{predicted}_i - \text{actual}_i|}. \quad (3)$$

Here, N is the number of data points.

3.4. Feature Selection. Feature selection (reduction in irrelevant variables) is the preprocessing step in ML that selects the best subset from the original dataset by evaluating the properties according to the used algorithm [48]. The ReliefF algorithm was developed by Kira and Rendell [49]. It weights the features according to the relationship between the effect variables. Although this method was successfully applied to two classes of the datasets, it was not proved functional for the datasets with multiple classes. To solve this problem, in 1994, Kononenko developed the ReliefF algorithm that works for the multiclass datasets [50]. The algorithm determines the weights of the continuous and discrete attributes based on a distance between the instances.

4. Results and Discussion

The cross-correlation between the datasets representing the parameters D_{112} and D_{224} is depicted in Figure 2. The correlation coefficient provides information on the effect level and direction of the linear relationship between two variables. The Pearson correlation is used when the dataset has a normal distribution, whereas the Spearman correlation is applied when the normal distribution cannot be reached.

According to the correlation results of the D_{112} dataset, the response variable f_c is highly correlated with the effect variable f_{cc} (0.88). Moreover, the highest correlation is observed between the response variable S and the effect variable TA (-0.57 for basalt and 0.57 for limestone). According to the correlation results of the D_{224} dataset, the response variable f_c is highly correlated with the effect variable f_{cc} (0.91). Besides, the highest correlation is obtained between the response variable S and the effect variable TA (-0.55 for basalt and 0.55 for limestone).

Before the data analysis begins, the data must be checked in accordance with the normal distribution. In this study, the normality test was performed using the Shapiro–Wilk normality test with the Gaussian error [51]. In the Shapiro–Wilk normality test, when the probability is >0.05 , the data are normally distributed, whereas when the probability is <0.05 , the data demonstrate a nonnormal data distribution. The small W value in the Shapiro–Wilk normality test indicates that the sample is not normally distributed. The Shapiro–Wilk normality test results for the D_{112} and D_{224} datasets are presented in Table 4.

According to the Shapiro–Wilk normality test results (Table 4), the D_{112} and D_{224} datasets are not normally distributed with the probability of the variables <0.05 and very high W values for both datasets. Furthermore, the box-plot graphs (Figure 3) prove that the dataset is not normally distributed. With the box-plot graph, it is possible to examine both ranges of the value and the numeric variable distribution.

TABLE 3: Hyperparameters of machine learning regression models.

Model	Method	Required package	Tuning parameter
Classification and regression trees (CART)	rpart	CRAN	method = "anova"
Random forest (RF)	rf	Caret	ntree = 100
Support vector machine (SVM)	svmLinear, svmPoly	Caret	gamma = 0.001, cost = 100
Partial least squares (PLS)	pls	Caret	tuneLength = 20
Artificial neural network (ANN)	mlp	RSNNS	size = 5, maxit = 100, learnFuncParams = 0.1
Bootstrap aggregation (bagging)	bagging	ipred	na.action = na.rpart method.type = "WM", num.labels = 7 max.iter = 30
Fuzzy logic (FL)	frbs.learn	frbs	step.size = 0.01, gradient descent = 00.1 type.implication.func = "ZADEH"

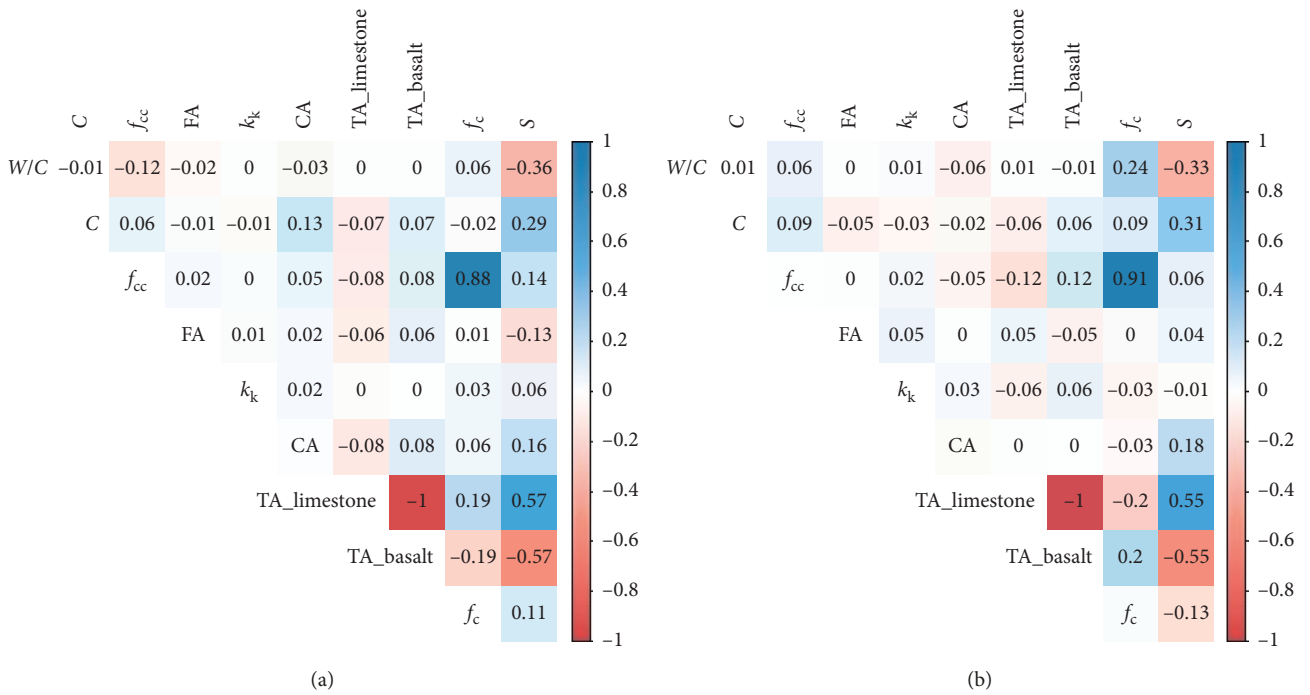
FIGURE 2: Correlation matrix of D_{112} (a) and D_{224} (b) datasets.

TABLE 4: Shapiro–Wilk normality test results for datasets.

Variables	D_{112} dataset		D_{224} dataset	
	P value	W	P value	W
W/C	$1.21 \cdot 10^{-07}$	0.792	$9.46E-08$	0.780
C	$1.36 \cdot 10^{-07}$	0.794	$8.11E-08$	0.777
f_{cc}	$2.75 \cdot 10^{-08}$	0.764	$2.32E-08$	0.752
FA	$7.11 \cdot 10^{-08}$	0.782	$3.73E-07$	0.805
k_k	$3.40 \cdot 10^{-07}$	0.810	$6.73E-08$	0.773
CA	$9.28 \cdot 10^{-08}$	0.787	$4.74E-08$	0.767

In this study, four different normalization techniques, namely, min-max, decimal, sigmoid, and z-score were applied to four different datasets. As a result, the most successful method was determined. After the normalization of the datasets by these methods, their success rate was compared using the KNN regression method. The KNN regression method was chosen being distance-based and

rapid in application. In this study, the k-values were selected at 3, 5, and 7. The results are provided in Table 5. According to the KNN regression results, the f_c (D_{112} , D_{224}) and S (D_{112} , D_{224}) values were normalized by the decimal scaling and min-max normalization methods, respectively.

The results of the RF, SVM linear, SVM linear (SVMLin), SVM polynomial (SVMPoly), PLS, Bagging, DT, MLP, and FL models for the prediction of the compressive strength and the slump value are presented in Table 6.

The reason for the selection of these regression methods was the successful employment of those prediction algorithms in published literature. As mentioned earlier, the datasets were randomly divided into the training (70%) and individual test sets (30%). Herein, the training and individual test sets consisted of 40 and 18 instances for the D_{112} dataset, respectively, and 39 and 17 instances for the D_{224} dataset, respectively. Prediction results for the models were obtained from the 10-fold cross-validation process. The

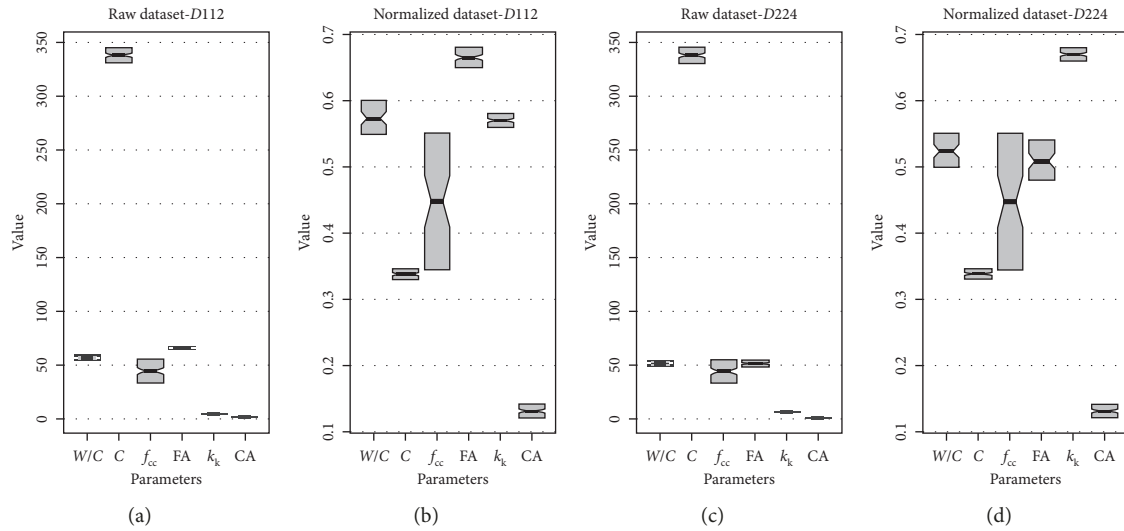


FIGURE 3: Box-plot graphs for the raw and decimal normalized dataset.

TABLE 5: The results of the normalization methods.

Regression method	Normalization method	D_{112-f_c} dataset		D_{112-S} dataset		D_{224-f_c} dataset		D_{224-S} dataset	
		RMSE	MAE	RMSE	MAE	RMSE	MAE	RMSE	MAE
3NN	Min-max	5.32	3.96	19.93	18.24	5.51	3.42	27.87	26.34
	Decimal	3.13	2.41	25.46	24.79	3.39	2.70	29.09	27.80
	Sigmoid	5.21	3.35	26.41	25.21	5.65	3.61	28.13	26.64
	Z-norm	5.22	3.62	25.84	24.68	5.60	3.50	28.22	26.69
5NN	Min-max	6.53	5.09	19.70	17.99	5.33	4.64	30.17	28.92
	Decimal	2.78	2.32	23.44	22.61	3.46	3.07	34.17	33.12
	Sigmoid	6.03	5.24	22.82	21.26	5.50	4.66	30.73	29.56
	Z-norm	6.01	5.22	22.81	21.16	5.66	4.87	30.34	29.22
7NN	Min-max	5.51	4.36	20.25	19.09	5.51	4.57	27.61	26.53
	Decimal	3.60	2.89	21.97	21.26	3.78	3.12	29.40	28.18
	Sigmoid	5.69	4.77	21.65	20.70	5.50	4.25	26.63	25.66
	Z-norm	5.63	4.72	21.63	20.67	5.46	4.20	26.63	25.64

TABLE 6: Metrics results of the different regression methods.

Dataset	Metric	RF	SVMLin	SVMPoly	PLS	Bagging	DT	ANN	FL
D_{112-f_c}	R	0.916	0.912	0.920	0.907	0.915	0.857	0.932	0.945
	RMSE	2.362	2.518	3.046	2.604	2.419	2.878	2.855	1.090
	MAE	1.957	1.837	2.423	2.001	2.117	2.511	2.625	0.933
D_{112-S}	R	0.833	0.758	0.761	0.705	0.705	0.693	0.897	0.947
	RMSE	4.748	4.983	5.094	5.380	6.100	5.942	2.686	2.477
	MAE	4.302	3.702	3.933	4.476	5.776	5.465	3.409	1.954
D_{224-f_c}	R	0.853	0.816	0.816	0.779	0.736	0.408	0.899	0.928
	RMSE	2.054	3.285	2.943	3.243	2.689	3.008	2.107	1.442
	MAE	1.641	2.678	2.316	2.724	2.192	2.364	2.926	0.995
D_{224-S}	R	0.772	0.654	0.765	0.645	0.730	0.518	0.896	0.977
	RMSE	3.778	5.114	4.005	5.015	4.094	5.424	2.534	1.413
	MAE	2.428	3.994	2.708	4.050	3.254	4.442	3.842	1.152

performance of these regression methods was evaluated according to the R, RMSE, and MAE statistical criteria. R was employed to evaluate the good fit between the predicted and actual values. A combination of the R, RMSE, and MAE

results was sufficient to reveal any significant differences between the predicted and actual values.

According to the statistical results of the regression method (Table 6), the FL regression model delivered the

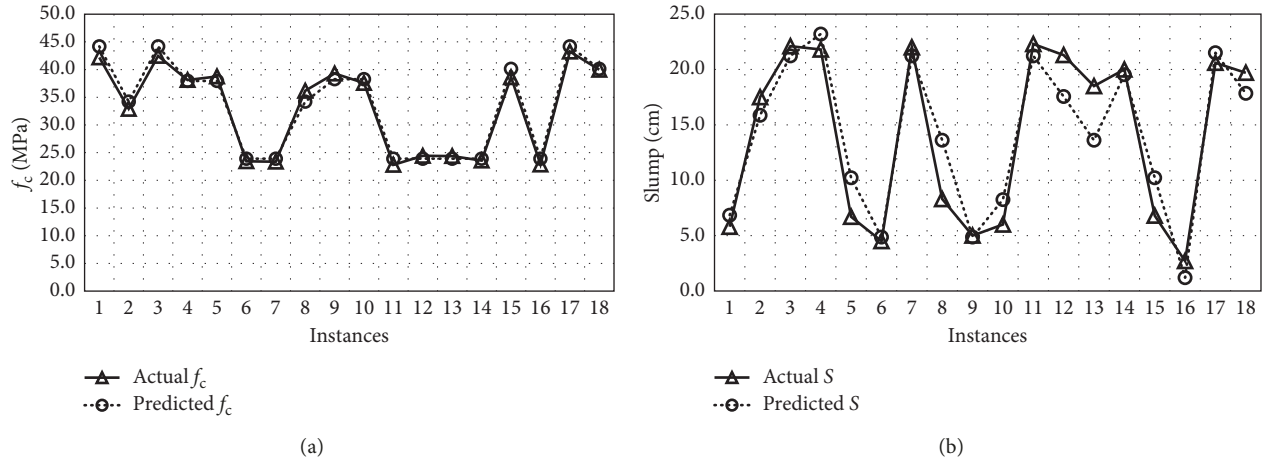


FIGURE 4: Comparison between actual and predicted values of f_c and S values using the FL model for the D_{112} dataset.

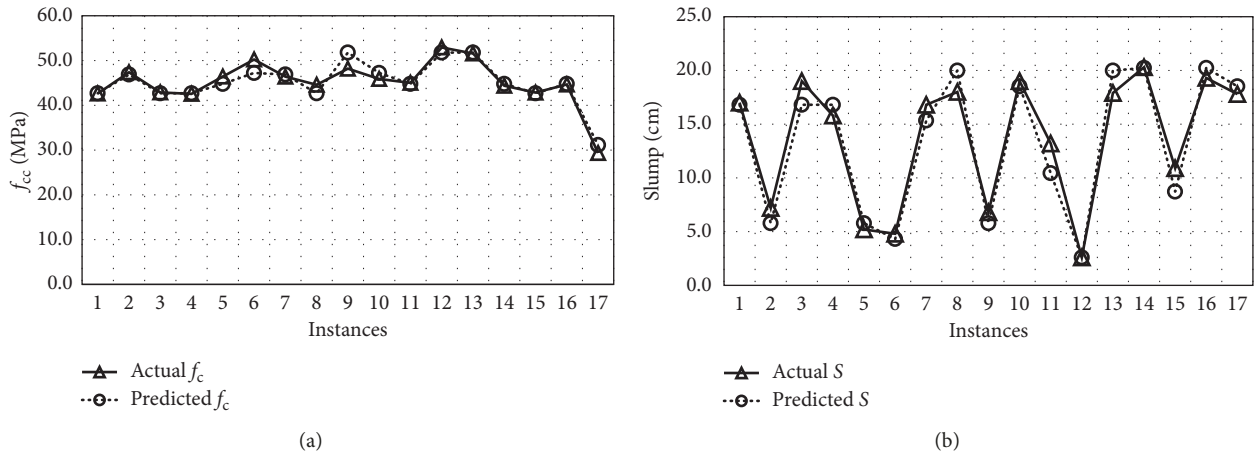


FIGURE 5: Comparison between actual and predicted values of f_c and S values using the FL model for the D_{224} dataset.

highest prediction accuracy for the prediction of the response variables f_c and S according to the maximum aggregate sizes (D_{112} and D_{224}). The FL model achieved the best prediction accuracy results among all the performance criteria according to seven benchmark models.

The prediction results obtained from the FL regression model and actual results are depicted in Figures 4 and 5. The prediction values for the compressive strength and slump are similar to the actual values.

To reduce the number of the effect variables, the ReliefF feature selection method was used to determine the high-level effect variables. As a result, the f_{cc} , k_k , C , and W/C effect variables were selected as they had a high-level effect on f_c and S for the maximum aggregate size. The results of R , RMSE, and MAE obtained after applying the FL model to all the effect variables and reduced effect variables are presented in Table 7. This table also indicates that there is no significant change in the R , RMSE, and MAE results when the number of features was reduced from seven to four. Therefore, the FL model with fewer features can still make successful predictions.

The effect levels of the simultaneously controllable effect variables on the response variables exhibit some variations [28–30]. Considering the selected variation intervals, the f_{cc} , k_k , C , and W/C variables had a significant effect level on the response variables for the maximum aggregate sizes. Cement strength (f_{cc}), cement dosage (C), and water/cement (W/C) ratio tend to have a significant effect on the compressive strength. Furthermore, the fineness modulus (k_k), which expresses the fineness and distribution of the mixture aggregate, is one of the essential variables that affects the concrete compactness. Moreover, the concrete compactness directly affects the compressive strength.

The workability of concrete is directly influenced by the cement properties (e.g., cement fineness), aggregate properties (e.g., roughness of the aggregate surface), and amount of mixing water. Particularly, it is not expected that the chemical additive variable does not have a significant effect on workability. The variation intervals of the chemical additive are negligible and do not show a significant effect on the workability of concrete. However, the variation intervals of the other effect variables can be considerable. Therefore,

TABLE 7: The results of the FL regression for the original dataset and selected subset.

Dataset	Metric	FL	FL after FS
D_{112-f_c}	R	0.945	0.962
	RMSE	1.090	1.245
	MAE	0.933	0.961
D_{112-S}	R	0.947	0.946
	RMSE	2.477	2.546
	MAE	1.954	1.514
D_{224-f_c}	R	0.928	0.954
	RMSE	1.442	1.461
	MAE	0.995	1.062
D_{224-S}	R	0.977	0.927
	RMSE	1.413	1.743
	MAE	1.152	1.183

the predicted accuracy does not decrease due to the FA, CA, and TA variables, which do not have a significant effect on response variables in the selected variation intervals.

5. Conclusions

The goals of this study were (i) to determine the most successful normalization technique for the datasets, (ii) to obtain the prime regression method to predict the f_c and S values, (iii) to choose the best subset using the ReliefF feature selection method, and (iv) to compare the regression results for the original and selected subsets.

To determine the effect levels of the effect variables on the response variables (i.e., f_c and S) with precision, data were analyzed for normalization. If the data were not normally distributed, it was necessary to determine the most appropriate normalization method. In this study, the Shapiro–Wilk normality test results demonstrated that the datasets were not normally distributed. The most successful techniques for the determination of the f_c (D_{112} , D_{224}) and S (D_{112} , D_{224}) values were the decimal scaling and min-max normalization methods, respectively. Therefore, as the variation ranges of the effect variables influencing the concrete properties varied substantially, it was necessary to preprocess the raw data for the estimation of the concrete properties.

Herein, seven different ML methods, such as DT, RF, SVM, PLS, ANN, bagging, and FL were experimented with to predict the f_c and S values. According to the R , RMSE, and MAE statistical results, FL is the best regression method for the maximum aggregate size. Generally, the similarity between the actual and predicted values is high for the compressive strength (Figures 4 and 5). A minimal difference between the actual and predicted slump values indicates that the slump values are more sensitive to the experimental error, simultaneously uncontrollable effect variables, and variation intervals of the effect variables. The flexibility of the computational structure of the FL approximated the results instead of providing the exact results. In particular, the uncertainties in the problem-solving and decision-making processes can be clarified by the application of the FL. Thus, complicated problems can be solved, making the FL more functional than any other ML method.

In experimental designs, where the number of the simultaneously uncontrollable effect variables is high, it is crucial to reduce the number of the experiments to save costs and time. Therefore, the predicted values close to the actual values need to be obtained with the minimum number of the experiments. In this study, seven simultaneously controllable effect variables were reduced to four effect variables (i.e., f_{cc} , k_k , C , and W/C) using the ReliefF feature selection method. The metric results obtained by the FL regression were similar for four and seven effect variables (Table 7). Therefore, the experimental designs with fewer effect variables are sufficient for estimating the concrete properties.

Data Availability

Previously reported “compressive strength and slump of concrete” data were used to support this study and are available in the author’s PhD thesis, report, and article. These prior studies (and datasets) are cited at relevant places within the text as references [28–30].

Conflicts of Interest

The author declares that there are no conflicts of interest.

References

- [1] D. C. Montgomery, *Design and Analysis of Experiments*, John Wiley & Sons, Hoboken, NJ, USA, 2017.
- [2] M. Awad and R. Khanna, *Efficient Learning Machines: Theories, Concepts, and Applications for Engineers and System Designers*, Apress, New York, NY, USA, 2015.
- [3] M. Hofmann and R. Klinkenberg, *RapidMiner: Data Mining Use Cases and Business Analytics Applications*, CRC Press, Boca Raton, FL, USA, 2013.
- [4] B. Boukhateem, S. Kenai, A. Tagnit-Hamou, and M. Ghrici, “Application of new information technology on concrete: an overview/naujų informacinių technologijų naudojimas ruošiant betoną. Apžvalga,” *Journal of Civil Engineering and Management*, vol. 17, no. 2, pp. 248–258, 2011.
- [5] P. Cihan, E. Gökçe, and O. Kalıpsız, “A review of machine learning applications in veterinary field,” *Kafkas Univ Vet Fak Derg*, vol. 23, no. 4, pp. 673–680, 2017.
- [6] E. E. Ozbas, D. Aksu, A. Ongen, M. A. Aydin, and H. K. Ozcan, “Hydrogen production via biomass gasification, and modeling by supervised machine learning algorithms,” *International Journal of Hydrogen Energy*, vol. 44, no. 32, pp. 17260–17268, 2019.
- [7] H.-G. Ni and J.-Z. Wang, “Prediction of compressive strength of concrete by neural networks,” *Cement and Concrete Research*, vol. 30, no. 8, pp. 1245–1250, 2000.
- [8] S. Akkurt, G. Tayfur, and S. Can, “Fuzzy logic model for the prediction of cement compressive strength,” *Cement and Concrete Research*, vol. 34, no. 8, pp. 1429–1433, 2004.
- [9] A. Öztaş, M. Pala, E. A. Özbay, E. Kanca, N. Caglar, and M. A. Bhatti, “Predicting the compressive strength and slump of high strength concrete using neural network,” *Construction and Building Materials*, vol. 20, no. 9, pp. 769–775, 2006.
- [10] M. Pala, E. Özbay, A. Öztaş, and M. I. Yuca, “Appraisal of long-term effects of fly ash and silica fume on compressive strength of concrete by neural networks,” *Construction and Building Materials*, vol. 21, no. 2, pp. 384–394, 2007.

- [11] M. Ozturan, B. Kutlu, and T. Ozturan, "Comparison of concrete strength prediction techniques with artificial neural network approach," *Building Research Journal*, vol. 56, no. 1, pp. 23–36, 2008.
- [12] M. M. Alshihri, A. M. Azmy, and M. S. El-Bisy, "Neural networks for predicting compressive strength of structural light weight concrete," *Construction and Building Materials*, vol. 23, no. 6, pp. 2214–2219, 2009.
- [13] M. Saridemir, "Prediction of compressive strength of concretes containing metakaolin and silica fume by artificial neural networks," *Advances in Engineering Software*, vol. 40, no. 5, pp. 350–355, 2009.
- [14] A. M. Diab, H. E. Elyamany, A. E. M. Abd Elmoaty, and A. H. Shalan, "Prediction of concrete compressive strength due to long term sulfate attack using neural network," *Alexandria Engineering Journal*, vol. 53, no. 3, pp. 627–642, 2014.
- [15] P. Chopra, R. K. Sharma, and M. Kumar, "Artificial neural networks for the prediction of compressive strength of concrete," *International Journal of Applied Science & Engineering*, vol. 13, pp. 187–204, 2015.
- [16] P. Chopra, R. K. Sharma, and M. Kumar, "Prediction of compressive strength of concrete using artificial neural network and genetic programming," *Advances in Materials Science and Engineering*, vol. 2016, Article ID 7648467, 10 pages, 2016.
- [17] P. Chopra, R. K. Sharma, M. Kumar, and T. Chopra, "Comparison of machine learning techniques for the prediction of compressive strength of concrete," *Advances in Civil Engineering*, vol. 2018, Article ID 5481705, 9 pages, 2018.
- [18] S. Wu, B. Li, J. Yang, and S. Shukla, "Predictive modeling of high-performance concrete with regression analysis," in *Proceedings of the 2010 IEEE International Conference on Industrial Engineering and Engineering Management*, pp. 1009–1013, Macao, China, December 2010.
- [19] M. F. M. Zain and S. M. Abd, "Multiple regression model for compressive strength prediction of high performance concrete," *Journal of Applied Sciences*, vol. 9, no. 1, pp. 155–160, 2009.
- [20] J. Namyong, Y. Sangchun, and C. Hongbum, "Prediction of compressive strength of in-situ concrete based on mixture proportions," *Journal of Asian Architecture and Building Engineering*, vol. 3, no. 1, pp. 9–16, 2004.
- [21] İ. B. Topçu and M. Saridemir, "Prediction of compressive strength of concrete containing fly ash using artificial neural networks and fuzzy logic," *Computational Materials Science*, vol. 41, no. 3, pp. 305–311, 2008.
- [22] C. Başıyigit, I. Akkurt, S. Kilincarslan, and A. Beycioglu, "Prediction of compressive strength of heavyweight concrete by ANN and FL models," *Neural Computing and Applications*, vol. 19, no. 4, pp. 507–513, 2010.
- [23] M. Wankhade and A. Kambekar, "Prediction of compressive strength of concrete using artificial neural network," *International Journal of Scientific Research and Reviews*, vol. 2, pp. 11–26, 2013.
- [24] P. Chopra, R. K. Sharma, and M. Kumar, "Predicting compressive strength of concrete for varying workability using regression models," *International Journal of Engineering & Applied Sciences*, vol. 6, no. 4, p. 10, 2014.
- [25] M. Nikoo, F. T. Moghadam, and L. Sadowski, "Prediction of concrete compressive strength by evolutionary artificial neural networks," *Advances in Materials Science and Engineering*, vol. 2015, Article ID 849126, 8 pages, 2015.
- [26] A. Khashman and P. Akpınar, "Non-destructive prediction of concrete compressive strength using neural networks," *Procedia Computer Science*, vol. 108, pp. 2358–2362, 2017.
- [27] F. Khademi, M. Akbari, S. M. Jamal, and M. Nikoo, "Multiple linear regression, artificial neural network, and fuzzy logic prediction of 28 days compressive strength of concrete," *Frontiers of Structural and Civil Engineering*, vol. 11, no. 1, pp. 90–99, 2017.
- [28] A. Güner, *Normal Betonun Alışılacağı Uygulama Özelliklerinin Kontrol Edilebilir Değişkenlere Göre Tepki Yüzeylerinin Belirlenmesi*, TUBITAK-Project No: 109M748, Türkiye Bilimsel ve Teknolojik Araştırma Kurumu, Ankara, Turkey, 2011.
- [29] M. T. Cihan, *Tepki yüzeyi yöntem bilgisinin beton uygulamasında kullanılabilirliğinin geliştirilmesi*, Ph.D. thesis, Fen Bilimleri Enstitüsü, Yıldız Teknik Üniversitesi, İstanbul, Turkey, 2012.
- [30] M. T. Cihan, A. Güner, and N. Yüzer, "Response surfaces for compressive strength of concrete," *Construction and Building Materials*, vol. 40, pp. 763–774, 2013.
- [31] P. Royston, "Approximating the Shapiro-Wilk W-test for non-normality," *Statistics and Computing*, vol. 2, no. 3, pp. 117–119, 1992.
- [32] A. F. Dutka and H. H. Hansen, *Fundamentals of Data Normalization*, Addison-Wesley Longman Publishing Co., Inc., Boston, MA, USA, 1991.
- [33] R. Ihaka and R. Gentleman, "R: a language for data analysis and graphics," *Journal of Computational and Graphical Statistics*, vol. 5, no. 3, pp. 299–314, 1996.
- [34] L. A. Shalabi, Z. Shaaban, and B. Kasasbeh, "Data mining: a preprocessing engine," *Journal of Computer Science*, vol. 2, no. 9, pp. 735–739, 2006.
- [35] P. Cihan, O. Kalipsiz, and E. Gökçe, "Hayvan hastalığı teşhisinde normalizasyon tekniklerinin yapay sinir ağı ve özellik seçim performansına etkisi," *Electronic Turkish Studies*, vol. 12, 2017.
- [36] E. Alpaydin, *Introduction to Machine Learning*, MIT Press, Cambridge, MA, USA, 2009.
- [37] J. R. Quinlan, "Induction of decision trees," *Machine Learning*, vol. 1, no. 1, pp. 81–106, 1986.
- [38] L. Breiman, J. Friedman, R. Olshen, and C. Stone, *Classification and Regression Trees*, vol. 37, Wadsworth International Group, Belmont, CA, USA, 1984.
- [39] A. Liaw and M. Wiener, "Classification and regression by randomForest," *R News*, vol. 2, pp. 18–22, 2002.
- [40] V. Vapnik, *The Nature of Statistical Learning Theory*, Springer Science & Business Media, Berlin, Germany, 2013.
- [41] S. Wold, A. Ruhe, H. Wold, and W. J. Dunn III, "The collinearity problem in linear regression. The partial least squares (PLS) approach to generalized inverses," *SIAM Journal on Scientific and Statistical Computing*, vol. 5, no. 3, pp. 735–743, 1984.
- [42] J. M. Zurada, *Introduction to Artificial Neural Systems*, West publishing Company, St. Paul, MN, USA, 1992.
- [43] L. Breiman, "Bagging predictors," *Machine Learning*, vol. 24, no. 2, pp. 123–140, 1996.
- [44] L. A. Zadeh, "Fuzzy sets," *Information and Control*, vol. 8, no. 3, pp. 338–353, 1965.
- [45] O. Kramer, *Dimensionality Reduction with Unsupervised Nearest Neighbors*, Springer, Berlin, Germany, 2013.
- [46] A. Beygelzimer, S. Kakadet, J. Langford, S. Arya, D. Mount, and S. Li, *Package "FNN"*, 2015.
- [47] T. Chai and R. R. Draxler, "Root mean square error (RMSE) or mean absolute error (MAE)?—arguments against avoiding

- RMSE in the literature,” *Geoscientific Model Development*, vol. 7, no. 3, pp. 1247–1250, 2014.
- [48] E. Alpaydin, *Machine Learning: The New AI*, MIT press, Cambridge, MA, USA, 2016.
- [49] K. Kira and L. A. Rendell, “A practical approach to feature selection,” in *Machine Learning Proceedings 1992*, pp. 249–256, Elsevier, Amsterdam, Netherlands, 1992.
- [50] I. Kononenko, “Estimating attributes: analysis and extensions of Relief,” in *European Conference on Machine Learning*, pp. 171–182, Springer, Berlin, Germany, 1994.
- [51] J. P. Royston, “An extension of Shapiro and Wilk’s W test for normality to large samples,” *Applied Statistics*, vol. 31, no. 2, pp. 115–124, 1982.

Research Article

Fuzzy Multicriteria Decision-Making Model for Time-Cost-Risk Trade-Off Optimization in Construction Projects

M. Ammar Alzarrad ¹, Gary P. Moynihan,² Muhammad T. Hatamleh,² and Siyuan Song³

¹Department of Civil Engineering and Construction, Bradley University, Peoria, IL 61625, USA

²Department of Civil, Construction and Environmental Engineering, The University of Alabama, Tuscaloosa, AL 35487, USA

³School of Construction and Design, The University of Southern Mississippi, Hattiesburg, MS 39406, USA

Correspondence should be addressed to M. Ammar Alzarrad; malzarrad@fsmail.bradley.edu

Received 13 September 2019; Accepted 6 November 2019; Published 27 November 2019

Academic Editor: Tayfun Dede

Copyright © 2019 M. Ammar Alzarrad et al. This is an open access article distributed under the Creative Commons Attribution License, which permits unrestricted use, distribution, and reproduction in any medium, provided the original work is properly cited.

As is often the case in project scheduling, when the project duration is shortened to decrease total cost, the total float is lost resulting in added critical or nearly critical activities. This, in turn, results in decreasing the probability of completing the project on time and increases the risk of schedule delays. To solve this problem, this research developed a fuzzy multicriteria decision-making (FMCDM) model. The objective of this model is to help project managers improve their decisions regarding time-cost-risk trade-offs (TCRTO) in construction projects. In this model, an optimization algorithm based on fuzzy logic and analytic hierarchy process (AHP) has been used to analyze the time-cost-risk trade-off alternatives and select the best one based on selected criteria. The algorithm was implemented in the MATLAB software and applied to two case studies to verify and validate the presented model. The presented FMCDM model could help produce a more reliable schedule and mitigate the risk of projects running overbudget or behind schedule. Further, this model is a powerful decision-making instrument to help managers reduce uncertainties and improve the accuracy of time-cost-risk trade-offs. The presented FMCDM model employed fuzzy linguistic terms, which provide decision-makers with the opportunity to give their judgments as intervals comparing to fixed value judgments. In conclusion, the presented FMCDM model has high robustness, and it is an attractive alternative to the traditional methods to solve the time-cost-risk trade-off problem in construction.

1. Introduction

Project management has a vital role in modern management. It is noted as the application of knowledge, skills, tools, and techniques in project activities to reach the project requirements [1]. In project management, the fundamental project concepts of time, cost, and risk are conflicting terms which should be appropriately assigned to project activities to achieve the desired objectives of project stakeholders [2]. There are many occasions where the owner informs the contractor that the schedule must be shortened. This action could lead to increases in total cost as well as risk. To accelerate the execution of a project, project managers need to reduce the scheduled execution time by hiring additional labor or using productive equipment. But, this idea will

increase cost and risk, hence shortening the completion time of jobs on critical path network is needed.

Time-cost trade-off (TCT) is a common approach applied by project managers to reach the required completion time of the projects with the least extra cost [3]. In fact, TCT deals with modifying implementation time of project activities while doing a trade-off between the completion time and the project cost [4]. Several approaches were introduced in addressing risk in time-cost trade-off problems (TCTPs). He et al. addressed the preemptive time-cost-risk trade-off project scheduling through a multiobjective multimode model [5]. Hosseini-Nasab et al. applied variable neighborhood search and tabu search to handle the TCT problem [6]. Mohagheghi et al. introduced a multicriteria decision-making model

for Time-cost-quality trade-off problem in construction projects [7]. The NSGA-II procedure was used to identify Pareto optimal solutions [7]. Eirgash et al. determined the optimal set of time-cost alternatives using a multiobjective teaching-learning-based optimization (TLBO) algorithm to successfully optimize small to medium projects [8]. Tran et al. presented fuzzy earned value management into a TCTP and used a statistical-based approach [9]. Tseng et al. proposed a two-phase differential evolution model to address construction project TCTP under resource-constrained limitations [10]. Zhang and Zhong, presented a multiobjective approach for solving discrete time-cost-risk trade-off problems with mode-identity and resource-constrained situations [11]. In this paper, a FMCDM model has been developed based on the fuzzy analytic hierarchy process (FAHP) algorithm. The objective of the presented model is to analyze the time-cost-risk trade-off alternatives and select the best one based on selected criteria. The presented algorithm was implemented in the MATLAB software and compared with other methods to qualify the magnitude of improvement that the proposed FMCDM model presents.

2. Fuzzy Multicriteria Decision-Making (FMCDM)

Some decision situations involve a multitude of objectives or decision criteria that may be inaccurate and conflict with each other. Decision analysis considers the paradigm in which decision-makers contemplate a choice of action in a risky environment. Decision analysis is designed to help decision-makers choose between a set of predetermined alternatives [12]. The variety in the quality of the available data about a decision-related problem calls for models and tools that can help in data processing. The analytic hierarchy process (AHP) is a decision-making procedure to help decision-makers establish priorities to take the best possible decision. Analytic hierarchy process (AHP) is a system of measurement using pairwise comparisons and depends mainly on the experts' opinions [13]. Al-Harbi [14] led a study in which the AHP is applied as a decision-making technique to assess the problem of contractor qualification. The traditional AHP technique is not considered to be able to deal with the risks involved in the criteria [15]. There is an extensive literature which addresses the situation in the real world where the AHP comparison criteria are imprecise judgments. To reduce the bias associated with traditional AHP, this paper utilizes fuzzy analytic hierarchy process (FAHP) as a tool to provide decision support for construction project managers. The presented FAHP utilizes triangular fuzzy numbers (TFN) to capture expert opinions. A triangular fuzzy number (μ) can be defined as a triplet (a_1, a_M, a_2) . This parameter (a_1, a_M, a_2) signifies the smallest possible value, the most promising value, and the largest possible value, respectively [12]. In FAHP, the pairwise evaluations of both criteria and the alternatives are completed using linguistic terms, which are represented by TFN. The α -cut

method is a common technique to do arithmetic operations on a triangular membership function [16].

The α -cut signifies the degree of risk that the project managers are ready to take (i.e., no risk to full risk). Because the value of α could significantly affect the solution, it should be wisely chosen by project managers. Figure 1 shows a TFN with α -cut. The higher the value of α , the lower the risk ($\alpha = 1$ means no risk) [17].

In this paper, triangular fuzzy number with α -cut and analytic hierarchy process (AHP) is used to help decision-makers establish priorities to take the best possible decision regarding the TCRTO problem. The presented FMCDM model consists of four stages, as follows.

2.1. FMCDM Model Stage 1. In stage one, the cost, time, and risk alternatives are calculated using the following objective functions:

$$\min f_1 = \sum_{i=1}^n t_{ij}(x_{ij}), \quad (1)$$

$$\min f_2 = \sum_{i=1}^n C_{ij}(x_{ij}) + \sum_{i=1}^n C_f, \quad (2)$$

$$\min f_3 = \sum_{i=1}^n R_{ij}, \quad (3)$$

$$S_j - S_i \geq t_{ij}(x_{ij}), \quad (4)$$

$$I_{ij} \leq X_{ij} \leq U_{ij}, \quad (5)$$

$$X_1 = 0, \quad (6)$$

$$\begin{aligned} C_R &\geq 0, \\ t_{ij}(x_{ij}) &\geq 0, \\ x_i &\geq 0. \end{aligned} \quad (7)$$

Equations (1)–(3) are the objective functions. They minimize the time, cost, and risk, respectively. The constraints are represented by equations (4) and (7). Equation (4) represents the precedence constraint. Equation (5) ensures normal and crash times represent the upper and lower limits of project duration which should not be violated. Equation (6) represents the start time which should always be zero. Equation (7) represents the nonnegativity constraint. The notations and variables used in the above equations are as follows:

i : index of activities

j : index of nodes in project network

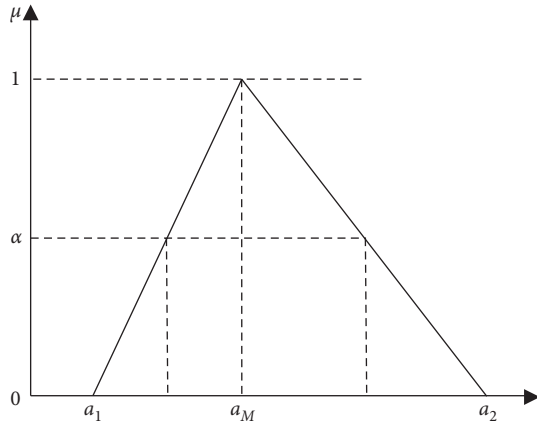
$t_{ij}(x_{ij})$: expected duration of an activity

$C_{ij}(x_{ij})$: the normal cost of an activity

R_{ij} : total value of risk for project activities

S_i : start time of activity i

S_j : start time of node j

FIGURE 1: Triangular fuzzy number with α -cut [7].

This step generates ten alternatives for cost, time, and risk based on different α -cut values that range from 0.1 to 1 with an increment of 10%.

2.2. FMCDM Model Stage 2. In stage two, data are gathered from decision-makers to compare alternatives based on a fuzzy scale. In traditional AHP, a scale of real numbers from one to nine is used to assign preferences [13]. When comparing two alternatives, the significance of the assigned number can be gauged by using the pairwise comparison measurement scale shown in Table 1 as suggested by Saaty [13]. Intermediate numbers are used to add further resolution to the judgments.

To fuzzify this numeric scale, TFN is used to represent uncertainty in the traditional AHP approach. This model uses the linguistic variables and the fuzzy triangular scale that are shown in Table 2, as suggested by Alzarrad and Fonseca [12].

The decision-makers compare the criteria or alternatives using the linguistic terms shown in Table 2, according to the matching TFN of these terms. For example, if the decision-makers state, "Time (criterion 1) is very strongly favored compared to cost (criterion 2)," then it takes the scale of (6, 7, 8). Conversely, comparison of cost (criterion 2) to time (criterion 1) will take the scale of (1/8, 1/7, 1/6). This step involves two objectives:

- (1) Compare the alternatives with respect to criteria
- (2) Compare the criteria with respect to the goal

2.3. FMCDM Model Stage 3. The third stage is to develop pairwise fuzzy comparison matrices. This consists of matrices of pairwise assessments of the contribution of elements at one level, to achieve the objectives of the next higher level. The diagonal elements of all three matrices are (1, 1, 1) because they are the result of comparing identical criteria. A pairwise fuzzy comparison matrix (\tilde{A}) is shown as follows:

TABLE 1: Traditional AHP numerical scale.

Location	Saaty scale
Extremely favored (E. Fav)	9
Very strong favored (V.S. Fav)	7
Strongly favored (S. Fav)	5
Moderately favored (M. Fav)	3
Equal (equal)	1
Moderately disfavored (M. Disfav)	1/3
Strongly disfavored (S. Disfav)	1/5
Very strongly disfavored (V.S. Disfav)	1/7
Extremely disfavored (E. Disfav)	1/9
Intermediate values	2, 4, 6, 8

TABLE 2: Fuzzy triangular scale for fuzzy AHP.

Location	Saaty scale
Extremely favored (E. Fav)	(9, 9, 9)
Very strong favored (V.S. Fav)	(6, 7, 8)
Strongly favored (S. Fav)	(4, 5, 6)
Moderately favored (M. Fav)	(2, 3, 4)
Equal (equal)	(1, 1, 1)
Moderately disfavored (M. Disfav)	(1/4, 1/3, 1/2)
Strongly disfavored (S. Disfav)	(1/6, 1/5, 1/4)
Very strongly disfavored (V.S. Disfav)	(1/8, 1/7, 1/6)
Extremely disfavored (E. Disfav)	(1/9, 1/9, 1/9)
Middle value of 1 and 3	(1, 2, 3)
Middle value of 3 and 5	(3, 4, 5)
Middle value of 5 and 7	(5, 6, 7)
Middle value of 7 and 9	(7, 8, 9)

$$\tilde{A} = \begin{bmatrix} d_{11} & d_{12} & \dots & d_{1n} \\ d_{21} & d_{22} & \dots & d_{2n} \\ \dots & \dots & \dots & \dots \\ d_{n1} & d_{n2} & \dots & d_{nn} \end{bmatrix}, \quad (8)$$

where d_{ij} indicates the decision maker's preference of i^{th} criterion over j^{th} criterion through TFN.

2.4. FMCDM Model Stage 4. This step involves the determination of the relative priorities of each element, at a specific level, with respect to the level immediately above. The relative weights of all the elements at the various levels are aggregated in order to find a vector of composite weights, which will serve as a rating of the decision alternatives to attain the general goal of the problem. The relative weights are denoted by a vector (w) called the priority vector. There are a number of techniques to determine the relative weights. The most commonly used technique is the eigenvalue method [18]. According to the eigenvalue method, the relative priorities of each element at a particular level can be calculated using the following steps:

- (1) Find the geometric mean of fuzzy comparison values of each criterion and alternative using the following equation:

$$r_i = \left(\prod_{j=1}^n d_{ij} \right)^{1/n}, \quad (9)$$

where r_i = geometric mean and n = number of criteria or alternatives

- (2) Find the reciprocal value of the r_i summation ($1/\sum r_i$) and arrange these values in increasing order
- (3) The priority vector (w_i) for each criterion or alternative can be calculated using the following equation:

$$w_i = r_i * \left(\frac{1}{\sum r_i} \right). \quad (10)$$

- (4) Since w_i are still TFN, they need to defuzzified by the Centre of Gravity method via applying the following equation:

$$w_{\text{crisp}} = \frac{lw_i + mw_i + hw_i}{3}, \quad (11)$$

where lw_i = the low value of w_i in the comparison rating, mw_i = the medium value of w_i in the comparison rating, hw_i = the high value of w_i in the comparison rating, and w_{crisp} = the defuzzified value priority vector (w_i) for each criterion or alternative

- (5) Normalize w_{crisp} by using the following equation:

$$w_n = \frac{w_{\text{crisp}}}{\sum w_{\text{crisp}}}. \quad (12)$$

By using these five steps, the normalized weights can be found. Then, the scores for each alternative can be calculated. Finally, the alternative with the largest score is recommended as the first priority of decision-makers.

3. Verification and Validation

To illustrate an implementation of the FMCDM model, two case studies are used to verify and validate the model.

3.1. Case One. The first case study is proposed initially by Gen and Cheng [19]. The FMCDM model is applied to this case to help the decision-makers determine the project optimal time-cost-risk balance. The case study shows a construction project that has seven activities as shown in Table 3. The calculated project duration is 60, 81, and 92 days for the optimistic, moderate, and pessimistic times, respectively. The calculated project cost is \$270K, \$245K, and \$220K for pessimistic, moderate, and optimistic.

The presented model generates the result as shown in Table 4.

TABLE 3: Activity duration and cost.

Activity	Predecessor	Optimistic time	Moderate time	Pessimistic time
A	—	14	20	24
B	A	15	18	20
C	A	15	22	33
D	A	12	16	20
E	B, C	22	24	28
F	D	14	18	24
G	E, F	9	15	18

Based on the results in Table 4, alternative 10 has the largest total score which is 0.255. Therefore, it is recommended as the best choice to minimize the risk and maintain the time-cost balance. To evaluate the result, a software called Expert Choice © is used. Expert Choice is a decision-making software that uses traditional AHP to select the best choice from a group of existing options [20].

Figure 2 shows a comparison between the Expert Choice result and the result obtained by using the FMCDM model.

At first glance, the results look similar, but to further compare the results, a test called Wilcoxon signed-rank test is performed. The method to perform the Wilcoxon test starts with two hypotheses. A null hypothesis (H_0) states that the results obtained from the two approaches are the same. An alternative hypothesis (H_1) states that the results obtained from the two approaches are not the same [21]. Table 5 shows the Wilcoxon signed-rank test result.

Table 5 shows that the p value is 0.006 which is less than the significance level of 0.05. As a result, there is enough evidence to reject the H_0 hypothesis and to conclude that the difference between the results obtained from the two approaches is significant. Although alternative 10 is recommended as the best choice by both the presented model and the Expert Choice software, the scores assigned by each approach are different.

3.2. Case Two. Case two is a concrete bridge project, which was first introduced by Zhang and Zhong [11]. This case consists of six activities as shown in Table 6. The calculated project duration is 180, 199, and 217 days for the optimistic, moderate, and pessimistic times, respectively. The calculated project cost is \$1500, \$1900, and \$2500 for pessimistic, moderate, and optimistic, respectively.

The presented model generates the result as shown in Table 7.

Based on the results in Table 7, alternative one has the highest score, which is 0.240. Therefore, it is recommended as the best choice. Expert Choice has been used to evaluate the result of the presented model. Figure 3 shows a comparison between the Expert Choice result and the result obtained by using the FMCDM model. Wilcoxon test has been used to further evaluate the results. Table 8 shows the Wilcoxon signed-rank test result.

Table 8 shows that the P value is 0.005 which is less than the significance level of 0.05. As a result, there is enough evidence to conclude that the difference between the results obtained from the two approaches is significant. Although

TABLE 4: Results of the FMCDM model (case one).

	Weights	Alt. 1	Alt. 2	Alt. 3	Alt. 4	Alt. 5	Alt. 6	Alt. 7	Alt. 8	Alt. 9	Alt. 10
Time	0.111	0.290	0.242	0.148	0.107	0.070	0.047	0.038	0.028	0.017	0.013
Cost	0.111	0.013	0.016	0.027	0.037	0.058	0.084	0.105	0.144	0.231	0.286
Risk	0.777	0.013	0.016	0.027	0.037	0.058	0.084	0.105	0.144	0.231	0.286
Total scores		0.044	0.041	0.040	0.044	0.059	0.080	0.097	0.131	0.207	0.255

The bold values represent the total weight score for each alternative.

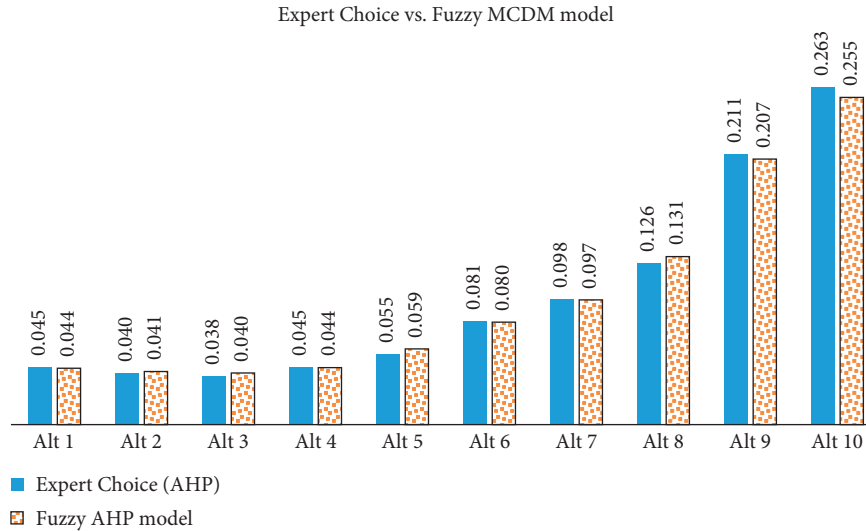


FIGURE 2: Expert Choice results vs FMCDM model results (case one).

TABLE 5: Activity duration and cost.

Source	N	Wilcoxon statistic	P value	Estimated median
FMCDM	10	55.0	0.006	0.086
Expert Choice	10	55.0	0.006	0.083

TABLE 6: Activity duration.

Activity	Optimistic time	Moderate time	Pessimistic time
A	26	28	30
B	40	42	46
C	36	38	40
D	83	85	87
E	18	20	22
F	22	25	28

TABLE 7: Results of the FMCDM model (case two).

	Weights	Alt. 1	Alt. 2	Alt. 3	Alt. 4	Alt. 5	Alt. 6	Alt. 7	Alt. 8	Alt. 9	Alt. 10
Time	0.819	0.290	0.242	0.148	0.107	0.070	0.047	0.038	0.028	0.017	0.013
Cost	0.091	0.013	0.016	0.027	0.037	0.058	0.084	0.105	0.144	0.231	0.286
Risk	0.091	0.013	0.016	0.027	0.037	0.058	0.084	0.105	0.144	0.231	0.286
Total scores		0.240	0.201	0.126	0.094	0.068	0.054	0.050	0.049	0.055	0.063

The bold values represent the total weight score for each alternative.

Alternative one is recommended as the best choice by both the presented model and the Expert Choice software, and the scores assigned by each approach are different. Further, the proposed FMCDM model allows better modeling of the uncertainty, and it takes care of more decision-makers' preferences compared with classical AHP.

4. Results and Limitations

In this paper, a FMCDM model is presented and compared with the classical AHP method that is implemented by use of the Expert Choice software. Two case studies have been used to verify and validate the presented model. Using the first

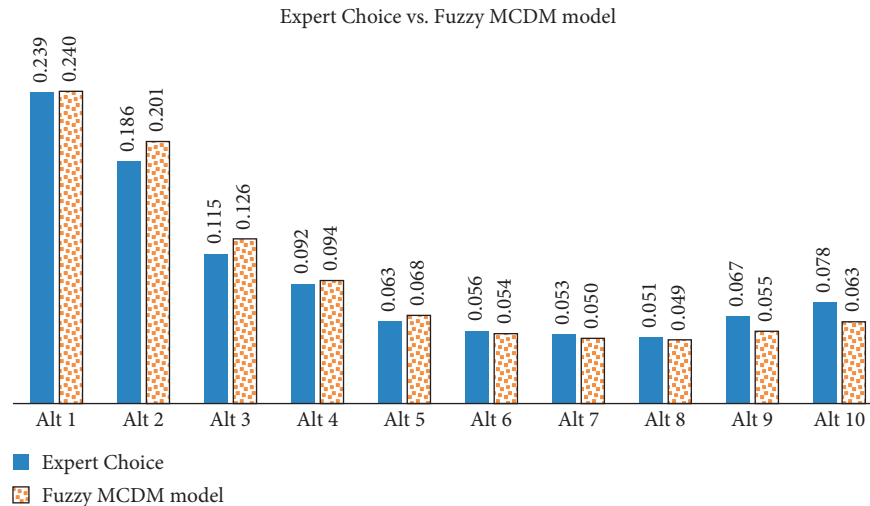


FIGURE 3: Expert Choice results vs FMCDM model results (case two).

TABLE 8: Activity duration and cost.

Source	N	Wilcoxon statistic	P value	Estimated median
FMCDM	10	55.0	0.005	0.0840
Expert choice ©	10	55.0	0.005	0.0875

case study data, the result of the FMCDM model shows that alternative ten has higher priority (0.255) than the other alternatives. The result of the Expert Choice software also shows that alternative ten has higher priority (0.263) than the other alternatives. Using the second case study data, the result of the FMCDM model shows that alternative one has higher priority (0.240) than the other alternatives. The result of the Expert Choice software also shows that alternative one has higher priority (0.239) than the other alternatives. However, the statistical analysis of the results obtained by the presented model and the Expert Choice software shows that there is a significant difference between the two approaches. The presented model is better than other available methods because it used fuzzy linguistic variables for enabling the comparisons between the criteria. This provides decision-makers with the opportunity to provide their judgments as intervals compared to the fixed value judgments. The presented model is much easier to use because the decision-makers feel much more comfortable with using linguistic variables compared to providing precise, crisp judgments [22]. The main limitation of the proposed model is the α -cut values that have been used in this research. Further research could be done to evaluate α -cut effect on the FMCDM model results. This will help investigate further the sensitivity of the model to α -cut change. Finally, the presented FMCDM model is a flexible decision-making model to help managers reduce uncertainties and improve the accuracy of their decision.

Data Availability

The data used in this study can be accessed at DOI: 10.1002/9780470172261.

Conflicts of Interest

The authors declare that there are no conflicts of interest regarding the publication of this paper.

Acknowledgments

The research leading to the publication of this article was partially supported by the Department of Civil Engineering and Construction at Bradley University in Peoria, Illinois, United States of America.

References

- [1] Ö. H. Bettemir and M. Talat Birgönül, "Network analysis algorithm for the solution of discrete time-cost trade-off problem," *KSCE Journal of Civil Engineering*, vol. 21, no. 4, pp. 1047–1058, 2017.
- [2] M. A. Alzarrad, G. P. Moynihan, and S. C. Vereen, "Weather derivatives as a risk management tool for construction projects," in *Proceedings of the 6th CSCE/CRC International Construction Specialty Conference*, pp. 1–9, Vancouver, Canada, May–June 2017.
- [3] J. H. Dahooie, E. K. Zavadskas, M. Abolhasani, A. Vanaki, and Z. Turskis, "A novel approach for evaluation of projects using an interval-valued fuzzy additive ratio assessment (ARAS) method: a case study of oil and gas well drilling projects," *Symmetry Open Access Journal*, vol. 10, no. 2, pp. 1–45, 2018.
- [4] N. Foroozesh, R. Tavakkoli-Moghaddam, and S. Meysam Mousavi, "Sustainable-supplier selection for manufacturing services: a failure mode and effects analysis model based on interval-valued fuzzy group decision-making," *The International Journal of Advanced Manufacturing Technology*, vol. 95, no. 9–12, pp. 3609–3629, 2018.

- [5] Z. He, H. He, R. Liu, and N. Wang, "Variable neighbourhood search and tabu search for a discrete time/cost trade-off problem to minimize the maximal cash flow gap," *Computers & Operations Research*, vol. 78, no. 4, pp. 564–577, 2017.
- [6] H. Hosseini-Nasab, M. Pourkheradmand, and N. Shahsavari-pour, "Solving multi-mode time-cost-quality trade-off problem in uncertainty condition using a novel genetic algorithm," *International Journal of Management and Fuzzy Systems*, vol. 3, no. 3, pp. 1–32, 2017.
- [7] V. Mohagheghi, S. M. Mousavi, and B. Vahdani, "Analyzing project cash flow by a new interval type-2 fuzzy model with an application to construction industry," *Neural Computing and Applications*, vol. 28, no. 4, pp. 3393–3411, 2017.
- [8] M. A. Eirgash, V. Togan, and T. Dede, "A multi-objective decision-making model based on TLBO for the time-cost trade-off problems," *Structural Engineering and Mechanics*, vol. 71, no. 2, pp. 139–151, 2019.
- [9] D. H. Tran, D. L. Luong, M. T. Duong, T. N. Le, and A. D. Pham, "Opposition multiple objective symbiotic organisms search (OMOSOS) for time, cost, risk and work continuity trade-off in repetitive projects," *Journal of Computational Design and Engineering*, vol. 5, no. 2, pp. 160–172, 2017.
- [10] M.-L. Tseng, M. Lim, K.-J. Wu, L. Zhou, and D. T. D. Bui, "A novel approach for enhancing green supply chain management using converged interval-valued triangular fuzzy numbers-grey relation analysis," *Resources, Conservation and Recycling*, vol. 128, no. 6, pp. 122–133, 2018.
- [11] Z. Zhang and X. Zhong, "Time/resource trade-off in the robust optimization of resource-constraint project scheduling problem under uncertainty," *Journal of Industrial and Production Engineering*, vol. 35, no. 4, pp. 243–254, 2018.
- [12] M. A. Alzarrad and D. Fonseca, "A new model to optimize project time-cost trade-off in an uncertain environment," in *Contemporary Issues and Research in Operations Management: Gary Moynihan*, pp. 95–112, InTechOpen, Rijeka, Croatia, 2018.
- [13] T. L. Saaty, "Decision making with the analytic hierarchy process," *International Journal of Services Sciences*, vol. 1, no. 1, pp. 95–122, 2008.
- [14] K. M. A.-S. Al-Harbi, "Application of the AHP in project management," *International Journal of Project Management*, vol. 19, no. 1, pp. 19–27, 2001.
- [15] N.-F. Pan, "Fuzzy AHP approach for selecting the suitable bridge construction method," *Automation in Construction*, vol. 17, no. 8, pp. 958–965, 2008.
- [16] J. Li, O. Moselhi, and S. Alkass, "Forecasting project status by using fuzzy logic," *Journal of Construction Engineering and Management*, vol. 132, no. 11, pp. 1193–1202, 2006.
- [17] A. R. Fayek and J. R. Rodriguez Flores, "Application of fuzzy logic to quality assessment of infrastructure projects at conceptual cost estimating stage," *Canadian Journal of Civil Engineering*, vol. 37, no. 8, pp. 1137–1147, 2010.
- [18] M. B. Ayhan, "Fuzzy topsis application for supplier selection problem," *International Journal of Information Management*, vol. 5, no. 2, pp. 159–174, 2013.
- [19] M. Gen and R. Cheng, *Genetic Algorithms and Engineering Optimization*, John Wiley & Sons, NY, USA, 2000.
- [20] A. Ishizaka and A. Labib, "Analytic hierarchy process and expert choice: benefits and limitations," *OR Insight*, vol. 22, no. 4, pp. 201–220, 2009.
- [21] J. L. Devore, *Probability and Statistics for Engineering and Sciences*, Cengage Learning, Boston, MA, USA, 2016.
- [22] G. Kabir and M. A. A. Hasin, "Comparative analysis of AHP and fuzzy AHP models for multicriteria inventory classification," *International Journal of Fuzzy Logic Systems*, vol. 1, no. 1, pp. 1–16, 2011.

Research Article

A Multiobjective Bilevel Programming Model for Environmentally Friendly Traffic Signal Timings

Ozgur Baskan 

Department of Civil Engineering, Faculty of Engineering, Pamukkale University, Denizli 20160, Turkey

Correspondence should be addressed to Ozgur Baskan; obaskan@pau.edu.tr

Received 6 July 2019; Accepted 23 August 2019; Published 20 October 2019

Academic Editor: Tayfun Dede

Copyright © 2019 Ozgur Baskan. This is an open access article distributed under the Creative Commons Attribution License, which permits unrestricted use, distribution, and reproduction in any medium, provided the original work is properly cited.

Rapid urbanization and mobility needs of road users increase traffic congestion and delay on urban road networks. Thus, local authorities aim to reduce users' total travel time through providing a balance between traffic volume and capacity. To do this, they optimize traffic signal timings, which is one of the most preferred methods, and thus they can increase the reserve capacity of a road network. However, more travel demand along with more reserve capacity leads to vehicle emissions problem which has become quite dangerous for road users, especially in developing countries. Therefore, this study presents a multiobjective bilevel programming model which considers both the maximization of reserve capacity of a road network and the minimization of vehicle emissions by aiming to achieve environmentally friendly signal timings. At the upper level, Pareto-optimal solutions of the proposed multiobjective model are found based on differential evolution algorithm framework by using the weighted sum method. Stochastic traffic assignment problem is presented at the lower level to evaluate the users' reactions. Two signalized road networks are chosen to show the effectiveness of the proposed model. The first one is a small network consisting two signalized intersections that are used to show the effect of the weighting factor on the proposed multiobjective model. The other road network with 96 O-D pairs and 9 signalized intersections is chosen as the second numerical application to investigate the performance of the proposed model on relatively large road networks. It is believed that results of this study may provide useful insights to local authorities who are responsible for regulating traffic operations with environmental awareness at the same time.

1. Introduction

Traffic congestion has become a serious problem worldwide especially in dense urban road networks and causes an increase in overall delay, which is the most significant effect of traffic congestion in a road network. As it is well known, major delays occurring in urban road networks arise from signalized intersections. In fact, a significant decrease in delay can be provided by optimizing signal timings at intersections. Conversely, applying improper signal timings leads to increase in total delay by reducing network's capacity. It is therefore a common method to optimize signal timings at intersections in order to increase the performance of a road network. The concept of reserve capacity has been widely used for a long time to optimize traffic signal timings. Reserve capacity can be defined as the maximization of the origin-destination (O-D) demand multiplier by means of

ensuring that flow on each link in the network does not exceed its capacity. It means that how large a multiplier can be applied to the base travel demand matrix by optimizing traffic signal timings. On the contrary, O-D demand multiplier represents increasing travel demand that occurs as a result of growing population, changing land use pattern, etc. Besides, the concept of reserve capacity describes the border between applying physical improvements and optimizing signal timings to increase the performance of a road network. In other words, local authorities can manage a road network by optimizing traffic signal timings until travel demand reaches a certain level. This concept was taken into consideration with the study proposed by Webster and Cobbe [1]. Allsop [2] took this pioneer work a step further in order to provide an opportunity for intersections with complicated signal plans. Yagar [3, 4] proposed new methods for maximizing capacity at a signalized intersection

by introducing different saturation flows from one stage to another in a cycle to overcome shortcomings in the study by Allsop [2]. While the reserve capacity has been successfully considered for signalized intersections, this concept has also been applied to roundabouts and priority junctions by Wong [5]. Considering a road network rather than a single intersection, Wong and Yang [6] aimed to maximize the reserve capacity of a signalized road network by using deterministic user equilibrium link flows. After that, Yang and Wang [7] explored the relationship between the reserve capacity maximization and travel cost minimization at a signalized road network. At the same year, Ziyou and Yifan [8] pointed out that the concept of reserve capacity and continuous network design problem must have been combined in order to reveal more realistic results for decision makers. Ge et al. [9] studied network's reserve capacity to reveal the impact of user information by using a bilevel programming model. Results showed that the relationship between reserve capacity and user information level depends on characteristics of a considered road network. Besides, a two-stage model to find optimal signal timings in the context of reserve capacity was proposed by Ceylan and Bell [10]. In view of network reliability, Chen et al. [11] developed a new index that examines the relationship between capacity and reliability of a signalized road network. Chiou [12] aimed to maximize the reserve capacity considering an explicit traffic model for a signalized road network. Furthermore, Chiou [13–16] investigated the concept of reserve capacity in the context of toll settings, expansions of link capacity, and minimizing of users' travel time. Similarly, Miandoabchi and Farahani [17] proposed a new framework which solves lane addition and street direction problems within the concept of reserve capacity. Chiou [18] attempted to maximize the reserve capacity of a road network by considering simultaneously the delay minimization problem. On the contrary, Wang et al. [19] extended the study conducted by [8], assuming drivers' decisions in the stochastic user equilibrium (SUE) manner. Baskan and Ozan [20] proposed a bilevel model based on the harmony search (HS) method to maximize the reserve capacity of a road network by taking equity issue into account. Recently, Baskan et al. [21] developed a biobjective bilevel programming model that simultaneously solves the reserve capacity maximization and delay minimization problems.

From another point of view, nowadays, many urban areas are faced with adverse environmental impacts such as noise and smog due to increasing travel demand. While noise can be prevented through enforcements and awareness of drivers, smog and its primary source vehicle emissions cannot be reduced in urban areas by such applications. As is known, significant emission reduction can be achieved by encouraging drivers to preserve their speed consistency. However, it is mostly not possible for drivers to maintain their speed constant due to traffic congestion and delay especially at intersections. Therefore, environmental effects arising from vehicle emissions should be taken into account in optimizing traffic signal timings. In this context, there are a limited number of

studies concerning environmentally friendly signal timings in urban road networks. Kwak et al. [22] investigated the effect of use of proper signal timings on vehicular emissions at an arterial road. Results of a case study showed that the proposed approach produces better solution than that of the best solution produced by Synchro. Ferguson et al. [23] developed a new model considering vehicle emissions in order to fill the gap in the literature-related road network design. Results clearly showed that minimizing network overall delay may increase vehicle emissions. Lv et al. [24] drew attention to the fact that minimizing delay does not reduce vehicle emission-based pollutants. To fill this gap in the literature, they developed an optimization model considering both delay and vehicle emissions as objectives. Liao [25] proposed a signal optimization model which consists of fuel consumption based upon the vehicle movements. The performance of the fuel-based signal optimization model is compared with other signal optimization models through simulations. Results showed that the fuel-based model is able to reduce fuel consumption and CO₂ equivalent (CO₂e) emissions with respect to compared models. Similarly, a vehicle-based emission model has been developed by Chang et al. [26] in order to estimate CO₂e emissions using intelligent transportation systems (ITSs). Findings indicated that the proposed model is capable of estimating CO₂e emissions using different types of ITS. Zhang et al. [27] developed a biobjective programming model to find optimal signal timings for coordinated arterials by minimizing delay and traffic-related emissions. A simulation-based genetic algorithm is used to solve the proposed model. Li and Ge [28] proposed a multiobjective bilevel programming model that maximizes the reserve capacity of a road network and minimizes vehicle emissions by considering equity issue. However, contrary to this study, they considered deterministic user equilibrium traffic assignment at the lower level to represent users' reactions. Khalighi and Christofa [29] investigated the relationship between traffic congestion and vehicle emissions at a signalized intersection. Results revealed that the proposed real-time signal control system is able to optimize traffic signal timings by minimizing vehicle emissions. Stevanovic et al. [30] presented a new method to integrate safety, traffic emission, and signal timing optimization to achieve more reliable decisions when local authorities face a choice between mobility, safety, and environment. Yao et al. [31] remarked that signal timings not only affect the capacity of an intersection but also vehicle emissions. They developed single objective and biobjective optimization models considering different travel demand levels and found that a proper signal timing plan can reduce both delay and vehicle emissions at a signalized intersection. Recently, Li and Sun [32] developed a multiobjective optimization method for signal timing optimization and turning-lane assignment problems considering three important performance measures, namely, transportation efficiency, road safety, and fuel consumption. The proposed methodology clearly showed that significant positive impacts on these measures can be observed with

combined optimization of turning-lane assignment and signal timings.

In the light of literature outlined, this study proposes a multiobjective bilevel programming model which considers both the maximization of reserve capacity of a road network and the minimization of vehicle emissions by aiming to achieve environmentally friendly signal timings. As it is well known, the reserve capacity can be utilized until the increasing travel demand reaches a certain level. On the contrary, this certain level of travel demand also causes significant increase on vehicle emissions in a road network. It indicates that only maximizing the reserve capacity rather than considering environmental effects does not mean that the road network can be managed effectively. Therefore, in this study, a multiobjective bilevel programming model has been developed to find Pareto-optimal solutions for these conflicting objectives. At the upper level, maximum O-D matrix multiplier and optimal signal timings are determined based on differential evolution algorithm frameworks, while the lower level is presented as an SUE assignment problem to evaluate users' reactions.

The remainder of this study is organized as follows. Section 2 is about statement of the problem. Solution algorithms are explained in detail in Section 3. The experimental evaluation of the proposed model is given in Section 4. Conclusions and future directions are provided in Section 5.

2. Statement of the Problem

The mutual interaction between two players, namely, local authority and road users, can be presented as a bilevel programming model. In this study, it is supposed that the local authority seeks to provide a sustainable traffic management through the maximization of the reserve capacity in a road network and the minimization of vehicle emissions. On the contrary, road users aim to minimize their own travel cost and to complete their travels within the shortest travel time. Therefore, road users are interested in neither maximizing the reserve capacity of a road network nor minimizing the total amount of vehicle emissions. The trade-off between the reserve capacity maximization and vehicle emission minimization can be investigated by defining a multiobjective bilevel programming model. At the upper level, reserve capacity maximization and vehicle emission minimization problems are simultaneously solved while SUE traffic assignment is performed at the lower level. The equilibrium link flows are determined by the path flow estimator (PFE) which is a logit-based SUE assignment tool [33]. The most important advantage of the PFE tool is that it does not involve path enumeration [21]. Considering a road network with a set of O-D pairs K , a set of links A , a set of paths D , a set of nodes N , and a set of intersections I , the problem can be formulated as

$$\max_{\xi, \mathbf{x}^*} \quad \psi, \quad (1)$$

$$\min_{\psi, \xi, \mathbf{x}^*} \quad E = \sum_{a \in A} x_a^* e_{ai}, \quad (2)$$

subject to

$$x_a^* (\psi, \xi) \leq p_a Q_a (\xi, s_a), \quad (3)$$

$$\mathbf{G}_i \xi_i \geq \mathbf{b}_i, \quad (4)$$

where ψ is the O-D matrix multiplier, e_{ai} is the amount of vehicle emissions on link a for vehicle class i , and x_a^* is the equilibrium link flow on link a . Equation (3) represents the link capacity constraint in which s_a is the saturation flow, Q_a is the capacity, and p_a is the saturation flow rate. ξ_i is a vector of signal timings and matrices, \mathbf{G}_i and \mathbf{b}_i are depended on signal timing specification for signalized intersection $i \in I$ (see for details [34]). E is the total amount of vehicle emissions in a road network which can be determined using a mesoscopic emission estimation model proposed by Behnke and Kirschstein [35]. According to their study, the amount of vehicle emissions (in kg CO₂e) on link a for vehicle class i can be formulated as

$$e_{ai} = e \cdot l_a \cdot (d_{ai}^{\text{fix}} + d_{ai}^{\text{load}} (m_i^t + \text{cap}_i)), \quad (5)$$

where e is the coefficient for diesel fuel, l_a is the length of link a (i.e. travel distance), d_{ai}^{fix} is the load-independent emission factor, d_{ai}^{load} is the load-dependent emission factor, m_i^t is the tare weight, and cap_i is the load capacity for vehicle class i . cap_i is taken between 0 and maxcap_i , which is the maximum load of vehicle class i . Emission factors dependent on load can be calculated as

$$d_{ai}^{\text{fix}} = \frac{r_i^{\text{idle}}}{v_{ai}} + \alpha_{ai} \cdot \frac{1}{2000} \cdot \frac{c_i^{\text{air}}}{3.6^3} \cdot \rho \cdot A_i \cdot v_{ai}^2, \quad (6)$$

$$d_{ai}^{\text{load}} = \alpha_{ai} \cdot \left(\frac{c_i^{\text{roll}}}{3.6} \cdot g + \frac{0.504}{2 \cdot 3600 \cdot 3.6^2} \cdot n_{ai}^{\text{acc}} \cdot v_{ai}^2 \right). \quad (7)$$

Here, r_i^{idle} is the minimum fuel consumption of vehicle class i , v_{ai} is average speed of vehicle class i on link a , c_i^{air} is the air resistance coefficient of vehicle class i , ρ is the density of air, A_i is the surface area of vehicle class i , c_i^{roll} is the rolling resistance coefficient of vehicle class i , g is the gravitational acceleration, n_{ai}^{acc} is the expected number of accelerations per km on link a , and α_{ai} represents the amount of fuel consumption per hour to provide one KW of energy, and α_{ai} is defined as

$$\alpha_{ai} = \frac{r_i^{\text{full}} - r_i^{\text{idle}}}{P_i \cdot (0.88 - 0.72 \cdot \exp(-0.077 \cdot v_{ai}^{1.41}))}, \quad (8)$$

where r_i^{full} and P_i are the maximum fuel consumption and rated power of engines in vehicles of class i , respectively.

The equilibrium link flows are needed to determine the total amount of vehicle emissions given in equation (2) in a road network. Thus, SUE link flows can be determined by solving traffic assignment problem given in equation [36].

$$\min_{\mathbf{x}} z(\mathbf{x}) = -\psi \mathbf{q}^T \boldsymbol{\mu}(\mathbf{x}) + \mathbf{x}^T \mathbf{t}(\mathbf{x}) - \sum_{a \in A} \int_0^{x_a} t_a(w) dw, \quad (9)$$

where \mathbf{q} is the vector of travel demand, $\mathbf{t}(\mathbf{x})$ represents a vector of link travel times for the given vector of link flows,

and $\boldsymbol{\mu}$ is the vector of expected minimum O-D costs. The proposed multiobjective bilevel programming model aims to maximize the reserve capacity and to minimize vehicle emissions in a road network. It is clear that these objectives are involved in an interaction, and it should be emphasized that one solution may not be existed for all objectives in case a multiobjective problem exists. Therefore, multiple objectives in a given optimization problem require finding well-known Pareto-optimal solutions. A solution for a multiobjective optimization problem is called Pareto-optimal if an objective function can only be improved by degrading some of the other objective function values. Therefore, the proper solution for a multiobjective problem can be provided by Pareto-optimal solutions using the weighted sum method. Before applying the weighted sum method, both objective functions have to be done unitless so that they can be directly added, that is,

$$f_1 = \frac{\psi^*}{\psi}, \quad (10)$$

$$f_2 = \frac{E}{E^*}, \quad (11)$$

where ψ^* and E^* represent upper and lower limits of objective functions given in equations (1) and (2). Since the objective functions are furthermore unitless, the weighted sum method can be applied to find the Pareto-optimal solutions of reserve capacity maximization and vehicle minimization problems subject to equations (3), (4), and (9) as given below:

$$\min f(\psi, \boldsymbol{\xi}, \mathbf{x}^*) = \lambda f_1 + (1 - \lambda) f_2, \quad (12)$$

where λ represents the weighting factor that is specified to find the Pareto-optimal solutions between two objective functions, namely, f_1 and f_2 . The reserve capacity is maximized when a larger value of λ is used by the local authority. Conversely, the minimization of vehicle emissions is taken much more into account for smaller values of λ .

3. Solution Algorithms

The differential evolution- (DE-) based solution algorithm has been introduced to solve the proposed multiobjective bilevel programming model by considering environmental issues. DE optimization algorithm developed by Storn and Price [37] is referred to as one of the most powerful metaheuristic methods [38, 39]. Its solution process is consists four fundamental steps, namely, initialization, mutation, crossover, and selection. As it is well known, few parameters are needed in DE to control the solution process. The first one is the number of population (NP) that represents the population size as used in all population-based metaheuristic methods. The solution vectors stored in the population are called *target vectors*. The second one is the mutation factor (F) used to create the mutant vector, and the last control parameter is the crossover rate (CR) that provides a probabilistic choice between the mutant and target vectors to generate the so-called *trial vectors* (see [37] for details).

It is clear that the maximum value of O-D multiplier, ψ^* and the minimum value of the total amount of vehicle emissions, E^* should be determined for solving the multiobjective model given in equation (12). For this purpose, both problems are solved separately by using the bilevel programming model within the DE framework. The maximization of the O-D multiplier and the minimization of the amount of vehicle emissions are handled at the upper level, while equilibrium link flows are obtained by means of solving SUE assignment problem at the lower level.

3.1. Maximization of Road Network's Capacity. Considering that DE is a minimization algorithm, equation (1) should be reformulated as a minimization problem as given in equation (13) subject to equations (3), (4), and (9) to maximize the reserve capacity of a road network.

$$\min Z(\psi, \mathbf{x}^* \boldsymbol{\xi}) = \frac{1}{\psi} + \sigma \left[\max \left(\sum_{a \in A} (x_a^*(\psi, \boldsymbol{\xi}) - Q_a(\boldsymbol{\xi}, s_a)), 0 \right) \right], \quad (13)$$

where σ is a penalty weighting factor. The right side of equation (13) is the penalty function that ensures link flows do not exceed their capacities. Pseudocode and solution steps for the reserve capacity maximization problem are given below in the line with the DE framework. Before starting Step 1, upper/lower bounds for cycle time for each signalized intersection and possible bounds for O-D multiplier are specified. Similarly, DE parameters and road network parameters, namely, saturation flows, free-flow travel times, and O-D demand matrix are initialized.

Step 1. Solution vectors (i.e., target vectors), Δ_u ($u = 1, 2, \dots, NP$), which include O-D multipliers, cycle times, and stage green timings generated randomly considering their upper and lower bounds. The generation of the decision variables can be formulated as

$$\psi_u = \text{rand}[0, 1] \times (\psi_u^{\max} - \psi_u^{\min}) + \psi_u^{\min}, \quad (14)$$

$$u = 1, 2, \dots, NP,$$

$$c_{u,i} = \text{int} \left[\text{rand}[0, 1] \times (c_{u,i}^{\max} - c_{u,i}^{\min}) + c_{u,i}^{\min} \right], \quad (15)$$

$$i = 1, 2, \dots, N,$$

$$Y_{u,i,j} = \text{int} \left[\text{rand}[0, 1] \times (c_{u,i} - Y_{u,i,j}^{\min}) + Y_{u,i,j}^{\min} \right], \quad (16)$$

$$i = 1, 2, \dots, N, j = 1, 2, \dots, z_n,$$

where $c_{u,i}$ is the cycle time for i^{th} signalized intersection for u^{th} target vector, $c_{u,i}^{\max}$ and $c_{u,i}^{\min}$ are its upper/lower bounds, $Y_{u,i,j}$ and $Y_{u,i,j}^{\min}$ are the j^{th} stage green and minimum green times of intersection i for u^{th} target vector, z_n is the number of stages at i^{th} intersection, and N is the number of intersections in a road network. It should be emphasized that the stage green timings generated according to equation (16) may not satisfy the condition in which the sum of all green and intergreen times should be equal to the cycle time.

Therefore, the stage green timings should be revised according to equation.

$$Y_{u,i,j} = \text{int} \left[Y_{u,i,j}^{\min} + \frac{Y_{u,i,j}}{\sum_{j=1}^{z_n} Y_{u,i,j}} \left[c_{u,i} - z_i \times (I + Y_{u,i,j}^{\min}) \right] \right], \quad (17)$$

subject to

$$\sum_{j=1}^{z_n} Y_{u,i,j} + I = c_{u,i}, \quad (18)$$

where I is the intergreen time. At this stage, the SUE link flows are needed to calculate the value of objective function given in (13). For this purpose, the PFE algorithm is used based on the logit route choice model. The details of the PFE algorithm are not provided to facilitate the presentation of the main contributions without loss of generality (see [33] for details).

Step 2. After creating the initial population, DE operators (mutation, crossover, and selection) are applied to each target vector in order to improve its solution quality. Thus, the solution vectors in the population may find an optimal/near-optimal solution through iterations for a given optimization problem. The mutation process is carried out by using three randomly selected solution vectors which should be different from each other [37]. A mutant vector, Φ_u^{iter} ($\text{iter} = 1, 2, \dots, \text{maxiter}$), for the u^{th} target vector Δ_u^{iter} , is created as

$$\Phi_u^{\text{iter}} = \Delta_{r_0}^{\text{iter}} + F \cdot (\Delta_{r_1}^{\text{iter}} - \Delta_{r_2}^{\text{iter}}), \quad (19)$$

where r_0, r_1 , and r_2 are indices of the selected target vectors which should be different from the u^{th} target vector.

Step 3. Crossover is conducted by using u^{th} target and mutant vectors. Each member of the trial vector, $\beta_{u,i}^{\text{iter}}$, from the u^{th} target or the mutant vectors by using probabilistic choice with CR as given in the following equation:

$$B_u^{\text{iter}} = \beta_{u,i}^{\text{iter}} = \begin{cases} \phi_{u,i}^{\text{iter}}, & \text{if } (\text{rand}(0, 1) \leq \text{CR} \text{ or } i = i_{\text{rand}}), \\ \delta_{u,i}^{\text{iter}}, & \text{otherwise, } i = 1, 2, \dots, \text{ND}, \end{cases} \quad (20)$$

where ND represents the number of decision variables. The statement $i = i_{\text{rand}}$ ensures that the u^{th} target and the trial vectors are different from each other in any case.

Step 4. Corresponding SUE link flows should be calculated for u^{th} trial vector by solving traffic assignment problem before applying the last step of DE. At this step, u^{th} target vector, Δ_u^{iter} , is replaced with the u^{th} trial vector, B_u^{iter} , if the trial vector provides lower objective function value as shown in equation (21). The DE optimization framework is terminated when the maximum number of iterations (maxiter) is reached.

$$\Delta_u^{\text{iter}+1} = \begin{cases} B_u^{\text{iter}}, & \text{if } Z(\mathbf{x}^*(B_u^{\text{iter}})) \leq Z(\mathbf{x}^*(\Delta_u^{\text{iter}})), \\ \Delta_u^{\text{iter}}, & \text{otherwise.} \end{cases} \quad (21)$$

3.2. Minimization of Total Amount of Vehicle Emissions. A bilevel programming model to minimize the total amount of vehicle emissions is explained based on the four-step DE framework. Algorithm 1 represents the main steps of the proposed model similar to Algorithm 2. Before applying Step 1, the upper and lower bounds for signal timing variables are specified. Similarly, DE parameters and road network parameters, namely, saturation flows, free-flow travel times, and O-D demand matrix are initialized. It should be emphasized that O-D demand matrix multiplier is taken as 1 in Algorithm 1. It means that the base travel demand is considered while the total amount of vehicle emissions, E^* , is minimized for a road network.

Step 1. Target vectors, T_u ($u = 1, 2, \dots, \text{NP}$), include cycle times and stage green timings generated randomly considering their upper and lower bounds. The generation of the decision variables is formulated based on equations (15) and (18) similar to Algorithm 2. SUE link flows are determined by the PFE algorithm, and the corresponding objective function value for each target vector is calculated as given in equation (2).

Step 2. At this step, the mutation operator is performed and a mutant vector, Φ_u^{iter} , ($\text{iter} = 1, 2, \dots, \text{maxiter}$), for the u^{th} target vector, T_u^{iter} , is created as

$$\Phi_u^{\text{iter}} = T_{r_0}^{\text{iter}} + F \cdot (T_{r_1}^{\text{iter}} - T_{r_2}^{\text{iter}}). \quad (22)$$

Step 3. At this step, u^{th} trial vector, B_u^{iter} , is generated from u^{th} target vector, T_u^{iter} , and mutant vector, Φ_u^{iter} . Each member of the trial vector, $\beta_{u,i}^{\text{iter}}$, is created as given in the following equation:

$$B_u^{\text{iter}} = \beta_{u,i}^{\text{iter}} = \begin{cases} \phi_{u,i}^{\text{iter}}, & \text{if } (\text{rand}(0, 1) \leq \text{CR} \text{ or } i = i_{\text{rand}}), \\ \tau_{u,i}^{\text{iter}}, & \text{otherwise, } i = 1, 2, \dots, \text{ND}. \end{cases} \quad (23)$$

Step 4. At the beginning of this step, equilibrium link flows are calculated for u^{th} trial vector by solving SUE assignment problem. Finally, u^{th} target vector, T_u^{iter} , is replaced with the u^{th} trial vector, B_u^{iter} , if the trial vector provides lower objective function value as shown in equation (24). The DE process is terminated in case the maximum number of iterations (maxiter) is reached.

$$T_u^{\text{iter}+1} = \begin{cases} B_u^{\text{iter}}, & \text{if } Z(\mathbf{x}^*(B_u^{\text{iter}})) \leq Z(\mathbf{x}^*(T_u^{\text{iter}})), \\ T_u^{\text{iter}}, & \text{otherwise.} \end{cases} \quad (24)$$

After the values of ψ^* and E^* are determined by applying Algorithms 1 and 2, the reserve capacity maximization and vehicle emission minimization problems can be simultaneously handled to find the Pareto-optimal solutions. To do

```

(1) for  $u \leftarrow 1$  to NP do
(2)   for  $i \leftarrow 1$  to ND do
(3)     Generate cycle time  $c_i$  for  $i^{\text{th}}$  intersection considering its upper and lower bounds
(4)     Generate green timings for  $i^{\text{th}}$  intersection between minimum green time and  $c_i$ 
(5)     Revise stage green times of  $i^{\text{th}}$  intersection providing signal timing constraints
(6)     Determine SUE flows for the  $u^{\text{th}}$  target vector
(7)     Determine objective function value given in equation (2) for  $u^{\text{th}}$  target vector
(8)   for iter  $\leftarrow 1$  to maxiter do
(9)     for  $u \leftarrow 1$  to NP do
(10)      Perform mutation to the  $u^{\text{th}}$  target vector to create a mutant vector
(11)      for  $i \leftarrow 1$  to ND do
(12)        Perform crossover to obtain the  $i^{\text{th}}$  decision variable of  $u^{\text{th}}$  trial vector
(13)        Revise cycle times considering their upper and lower bounds
(14)        Revise stage green times providing signal timing constraints
(15)        Determine SUE flows for the  $u^{\text{th}}$  trial vector
(16)        Determine objective function value given in equation (2) for the  $u^{\text{th}}$  trial vector
(17)        Include  $u^{\text{th}}$  trial vector to the population instead of  $u^{\text{th}}$  target vector if it provides lower objective function value
(18)   print optimal/near optimal signal timings

```

ALGORITHM 1: Pseudocode for the minimization of vehicle emissions.

```

(1) for  $u \leftarrow 1$  to NP do
(2) Generate O-D matrix multiplier as  $\psi \in \{\psi^{\min}, \dots, \psi^{\max}\}$  for the  $u^{\text{th}}$  target vector
(3)   for  $i \leftarrow 1$  to  $N$  do
(4)     Generate cycle time  $c_i$  for  $i^{\text{th}}$  intersection considering its upper and lower bounds
(5)     Generate green timings for  $i^{\text{th}}$  intersection between minimum green time and  $c_i$ 
(6)     Revise stage green times of  $i^{\text{th}}$  intersection providing signal timing constraints
(7)     Determine SUE flows for the  $u^{\text{th}}$  target vector
(8)     Determine objective function value given in equation (13) for  $u^{\text{th}}$  target vector
(9)   for iter  $\leftarrow 1$  to maxiter do
(10)    for  $u \leftarrow 1$  to NP do
(11)      Perform mutation to the  $u^{\text{th}}$  target vector
(12)      for  $i \leftarrow 1$  to ND do
(13)        Perform crossover to obtain the  $i^{\text{th}}$  decision variable of  $u^{\text{th}}$  trial vector
(14)        Revise cycle times considering related constraints
(15)        Revise O-D matrix multiplier considering their upper and lower bounds
(16)        Revise stage green times providing signal timing constraints
(17)        Determine SUE flows for the  $u^{\text{th}}$  trial vector
(18)        Determine objective function value given in equation (13) for the  $u^{\text{th}}$  trial vector
(19)        Include  $u^{\text{th}}$  trial vector to the population instead of  $u^{\text{th}}$  target vector if it provides lower objective function value
(20)   print optimal/near optimal signal timings and maximum O-D matrix multiplier,  $\psi$ 

```

ALGORITHM 2: Pseudocode for the maximization of reserve capacity.

this, a multiobjective bilevel programming model given in equation (12) subject to equations (3), (4), and (9) is solved by using Algorithm 3 based on the DE framework by taking weighting factor λ into account.

4. Numerical Applications

The applicability of the proposed algorithms is demonstrated by using two signalized test networks in this section. First network called Test Network-1 is used to reveal the effect of the weighting factor in solving the multiobjective optimization problem given in equation (12). A road network called

Test Network-2 is chosen as the second numerical application to investigate the performance of the proposed algorithms on relatively large networks.

4.1. Test Network-1. The first test network taken from [21] is a small road network which has 2 signalized intersections and 8 links. Layout, stage plans, and revised layout for the PFE are given in Figures 1 and 2, respectively.

The free-flow travel time, t_a^0 , and saturation flow, s_a , for link $a \in A$ are set to 20 sec and 1800 veh/hr, respectively. It is assumed that there is one O-D pair as shown in Figure 1, and travel demand for this O-D pair is taken as 1500 veh/hr. The intergreen time, I , is chosen as 5 sec. Upper and lower

```

(1) Specify the weighing factor  $\lambda \in (0, 1)$ 
(2) Initialize the values of  $\psi^*$  and  $E^*$  to calculate functions  $f_1$  and  $f_2$  given in equation (10) and (11)
(3) for  $u \leftarrow 1$  to NP do
(4) Generate O-D matrix multiplier as  $\psi \in \{\psi^{\min}, \dots, \psi^{\max}\}$  for the  $u^{\text{th}}$  target vector
(5)   for  $i \leftarrow 1$  to  $N$  do
(6)     Generate cycle time  $c_i$  for  $i^{\text{th}}$  intersection considering its upper and lower bounds
(7)     Generate green timings for  $i^{\text{th}}$  intersection between minimum green time and  $c_i$ 
(8)     Revise stage green times of  $i^{\text{th}}$  intersection providing signal timing constraints
(9)     Determine SUE flows for the  $u^{\text{th}}$  target vector
(10)    Determine objective function value given in equation (12)
(11)    for  $u^{\text{th}}$  target vector subject to equations (3) and (4) and equation (9)
(12)  for iter  $\leftarrow 1$  to maxiter do
(13)    for  $u \leftarrow 1$  to NP do
(14)      Perform mutation to the  $u^{\text{th}}$  target vector to create a mutant vector
(15)    for  $i \leftarrow 1$  to ND do
(16)      Perform crossover to obtain the  $i^{\text{th}}$  decision variable of  $u^{\text{th}}$  trial vector
(17)      Revise cycle times considering related constraints
(18)      Revise O-D matrix multiplier considering their upper and lower bounds
(19)      Revise stage green times providing signal timing constraints
(20)      Determine SUE flows for the  $u^{\text{th}}$  trial vector
(21)      Determine objective function value given in equation (12)
(22)      for  $u^{\text{th}}$  trial vector subject to equations (3), (4), equation (9)
(23)      Include  $u^{\text{th}}$  trial vector to the population instead of  $u^{\text{th}}$  target vector if it provides lower objective function value based on the rule given in equation (24)
(24) print optimal/near-optimal signal timings and maximum O-D matrix multiplier,  $\psi$ 

```

ALGORITHM 3: Pseudocode for the multiobjective bilevel programming model.

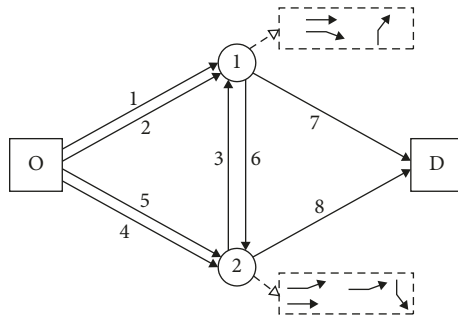


FIGURE 1: Test Network-1.

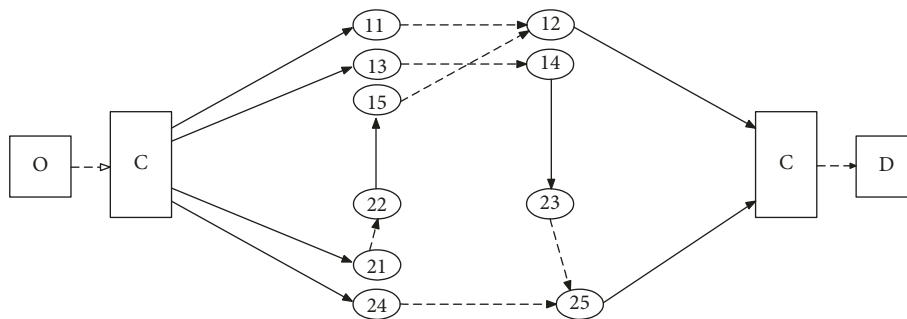


FIGURE 2: Test Network-1 revised for the PFE algorithm.

bounds for cycle time c_i for i^{th} intersection are set to 30 and 100 sec, respectively, in keeping with previous studies [21, 40]. $Y_{i,j}$ is set as being between minimum green time and

c_i where minimum stage green time is selected as 7 sec. Please note that all intersections in Test Network-1 are isolated. On the contrary, it is clear that the values of control

parameters of DE optimization algorithm have an impact on solution quality. In this context, the ranges for F and CR are recommended as $[0.5, 1.0]$ and $[0.8, 1.0]$ by [37], Storn and, Price, respectively. In addition, there are quite a few numbers of studies in the literature for setting of DE parameters in last decades. The recent study by [21] recommends that the value of 0.8 can be used for F and CR. In their study, a comparative sensitivity analysis has been performed and the parameter combination of $F=CR=0.8$ has been resulted in the lowest mean objective function and standard deviation values. Therefore, this parameter combination is selected for all numerical applications in this study. The population size, NP, is selected as 15 considering the number of decision variables, and the maxiter is set to 200 for all algorithms for Test Network-1 (see [21] for details). Note that the average computational time of each iteration of the Algorithm 2 for 30 independent runs, using PC with Intel Core i7 2.10 GHz, 8 GB RAM, was about 7.5 seconds of CPU. To maximize the reserve capacity of Test Network-1, the objective function in equation (13) subject to equations (3) and (4) and equation (9) was minimized by executing Algorithm 2. The best objective function value was found as 0.4680 after 200 iterations, that is, the O-D demand matrix for Test Network-1 can be increased by about 2.14 times as shown in Figure 3. In this case, link flows do not exceed their capacities although the travel demand was increased more than two times. Degree of saturation for links 1 and 4 is 100% that means flows on those links equal their capacities. Flows on other links in Test Network-1 are less than their capacities with the degree of saturation of 98%. In addition, optimal cycle time was found to be 100 sec, which is equally distributed to the stages in each intersection in Test Network-1. It should be emphasized that decision makers do not take the amount of vehicle emissions in the network into account in case they aim to maximize the network's reserve capacity.

On the contrary, the total amount of vehicle emissions represented in equation (2) subject to equations (4) and (9) was minimized for Test Network-1 by using Algorithm 1. The convergence graph is given in Figure 4. The objective function value was found to be about 145.25 after 200 iterations. The optimized signal timings are given in Table 1. The all parameters needed for the mesoscopic emission model were selected similarly as in [35] for small vehicle class.

Once the values of ψ^* and E^* are determined by applying Algorithms 1 and 2, the reserve capacity maximization and vehicle emission minimization problems can be simultaneously solved using equation (12) by applying Algorithm 3. The Ψ , E , and corresponding function values for different weighting factors are given in Table 2. As can be seen in Table 2, the network's reserve capacity cannot be increased when the weighting factor varies between 0 and 0.3 since local authorities try to minimize the total amount of vehicle emissions in the network and they are unwilling to increase the base travel demand in the network. In this case, f_1 is equivalent to ψ^* since ψ is 1.0 which represents the base O-D demand. On the contrary, the value of f_2 equals 1.0 since the value of E is equivalent to E^* . This means that local authority totally concentrates on minimization of vehicle emissions by

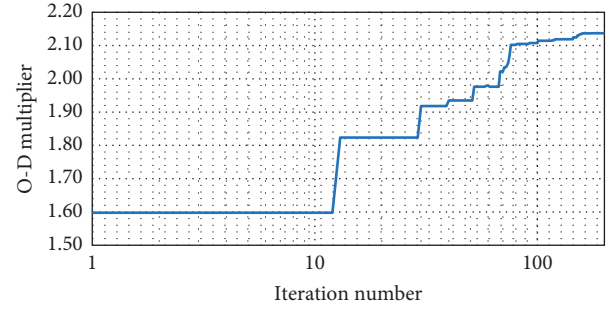


FIGURE 3: Convergence graph of the Algorithm 2 for Test Network-1.

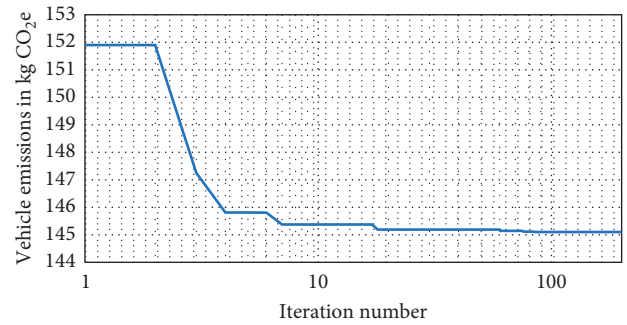


FIGURE 4: Convergence graph of the Algorithm 1 for Test Network-1.

TABLE 1: Optimal signal timings for E^* in Test Network-1.

Cycle time (sec) c_i	Green timing (sec) $Y_{i,1}$	Green timing (sec) $Y_{i,2}$
90	58	22
68	40	18

TABLE 2: The ψ , E , and corresponding function values for Test Network-1.

λ	ψ	E	f_1	f_2	f
0.0	1.000	145.25	2.137	1.000	1.000
0.1	1.000	145.25	2.137	1.000	1.114
0.2	1.000	145.25	2.137	1.000	1.227
0.3	1.000	145.25	2.137	1.000	1.341
0.4	1.121	164.47	1.906	1.132	1.442
0.5	1.353	200.03	1.579	1.377	1.478
0.6	1.372	206.00	1.557	1.418	1.501
0.7	1.606	356.78	1.331	2.456	1.668
0.8	1.811	421.37	1.180	2.901	1.524
0.9	2.000	515.20	1.068	3.546	1.316
1.0	2.137	674.15	1.000	4.641	1.000

optimizing traffic signal timings instead of increasing network's reserve capacity. Conversely, in case the weighting factor is equivalent to 1.0, local authority is not interested in minimizing vehicle emissions and tries to maximize the network's reserve capacity.

In this context, Figure 5 represents Pareto-optimal solutions for f_1 and f_2 with various values of weighting factor λ .

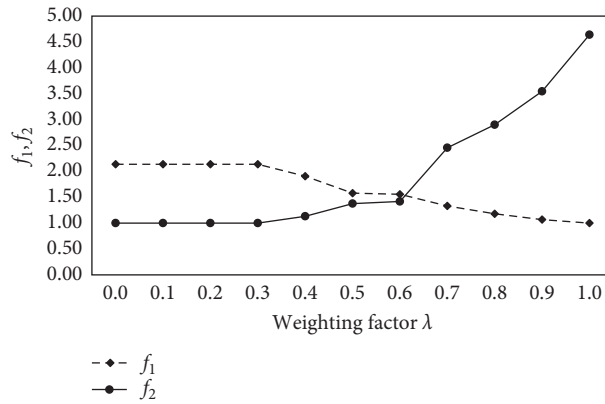


FIGURE 5: Solutions of f_1 and f_2 with various values of weighting factor λ for Test Network-1.

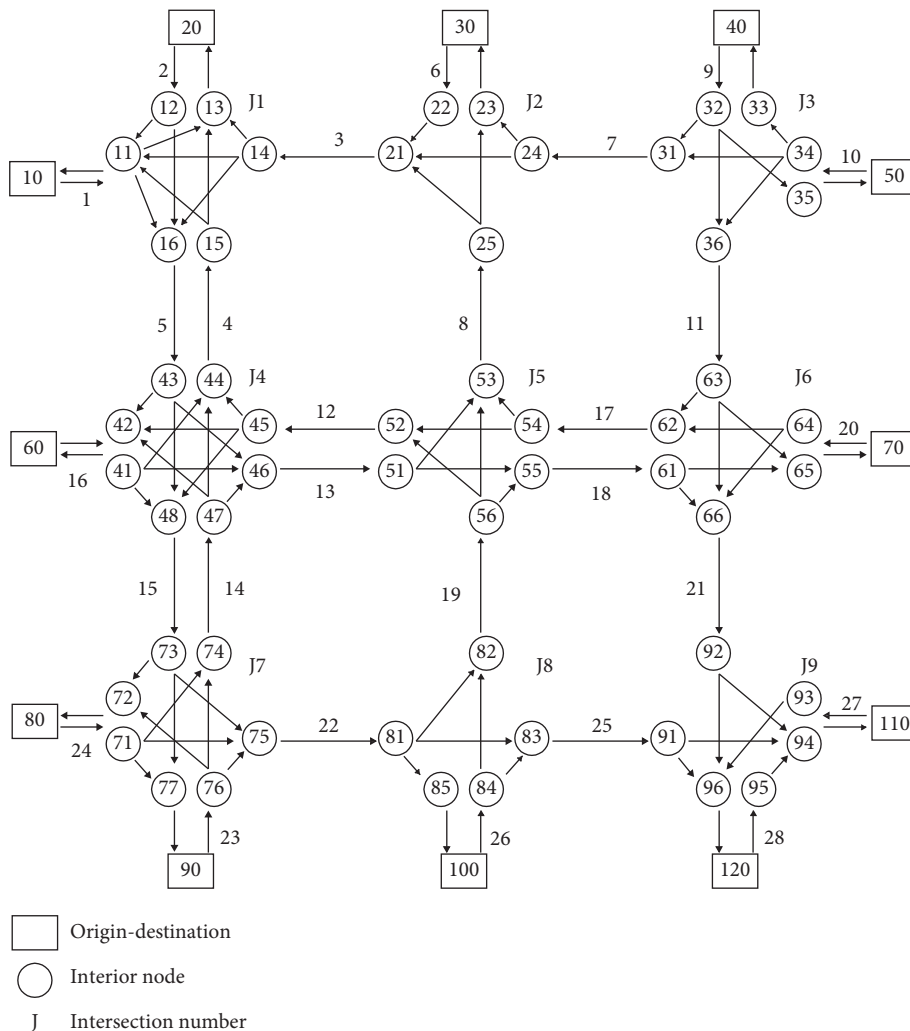


FIGURE 6: Test Network-2 and its representation for the PFE algorithm.

It can be clearly seen that the value of f_1 decreases when the weighting factor varies between 0.0 and 1.0. This result means at the same time that the O-D demand multiplier increases since local authority pays more attention to maximize the reserve capacity of the network.

Conversely, the value of f_2 increases as the weighting factor increases from 0.0 to 1.0. On the contrary, the total amount of vehicle emissions, E , has a decreasing trend when the weighting factor varies from 1.0 to 0.0 as can be seen in Table 2 since local authority focuses attention on minimizing

vehicle emissions in the network instead of maximizing the reserve capacity. In addition to these results, there is no change in f_1 and f_2 until the weighting factor is increased to 0.3. On the contrary, as the weighting factor continues to increase, the value of f_1 begins to decrease and the value of f_2 begins to increase. The value of f_1 shows almost a linear decrease while the weighting factor increases from 0.3 to 1.0. However, the value of f_2 increases significantly especially after the weighting factor's value reached to the value of 0.6 as shown in Figure 5. Thus, after this point, increasing the network's reserve capacity leads to significant increase in the total amount of vehicle emissions in the network.

4.2. Test Network-2. Test Network-2 previously proposed by Gartner et al. [41] and Jovanovic et al. [42] is selected as the second numerical application to show the effectiveness of the proposed algorithm on relatively large networks. Test Network-2 revised for this numerical application consisting 96 O-D pairs, 9 signalized intersections, and 28 links as shown in Figure 6.

Interior nodes are presented to indicate how the PFE algorithm works to solve SUE traffic assignment problem. Each intersection is operated by two stages as can be seen in Figure 7. The minimum stage green time, $Y_{i,j}^{\min}$, is set to 7 sec and the minimum and maximum cycle times for each intersection are taken as 30 and 120 sec, respectively. In addition, the intergreen time between successive stages is set to 5 sec and the minimum and maximum values of the O-D matrix multiplier are selected as 1 and 3, respectively. The saturation flow is taken as 1800 veh/hr. Table 3 presents link-related data for Test Network-2. The free-flow travel times of the entrance links (1, 2, 6, etc.) in the network are assumed to be 1 sec. O-D demand matrix is assumed as given in Table 4.

The population size, NP, is set to 60 considering the number of decision variables, and the maxiter for all algorithms is set to 300. Note that the average computational time of each iteration of Algorithm 2 for 15 independent runs was about 41 sec of CPU. To maximize the reserve capacity of Test Network-2, the objective function in equation (13) subject to equations (3), (4), and (9) was minimized by executing Algorithm 2. The maximum O-D matrix multiplier, ψ^* , was found as 1.24 for Test Network-2. Furthermore, E^* was determined as 1248 by using Algorithm 1. The Ψ , E , and corresponding function values for different weighting factors are given in Table 5.

Similar to the analysis performed for Test Network-1, local authority aims to minimize the total amount of vehicle emissions in the network, and travel demand increase is not permitted until the weighting factor reached to the value of 0.3. However, in case the weighting factor varies from 0.3 to 1.0, local authority focuses on the maximization of network's reserve capacity more than the minimization of vehicle emissions. Figure 8 represents Pareto-optimal solutions for f_1 and f_2 with various values of weighting factor λ for Test Network-2. The value of f_1 decreases when weighting factor increases from 0.3 to 1.0. On the contrary, the value of f_2 significantly increases especially after the value of weighting

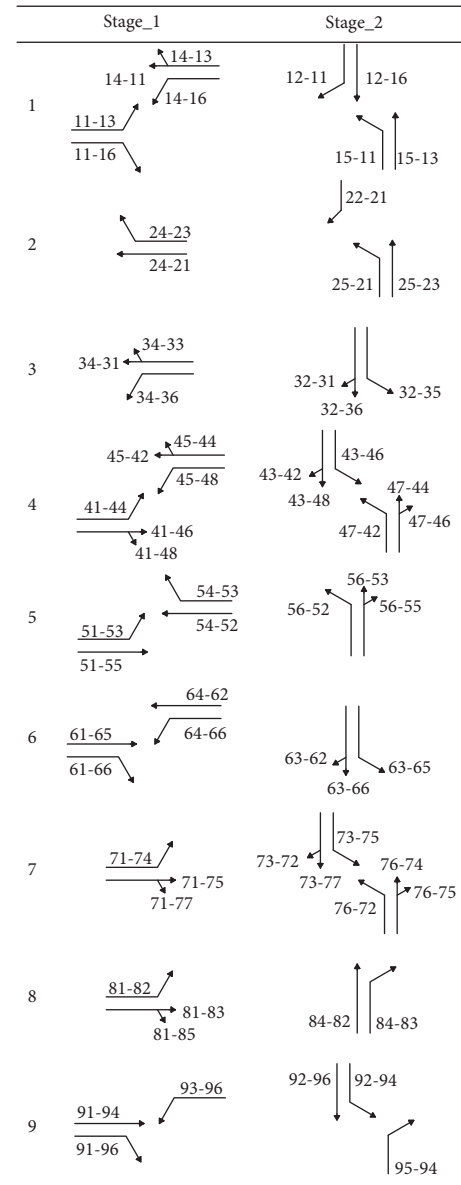


FIGURE 7: Stage plans for Test Network-2.

TABLE 3: Link-related data for Test Network-2.

Link number	Link length l_a (km)	Free-flow travel time t_a^0 (sec)
3	0.183	13.18
4	0.305	21.96
5	0.305	21.96
7	0.244	17.57
8	0.305	21.96
11	0.305	21.96
12	0.183	13.18
13	0.183	13.18
14	0.168	12.10
15	0.168	12.10
17	0.244	17.57
18	0.244	17.57
19	0.168	12.10
21	0.168	12.10
22	0.183	13.18
25	0.244	17.57

TABLE 4: O-D demand matrix for Test Network-2 (veh/hr).

O/D	10	20	30	40	50	60	70	80	90	100	110	120
10	—	100	100	—	—	100	100	100	100	100	100	100
20	60	—	60	—	—	60	60	60	60	60	60	60
30	60	60	—	—	—	60	60	60	60	60	60	60
40	60	60	60	—	60	60	60	60	60	60	60	60
50	40	40	40	40	—	40	40	40	40	40	40	40
60	50	50	50	—	—	—	50	50	50	50	50	50
70	70	70	70	—	—	70	—	70	70	70	70	70
80	110	110	110	—	—	110	110	—	110	110	110	110
90	90	90	90	—	—	90	90	90	—	90	90	90
100	30	30	30	—	—	30	30	30	30	—	30	30
110	—	—	—	—	—	—	—	—	—	—	—	45
120	—	—	—	—	—	—	—	—	—	—	69	—

TABLE 5: The ψ , E , and corresponding function values for Test Network-2.

λ	ψ	E	f_1	f_2	f
0.0	1.00	1248	1.240	1.000	1.000
0.1	1.00	1248	1.240	1.000	1.024
0.2	1.00	1248	1.240	1.000	1.048
0.3	1.00	1248	1.240	1.000	1.072
0.4	1.03	1290	1.203	1.034	1.101
0.5	1.04	1300	1.192	1.042	1.117
0.6	1.11	1350	1.119	1.082	1.104
0.7	1.17	1470	1.062	1.178	1.097
0.8	1.18	1620	1.047	1.298	1.097
0.9	1.21	1734	1.026	1.389	1.062
1.0	1.24	1872	1.000	1.499	1.000

TABLE 6: Optimal signal timings for Test Network-2 for weighting factor $\lambda = 0.6$.

Cycle time (sec) c_i	Green timing (sec) $Y_{i,1}$	Green timing (sec) $Y_{i,2}$
45	20	15
51	16	25
36	14	12
81	24	47
75	37	28
40	16	14
74	25	39
74	50	14
30	10	10

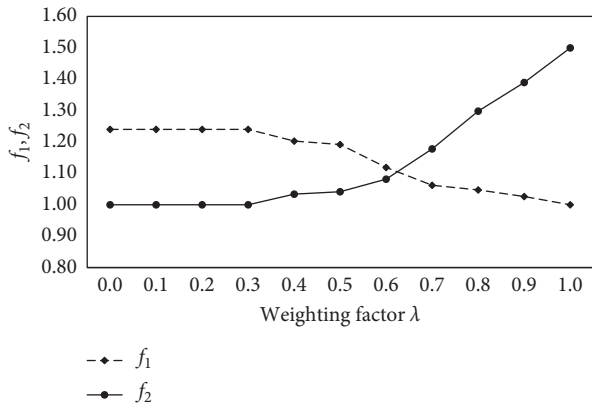


FIGURE 8: Solutions of f_1 and f_2 with various values of weighting factor λ for Test Network-2.

factor equals 0.6. This result is compatible with the results of the analysis performed for Test Network-1.

In case the weighting factor is equivalent to the value of 0.0, only the minimization of vehicle emissions is taken into account by local authority. Conversely, the maximization of network's reserve capacity is considered instead of the minimization of vehicle emissions in case weighting factor λ equals 1.0. The total amount of vehicle emissions has reached the value of 1872 in kg CO₂e as shown in Table 5 in case the O-D travel demand matrix has increased 24%. It should be

pointed out that link flows do not exceed their capacities although the maximum demand multiplier has been applied to the O-D matrix. Optimized signal timings for Test Network-2 for weighting factor $\lambda = 0.6$ are given in Table 6 since this value is assumed as a critical point.

5. Conclusions and Future Directions

This study presents a multiobjective bilevel programming model that considers the maximization of reserve capacity of a road network and the minimization of vehicle emissions by aiming to achieve environmentally friendly signal timings. A weighted sum method is introduced to find the Pareto-optimal solutions of the proposed multiobjective problem based on differential evolution algorithm framework. Two road networks are considered in order to show the applicability of the proposed model. Test Network-1 is used to reveal the effect of the weighting factor in solving the multiobjective optimization problem. It is found that the O-D demand matrix for Test Network-1 can be increased by about 2.14 times without links exceeding their capacities. According to the results of the Pareto-optimal analysis, it should be emphasized that the total amount of vehicle emissions significantly increases especially after the value of the weighting factor equals 0.6. In other words, increasing the network's reserve capacity leads to significantly increasing the amount of vehicle emissions in the network after this point. Test Network-2 is selected as the second

numerical application to show the effectiveness of the proposed algorithm on relatively large networks. Results show that the total amount of vehicle emissions is found as the value of 1872 in case the O-D matrix is increased 24%. Pareto-optimal analysis reveals that the results for Test Network-2 are compatible with those of Test Network-1.

In conclusion, results obtained from the Pareto-optimal analysis may give a good opportunity to authorities to provide a balance between two conflicting objectives, namely, reserve capacity maximization and vehicle emissions minimization. In addition, results also show that the proposed multiobjective model may be a useful tool to provide sustainable signal timings considering environmental issues. In future studies, an application on a realistic road network is necessary to validate the results of the proposed model even though the findings for the two test networks give some new insights.

Data Availability

The data used to support the findings of this study are included within the article.

Conflicts of Interest

The authors declare that there are no conflicts of interest regarding the publication of this paper.

References

- [1] F. V. Webster and B. M. Cobbe, *Traffic Signal*, Road Research Technical Paper No. 56, HMSO, London, UK, 1966.
- [2] R. E. Allsop, "Estimating the traffic capacity of a signalized road junction," *Transportation Research*, vol. 6, no. 3, pp. 245–255, 1972.
- [3] S. Yagar, "Capacity of a signalized road junction: critique and extensions," *Transportation Research*, vol. 8, no. 2, pp. 137–147, 1974.
- [4] S. Yagar, "Addressing errors and omissions in paper on intersection capacity maximization," *Transportation Research Part B: Methodological*, vol. 19, no. 1, pp. 81–84, 1985.
- [5] S. C. Wong, "On the reserve capacities of priority junctions and roundabouts," *Transportation Research Part B: Methodological*, vol. 30, no. 6, pp. 441–453, 1996.
- [6] S. C. Wong and H. Yang, "Reserve capacity of a signal-controlled road network," *Transportation Research Part B: Methodological*, vol. 31, no. 5, pp. 397–402, 1997.
- [7] H. Yang and J. Y. T. Wang, "Travel time minimization versus reserve capacity maximization in the network design problem," *Transportation Research Record: Journal of the Transportation Research Board*, vol. 1783, no. 1, pp. 17–26, 2002.
- [8] G. Ziyoun and S. Yifan, "A reserve capacity model of optimal signal control with user-equilibrium route choice," *Transportation Research Part B: Methodological*, vol. 36, no. 4, pp. 313–323, 2002.
- [9] Y. E. Ge, H. M. Zhang, and W. H. K. Lam, "Network reserve capacity under influence of traveler information," *Journal of Transportation Engineering*, vol. 129, no. 3, pp. 262–270, 2003.
- [10] H. Ceylan and M. G. H. Bell, "Reserve capacity for a road network under optimized fixed time traffic signal control," *Journal of Intelligent Transportation Systems: Technology, Planning, and Operations*, vol. 8, no. 2, pp. 87–99, 2004.
- [11] A. Chen, P. Chootinan, and S. C. Wong, "New reserve capacity model of signal-controlled road network," *Transportation Research Record: Journal of the Transportation Research Board*, vol. 1964, pp. 35–41, 2006.
- [12] S.-W. Chiou, "Reserve capacity of signal-controlled road network," *Applied Mathematics and Computation*, vol. 190, no. 2, pp. 1602–1611, 2007.
- [13] S.-W. Chiou, "An efficient search algorithm for road network optimization," *Applied Mathematics and Computation*, vol. 201, no. 1–2, pp. 128–137, 2008.
- [14] S.-W. Chiou, "A hybrid approach for optimal design of signalized road network," *Applied Mathematical Modelling*, vol. 32, no. 2, pp. 195–207, 2008.
- [15] S.-W. Chiou, "Optimization of limited network capacity with toll settings," *Information Sciences*, vol. 179, no. 1–2, pp. 109–119, 2009.
- [16] S.-W. Chiou, "Optimization for signal setting problems using non-smooth techniques," *Information Sciences*, vol. 179, no. 17, pp. 2985–2996, 2009.
- [17] E. Miandoabchi and R. Z. Farahani, "Optimizing reserve capacity of urban road networks in a discrete network design problem," *Advances in Engineering Software*, vol. 42, no. 12, pp. 1041–1050, 2011.
- [18] S.-W. Chiou, "Optimal signal-setting for road network with maximum capacity," *Information Sciences*, vol. 273, pp. 287–303, 2014.
- [19] J. Wang, W. Deng, and J. Zhao, "Road network reserve capacity with stochastic user equilibrium," *Transport*, vol. 30, no. 1, pp. 103–116, 2015.
- [20] O. Baskan and C. Ozan, "Reserve capacity model for optimizing traffic signal timings with an equity constraint," *Highway Engineering*, Wiley-Blackwell, Hoboken, NJ, USA, 2017.
- [21] O. Baskan, H. Ceylan, and C. Ozan, "A simultaneous solution for reserve capacity maximization and delay minimization problems in signalized road networks," *Journal of Advanced Transportation*, vol. 2019, Article ID 6203137, 18 pages, 2019.
- [22] J. Kwak, B. Park, and J. Lee, "Evaluating the impacts of urban corridor traffic signal optimization on vehicle emissions and fuel consumption," *Transportation Planning and Technology*, vol. 35, no. 2, pp. 145–160, 2012.
- [23] E. M. Ferguson, J. Duthie, and S. Travis Waller, "Comparing delay minimization and emissions minimization in the network design problem," *Computer-Aided Civil and Infrastructure Engineering*, vol. 27, no. 4, pp. 288–302, 2012.
- [24] J. Lv, Y. Zhang, and J. Zietsman, "Investigating emission reduction benefit from intersection signal optimization," *Journal of Intelligent Transportation Systems*, vol. 17, no. 3, pp. 200–209, 2013.
- [25] T.-Y. Liao, "A fuel-based signal optimization model," *Transportation Research Part D: Transport and Environment*, vol. 23, pp. 1–8, 2013.
- [26] X. Chang, B. Y. Chen, Q. Li, X. Cui, L. Tang, and C. Liu, "Estimating real-time traffic carbon dioxide emissions based on intelligent transportation system technologies," *IEEE Transactions on Intelligent Transportation Systems*, vol. 14, no. 1, pp. 469–479, 2013.
- [27] L. Zhang, Y. Yin, and S. Chen, "Robust signal timing optimization with environmental concerns," *Transportation Research Part C: Emerging Technologies*, vol. 29, pp. 55–71, 2013.
- [28] Z.-C. Li and X.-Y. Ge, "Traffic signal timing problems with environmental and equity considerations," *Journal of Advanced Transportation*, vol. 48, no. 8, pp. 1066–1086, 2014.
- [29] F. Khalighi and E. Christofa, "Emission-based signal timing optimization for isolated intersections," *Transportation*

- Research Record: Journal of the Transportation Research Board*, vol. 2487, no. 1, pp. 1–14, 2015.
- [30] A. Stevanovic, J. Stevanovic, J. So, and M. Ostojic, “Multi-criteria optimization of traffic signals: mobility, safety, and environment,” *Transportation Research Part C: Emerging Technologies*, vol. 55, pp. 46–68, 2015.
- [31] R. Yao, X. Wang, H. Xu, and L. Lian, “Emission factor calibration and signal timing optimisation for isolated intersections,” *IET Intelligent Transport Systems*, vol. 12, no. 2, pp. 158–167, 2018.
- [32] X. Li and J.-Q. Sun, “Turning-lane and signal optimization at intersections with multiple objectives,” *Engineering Optimization*, vol. 51, no. 3, pp. 484–502, 2019.
- [33] M. G. H. Bell and C. M. Shield, “A log-linear model for path flow estimation,” in *Proceedings of the 4th International Conference on the Applications of Advanced Technologies in Transportation Engineering*, Y. J. Stephanedes and F. Filippi, Eds., pp. 695–699, Capri, Italy, June 1995.
- [34] R. E. Allsop, “Evolving application of mathematical optimisation in design and operation of individual signal-controlled road junctions,” in *Mathematics in Transport and Planning and Control*, J. D. Griffiths, Ed., pp. 1–24, Clarendon Press, Oxford, UK, 1992.
- [35] M. Behnke and T. Kirschstein, “The impact of path selection on GHG emissions in city logistics,” *Transportation Research Part E: Logistics and Transportation Review*, vol. 106, pp. 320–336, 2017.
- [36] M. G. H. Bell and Y. Iida, *Transportation Network Analysis*, John Wiley & Sons, Chichester, UK, 1997.
- [37] R. Storn and K. Price, “Differential evolution—a simple and efficient heuristic for global optimization over continuous spaces,” *Journal of Global Optimization*, vol. 11, no. 4, pp. 341–359, 1997.
- [38] P. Civicioglu and E. Besdok, “A conceptual comparison of the Cuckoo-search, particle swarm optimization, differential evolution and artificial bee colony algorithms,” *Artificial Intelligence Review*, vol. 39, no. 4, pp. 315–346, 2013.
- [39] A. Deb, J. S. Roy, and B. Gupta, “Performance comparison of differential evolution, particle swarm optimization and genetic algorithm in the design of circularly polarized microstrip antennas,” *IEEE Transactions on Antennas and Propagation*, vol. 62, no. 8, pp. 3920–3928, 2014.
- [40] M. Dell’Orco, O. Baskan, and M. Marinelli, “A Harmony Search algorithm approach for optimizing traffic signal timings,” *Promet—Traffic & Transportation*, vol. 25, no. 4, pp. 349–358, 2013.
- [41] N. H. Gartner, J. D. C. Little, and H. Gabbay, “Optimization of traffic signal settings by mixed-integer linear programming,” *Transportation Science*, vol. 9, no. 4, pp. 321–343, 1975.
- [42] A. Jovanovic, M. Nikolic, and D. Teodorovic, “Area-wide urban traffic control: a bee colony optimization approach,” *Transportation Research Part C: Emerging Technologies*, vol. 77, pp. 329–350, 2017.

Research Article

Multiobjective Optimization Design for Structural Parameters of TBM Disc Cutter Rings Based on FAHP and SAMPGA

Laikuang Lin ^{1,2}, Yimin Xia ^{1,2} and Dun Wu³

¹College of Mechanical and Electrical Engineering, Central South University, Changsha 410083, China

²State Key Laboratory of High Performance Complex Manufacturing, Central South University, Changsha 410083, China

³China Railway 14th Bureau Group Tunnel Engineering Co., Ltd., Jinan 250014, China

Correspondence should be addressed to Laikuang Lin; linlaikuang@csu.edu.cn and Yimin Xia; xiaymj@csu.edu.cn

Received 11 July 2019; Accepted 22 August 2019; Published 12 September 2019

Guest Editor: Moacir Kripka

Copyright © 2019 Laikuang Lin et al. This is an open access article distributed under the Creative Commons Attribution License, which permits unrestricted use, distribution, and reproduction in any medium, provided the original work is properly cited.

As a key component of tunnel boring machines (TBMs), the disc cutter ring and its structural parameters are closely related to the TBM tunneling quality. Literature review shows that investigations on optimization design methods for cutter ring structure are seriously insufficient. Therefore, in this paper, a multiobjective optimization design model of structural parameters for disc cutter rings is developed based on the complex geological conditions and the corresponding cutter ring structure design requirements. The rock breaking capability, energy consumption, load-bearing capability, wear life, and wear uniformity of disc cutter are selected as the objectives, and the geometric structure of cutter rings, ultimate load-bearing capability, and cutterhead drive performance are determined as constraints. According to the characteristics of this model, a self-adaptive multipopulation genetic algorithm (SAMPGA) is utilized to solve the optimization problem, and the Fuzzy analytical hierarchy process (FAHP) is employed to calculate weight coefficients for multiple objectives. Finally, the applicability of the proposed method is demonstrated through a case study in a TBM project. The results indicated that the rock breaking performance and service life of the disc cutter are improved after optimization by using the proposed method. The utilization of SAMPGA effectively solves the premature local convergence problems during optimization. The geological adaptability should be considered in the cutter ring structure design, which can be realized by using the proposed method based on the suitable weight coefficients.

1. Introduction

With the rapid development of tunnel constructions, tunnel boring machines (TBMs) are widely employed in tunnel excavation due to their high excavation efficiency, excellent safety, and less ground disturbance [1, 2]. Disc cutters mounted on TBM cutterhead are the main rock breaking tools, and cutter rings interact with and cut rocks directly during the TBM tunneling process [3, 4]. When tunneling in the complex and harsh geological conditions, the cutter ring suffers from high contact stress and strong impact vibration. If the structural design of the cutter ring is unreasonable, it will not only limit the rock breaking capability and efficiency of the disc cutter but also cause serious wear and breakage failure of the cutter ring, which will significantly affect the tunneling efficiency and construction cost of the TBM

project. Nowadays, most of the existing cutter ring designs are based on engineering experience or adopt commonly used dimensions specified by several well-known cutter manufacturers. Relevant optimization design method for structural parameters of TBM disc cutter ring is rare. Therefore, it is of great necessity and attractiveness to develop geological adaptability and a multiobjective optimization design method for cutter ring structural parameters on the basis of the complex and changeable geological conditions.

At present, the research associated with cutter ring structure mainly focuses on the rock breaking characteristics of types of cutter rings and the influence of cutter ring structural parameters on its cutting performance. Rostami [5] studied the load characteristics and rock fragmentation induced by a disc cutter based on linear cutting experiments

and pointed out that the contact stress of cutter ring is closely related to the cutter tip width. Balci and Tumac [6, 7] compared and analyzed the rock breaking loads of constant cross-section (CCS) and V-type disc cutters through a series of rock breaking tests, and they established and modified the rock breaking load prediction model of the CCS disc cutter considering the influences of diameter, tip width, and edge angle of cutter ring. Choi et al. [8] investigated the effects of cutter ring shape on cutter forces by a series of full-scale linear cutting tests and found that the rolling stress acting on a V-shape disc cutter was much higher than on a CCS disc cutter. Chiaia [9] studied the rock breaking mechanisms using different types of cutters, including blunt rigid sphere, flat punch, and circular cone. Lislerud [10] compared the rock breaking characteristics of flat-edged disc cutter, wedge-shaped disc cutter, and studded roller disc cutter and put forward the rock breaking kinetic model of studded roller disc cutter. Zhang et al. [11] studied the rock fragmentation process subject to wedge cutters by physical experiments and bonded particle model simulations, and the AE distribution, crack pattern, and cutter force were obtained both for single cutter and double cutters. Roby et al. [12] introduced recent improvements in the disc cutter components and emphatically analyzed the distinctions of disc cutters with different sizes. Maidl et al. [13] presented that the cutter tip widths of commonly used disc cutters are mainly designed as 6.35 mm (1/4-inch), 12.7 mm (1/2-inch), 19.05 mm (3/4-inch), and 25.4 mm (1-inch). Marji [14] and Sun et al. [15] established rock breaking simulation models for disc cutters by using discrete element method and revealed the effects of cutter tip width and edge angle parameters on the cutter rock breaking performance (crack propagation, rock breaking volume, specific energy, etc.). Li et al. [16] analyzed the difference in rock breaking characteristics between small edge angle cutter ring and fat edge cutter ring through theoretical, simulation, and experimental analysis, and they found the performance of the small edge angle cutter ring better than that of the fat edge cutter ring in high abrasive strata. Xia et al. [17] used the orthogonal test method to analyze the influences of cutter ring structural parameters on rock breaking forces. Review of the literature shows that researches on cutter ring structural design mainly focus on the effects of the shape size or structural parameters of the cutter ring on its rock breaking performance based on parametric analysis method. However, the effects of cutter ring structural parameters on other cutter performances, e.g., wear resistance performance, are seldom considered as well as the influence of geological conditions on the structural design of cutter rings. In reality, disc cutter wear is an important factor that raises up the excavation cost and delays the project during TBM tunneling of hard rock [18]. Additionally, investigations on multiobjective optimization design methods for cutter ring structural parameters are seriously insufficient.

Cutter ring structural design problem contains several mutually conflicting objectives and constraints, which belong to a multiobjective optimization problem. To deal with this engineering problem, selecting a suitable multiobjective optimization approach is one of the aims in this study.

Traditional optimization techniques tend to provide a local optimum solution in scenarios where the size of the search space is large, a number of variables are to be handled, multiple objectives are to be achieved, and a number of constraints are to be satisfied simultaneously [19]. Therefore, a number of population-based optimization algorithms known as the advanced optimization algorithms have been developed in recent year and extensively used in engineering issues. These methods mainly include genetic algorithm (GA) [20], particle swarm optimization (PSO) [21], artificial immune system [22], differential evolution algorithms [23], ant colony algorithm (ACA) [24], and simulated annealing (SA) [25]. As a classical meta-heuristic algorithm, GA is frequently used as a search strategy to discover the optimal subset. However, there are some defects existed in simple GA (SGA), such as processing of single objective function, premature convergence, low efficiency of optimization, etc. To deal with multiobjective optimization problems, several extended GAs are presented based on the SGA. Muruta and Ishibuchi [26] developed a GA-based algorithm to solve multiobjective problems called multiobjective genetic algorithm (MOGA). Dynamic weighting is used in this algorithm to transfer the multiple objectives into a single objective. Deb et al. [27] proposed the nondominated sorting GA-II (NSGA-II) approach, which is implemented with an effective sorting method based on individual ranking by nondominated sorting and a crowded distance sorting evaluating the population density of solutions in the same rank [28]. Huo et al. [29] employed an SGA and a cooperative coevolutionary genetic algorithm (CCGA) to solve the disc cutters' multispiral and stochastic layout problems. Shahsavari et al. [30] compared three self-adaptive multi-objective evolutionary algorithms for a triple-objective project scheduling problem, including self-adaptive multi-population genetic algorithm (SAMPGA), two-phase sub-population genetic algorithm (TPSPGA), and nondominated ranked genetic algorithm (NRGA). Considering the characteristics of the above GAs and requirements in structure design of cutter rings, an SAMPGA [31] has been selected in this paper as an appropriate optimization algorithm.

In this paper, a multiobjective optimization design model of structural parameters for disc cutter rings, including five objectives and twelve constraints, is established based on the engineering technical requirements and the corresponding cutter ring structure design requirements. According to the characteristics of this model, an SAMPGA is applied to solve the multiobjective optimization design problem, and the fuzzy analytical hierarchy process (FAHP) is employed to deal with the multiobjective functions. Finally, the applicability and validity of the proposed approach are demonstrated through a case study in a TBM project.

2. Problem Description and Modeling

2.1. Requirements in Structure Design of Cutter Ring. A disc cutter ring is the only part of a disc cutter that contacts with rock, and its structure characteristics directly determine the cutter service performance. To obtain the disc cutter with high rock breaking efficiency and long service life, purpose,

and principle of the cutter ring structural design are summarized by consulting relevant literature and engineering data. (1) Excellent rock breaking performance: Disc cutter can break rock normally and break more rocks as much as possible under harsh geological conditions, which is the basic requirement of the cutter ring geological adaptability design. (2) Minimum cutter energy consumption for rock breaking: Breaking rocks efficiently with less energy consumption will improve the overall tunneling efficiency of disc cutter and cutterhead. (3) Long service life and uniform wear: Loads that cutter bearings suffered meet the design requirement, and the blade shape of cutter ring maintains stability during normal wear process. (4) Meet the basic structural parameters requirement of cutter ring: There is a correlation among the structural parameters of the CCS disc cutter ring; therefore, the setting of structural parameters should meet the relevant requirements. (5) Meet the requirements of cutterhead drive performance: Total loads on the disc cutter should not exceed the rated thrust and torque of the cutterhead. (6) Meet the ultimate load-bearing capability requirements of disc cutter: Average load of the disc cutter after optimization should not exceed the prescribed limit load.

2.2. Mathematical Model and Parameter Expression. Multiobjective optimization design model for cutter ring structural parameters mainly includes objective functions, constraints, and design variables, which can be defined as follows:

$$\begin{aligned} \min \quad & f_m(x_1, x_2, \dots, x_n), \quad m = 1, 2, \dots, M, \\ \text{s.t.} \quad & g_k(x_1, x_2, \dots, x_n) \geq 0, \quad k = 1, 2, \dots, K, \\ & h_l(x_1, x_2, \dots, x_n) = 0, \quad l = 1, 2, \dots, L, \\ & x_i^L \leq x_i \leq x_i^U, \quad i = 1, 2, \dots, N, \end{aligned} \quad (1)$$

where $f_m(x)$ is the objective functions, X denotes the decision space, $x = (x_1, x_2, \dots, x_n) \in X$, x^L and x^U are lower and upper boundaries of design variable x , respectively, $g_k(x)$ is the k -th inequality constraint, and $h_l(x)$ is the l -th equality constraint.

CCS disc cutter is the most commonly used type of cutter for TBM due to its balanced rock breaking and wear resistance performance. Thus, it is set as the structural design object in this paper. Sketch of disc cutter and cutter ring is shown in Figure 1. The key structural parameters of the cutter ring, including cutter tip width T , edge angle θ , and edge radius r , are selected as the design variables, which can be expressed as $x = (T, \theta, r)$.

2.3. Objective Functions

2.3.1. Rock Breaking Capability of Disc Cutter. Cutter rock breaking capability is the key factor to the smooth excavation for TBM in hard rock conditions, and it is a basic criterion reflecting the geological adaptability. Rock breaking induced by disc cutter is a process of crack generation, crack propagation,

crack intersection, and rock fragmentation. Therefore, the length of the side crack induced by disc cutter is used to characterize the cutter rock breaking capability, which can be calculated by Liu's semiempirical and semitheoretical model [32]:

Before the formation of the crushed zone,

$$L = \left[\left(\frac{F_V}{\sigma_c d^2} + 0.10848 \right) \times \frac{F_V}{38.49109} \right]^{2/3} \times \left(\frac{1 - \nu^2}{EG_{IC}} \right)^{1/3}. \quad (2)$$

After the formation of the crushed zone,

$$L = \left[\left(\frac{F_V}{\sigma_c d^2} - 2.45434 \right) \times \frac{F_V}{27.86853} \right]^{2/3} \times \left(\frac{1 - \nu^2}{EG_{IC}} \right)^{1/3}, \quad (3)$$

where F_V is the normal force of disc cutter, σ_c is uniaxial compressive strength (UCS) of rock, d is the size of the cutter tip, $d = T/\cos(\theta/2) + 2r$, ν is Poisson's ratio of rock, E is Young's modulus of rock, and G_{IC} is the energy release rate of rock.

Forces of disc cutter can be obtained by using the Colorado School of Mines (CSMs) model [33] as follows:

$$\begin{aligned} F_V &= F_t \cos\left(\frac{\varphi}{2}\right) = C \frac{\varphi RT}{1 + \psi} \left(\frac{S\sigma_c^2\sigma_t}{\varphi\sqrt{RT}} \right)^{1/3} \cos\left(\frac{\varphi}{2}\right), \\ F_R &= F_t \sin\left(\frac{\varphi}{2}\right) = C \frac{\varphi RT}{1 + \psi} \left(\frac{S\sigma_c^2\sigma_t}{\varphi\sqrt{RT}} \right)^{1/3} \sin\left(\frac{\varphi}{2}\right), \\ \varphi &= \arccos\left(\frac{R - h}{R}\right), \end{aligned} \quad (4)$$

where F_t denotes the total force of disc cutter, F_R is the rolling force of disc cutter, R is the radius of disc cutter, ψ is the distribution coefficient of cutter tip pressure, φ denotes the contact angle between cutter ring and rock, h is the cutting depth, S is the cutter spacing, C is a dimensionless coefficient with value of 2.12, and σ_t is the tensile strength of rock. The rest of the symbols have the same meaning as equations (2) and (3). Additionally, the meanings of the same symbolic variables used in the following equations are consistent.

Based on the linear elastic fracture theory, the relationship of the energy release rate G_{IC} and the fracture toughness K_{IC} can be defined as [34]

$$G_{IC} = \frac{(1 - \nu^2)K_{IC}^2}{E}. \quad (5)$$

According to Zhang's research [35], the fracture toughness K_{IC} can be approximately computed by the following equation:

$$K_{IC} = 0.145\sigma_t. \quad (6)$$

Therefore, the objective function of cutter rock breaking capability is defined as

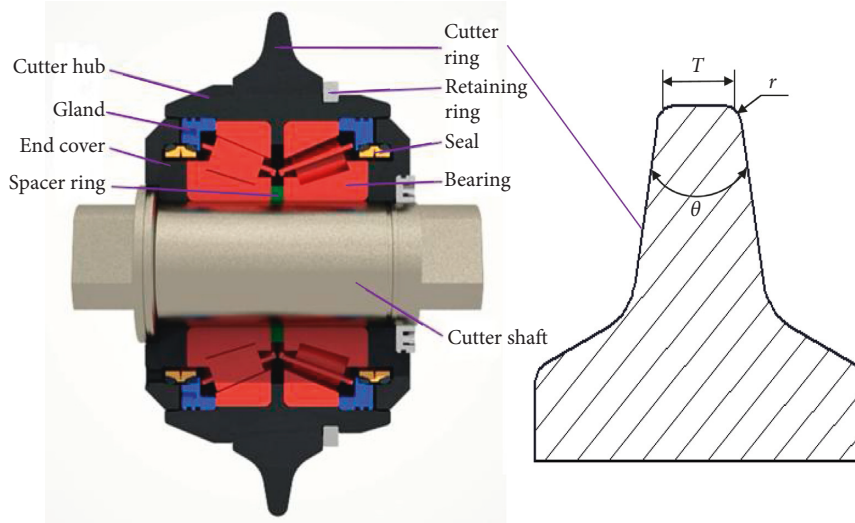


FIGURE 1: Sketch of disc cutter and cutter ring.

$$\min f_1(x) = \frac{1}{L}. \quad (7)$$

2.3.2. *Energy Consumption for Rock Breaking by Disc Cutter.* Specific energy (SE) of disc cutter refers to the energy consumed by breaking the unit volume of rock, and the greater the SE is, the lower the rock breaking efficiency is. The following equations can be used to calculate the value of SE [36, 37]:

For $L < h \tan(\beta/2)$,

$$E_S = \begin{cases} \frac{F_R}{\mu Sh}, & 0 < S \leq 2L + T, \\ \frac{F_R}{[Sh - ((S - T)^2/4 \tan(\beta/2))]}, & 2L + T < S \leq 2h \tan\left(\frac{\beta}{2}\right) + T, \\ \frac{F_R}{(h^2 \tan(\beta/2) + Th)}, & S > 2h \tan\left(\frac{\beta}{2}\right) + T. \end{cases} \quad (8)$$

For $L \geq h \tan(\beta/2)$,

$$E_S = \begin{cases} \frac{F_R}{\mu Sh}, & S \leq 2L + T, \\ \frac{F_R}{(h^2 \tan(\beta/2) + Th)}, & S > 2L + T, \end{cases} \quad (9)$$

where β is the rock breakage angle and μ is the coefficient characterizing the direction of side crack propagation.

Then, the objective function of cutter energy consumption for rock breaking is defined as

$$\min f_2(x) = E_S. \quad (10)$$

2.3.3. *Load-Bearing Capability of Cutter Bearing.* When the disc cutter breaks rock, the cutter bearings suffer large axial

and radial loads and high-intensity impact vibration. Failure of the bearing is an important reason for the abnormal failure of the disc cutter. When calculating the bearing life, it is necessary to convert the bearing's radial and axial loads into equivalent loads. The equation for calculating the equivalent dynamic bearing load is as follows:

$$P = f_p(XF_n + YF_a), \quad (11)$$

where X and Y are the radial load factor and axial load factor for the bearing, respectively, F_n is actual radial bearing load, F_a is the actual axial bearing load, and f_p is the load coefficient related to working conditions.

The bearing with relatively large load is selected as the design object, and its actual radial and axial loads are calculated as follows:

$$\begin{cases} F_n = \frac{\sqrt{F_V^2 + F_R^2}}{2} + \frac{F_S D_z}{2L_z}, \\ F_a = \frac{F_n}{2y} + F_S, \end{cases} \quad (12)$$

where D_z is the outside diameter of bearing, L_z is the center distance between two bearings, $L_z = T_b + l$, T_b is the bearing width, l is the thickness of spacer ring, y is the derived axial force coefficient, F_S is the side force of disc cutter [38], $F_S = (\tau/2) \cdot (R\phi)^2 \cdot \sin(R\phi/2\rho)$, τ is the shear strength of rock, and ρ is the installation radius of disc cutter.

The objective function for the load-bearing capability of cutter bearing is defined as

$$\min f_3(x) = P. \quad (13)$$

2.3.4. *Wear Life of Cutter Ring.* Wear life of the cutter ring is mainly characterized by wear loss, which is related to the cutter working conditions, the structural parameters of cutter ring, and the layout parameters of disc cutter. Based on Archard's abrasive wear theory, Zhu [39] established a

theoretical model of the front and side wear loss (wear step) for the cutter ring. The calculations are as follows:

Front wear step of the cutter ring:

$$dh_1 = k_D \times \int_0^{\varphi/\omega} \left[\left(C^3 \sqrt{\frac{S}{\varphi \sqrt{RT}}} \cdot \sigma_c^2 \sigma_t \left(1 - \frac{\varphi - \omega t}{\varphi} \right)^\psi \right) \times \sqrt{(\omega R (1 - \cos(\varphi - \omega t)) + v \sin(\varphi - \omega t))^2 + (\omega_1 R \sin(\varphi - \omega t))^2} \right] dt. \quad (14)$$

Side wear step of the cutter ring:

$$dh_2 = k_D \times \frac{c \cdot \cos(\xi) \cdot \cos(\theta/2) \cdot \cos(\gamma)}{\sin((\beta/2) - (\theta/2) - \xi - \gamma) \cdot \cos(\beta/2)} \times \int_0^{(\arccos((R-h)/r_c))/\omega} \left[fr_c \times \sqrt{(\omega \sqrt{r_c^2 + R^2 - 2Rr_c \cos(\varphi - \omega t)})^2 + v^2 + 2v\omega r_c \sin(\varphi - \omega t)} \right] dt, \quad (15)$$

where ω is the rotating angular velocity of disc cutter, $\omega = \rho\omega_1/R$, ω_1 is the rotating angular velocity of cutterhead, $\omega_1 = \pi n/30$, n is the rotating speed of cutterhead, v is the tunneling speed of cutterhead, $v = hn/60$, t is the wear time, K_D is the wear coefficient, c is the rock cohesion, ζ is the internal friction angle of rock, γ is friction angle between rock and cutter, r_c is the distance from a point on the cutter edge side to the center axis of disc cutter, and fr_c is the lateral pressure distribution coefficient.

In the actual TBM project, when the front of a cutter ring is worn to the limit value, the cutter ring will be replaced immediately. Therefore, the wear life of the cutter ring can be expressed as

$$w_h = \frac{w_{\max} R}{60 dh_1 \cdot n \cdot \rho}, \quad (16)$$

where w_{\max} is the limit wear volume of the cutter ring.

The objective function for wear life of the cutter ring can be defined as

$$\min f_4(x) = \frac{1}{w_h}. \quad (17)$$

2.3.5. Wear Uniformity of Cutter Ring. Changing trend of the cutter blade is different when disc cutter works and wears in different geological conditions. Actually, the shape of the worn blade is determined by both front wear and side wear [39]. If the cutter blade shape (blade angle) is stable in the wear process, the advantage of CCS disc cutter can be exerted and the optimal wear resistance performance will be obtained.

According to the geometric relationship between the front-side wear steps and the cutter blade shape, the objective function of the wear uniformity of cutter ring is defined as

$$\min f_5(x) = \left(\frac{dh_2}{dh_1} - \tan\left(\frac{\theta}{2}\right) \right)^2. \quad (18)$$

From the above optimization objective functions, it can be found that the cutter ring structural design problem contains several mutually conflicting objectives. The optimization objectives of disc cutter cannot be satisfied simultaneously under the same structural parameters, which require compromise among multiple objectives. In this paper, weight coefficient transformation method [40] is used to deal with the multiobjective optimization problem, which transforms the multiobjective functions into a single objective function. By giving different weight coefficients to the objective functions according to specific geological conditions, the geological adaptability optimization result can be achieved for cutter ring structural design. By using the weight coefficient transformation method, the combined objective function can be expressed as follows:

$$\min f(x) = \sum_{i=1}^5 \left(w_i \cdot \frac{f_i(x)}{\chi_i} \right), \quad (19)$$

where w_i is weight coefficient and χ_i is the elimination coefficient set for eliminating the order of magnitude difference [41].

2.4. Subject to Constraints

2.4.1. Dimensional Constraints of Geometric Structures. Cutter tip width is the main structural parameter of the cutter ring. A very small tip width will aggravate the cutter wear and increase the cost of cutter replacement, while a very large width will increase the rock breaking force and weaken the penetration capability of disc cutter. Considering the commonly used parameters, the dimensional constraint of the cutter tip width is given:

$$\begin{aligned} g_1(x) &= T - 0.012 \geq 0, \\ g_2(x) &= 0.03 - T \geq 0. \end{aligned} \quad (20)$$

Cutter edge angle has a great influence on the rock breaking performance of disc cutter. Choice of sharp-edged

and flat-edged cutters is the primary consideration in cutter structure design. Considering the changing trend of the blade shape in the wear process, the dimensional constraint for the cutter edge angle is defined as

$$\begin{aligned} g_3(x) &= \theta - 10^\circ \geq 0, \\ g_4(x) &= 30^\circ - \theta \geq 0. \end{aligned} \quad (21)$$

Too small cutter edge radius will result in stress concentration and difficulty in penetrating hard rocks. When the cutter edge radius is larger than 10 mm, the influence of edge radius parameter on cutting force will be reduced. Therefore, the dimensional constraint for the cutter edge radius is defined as

$$\begin{aligned} g_5(x) &= r - 0.0025 \geq 0, \\ g_6(x) &= 0.01 - r \geq 0. \end{aligned} \quad (22)$$

Spacer ring not only plays a role in positioning but also determines the starting torque of disc cutter. The dimensional constraint of spacer ring thickness is set as follows:

$$\begin{aligned} g_7(x) &= l - 0.01 \geq 0, \\ g_8(x) &= 0.018 - l \geq 0. \end{aligned} \quad (23)$$

2.4.2. Dimensional Correlation Constraint of Geometric Structures. In addition to satisfying the above dimensional constraints, the structural parameters of the cutter ring also need to satisfy the following correlation constraints:

$$g_9(x) = \frac{T}{2} - r \times \tan\left(\frac{\pi}{4} - \frac{\theta}{4}\right) > 0. \quad (24)$$

2.4.3. Constraint of Ultimate Load-Bearing Capability of Disc Cutter. The ultimate load-bearing capability of disc cutter varies with cutter ring size. Ultimate load-bearing capability of 17-inch disc cutter is 250 kN and that of 19-inch cutter is 315 kN [12]. Thus, the constraint of cutter ultimate load-bearing capability is given as

$$g_{10}(x) = F_V \leq F_{\text{rated}}. \quad (25)$$

2.4.4. Constraint of Cutterhead Drive Performance. The constraint of cutterhead drive performance is defined as

$$\begin{aligned} g_{11}(x) &= F_R \leq \frac{T_d}{0.3 DN}, \\ g_{12}(x) &= F_V \leq \frac{2F_d}{D}, \end{aligned} \quad (26)$$

where F_d and T_d are the rated thrust and torque of cutterhead, respectively, and D is the diameter of cutterhead.

3. Description of Methodologies

Cutter ring structural design problem contains several mutually conflicting objectives as well as linear and non-linear constraints, which belongs to a discontinuous multiobjective optimization problem. Therefore, an improved self-adaptive multipopulation genetic algorithm (SAMPGA) is used to solve this problem. Meanwhile, the fuzzy analytic hierarchy process (FAHP) is employed to deal with multiple objective functions and to obtain the combined objective function.

3.1. Self-Adaptive Multipopulation Genetic Algorithm. As is stated above, GA is one of the widely used evolutionary algorithms to deal with nonlinear optimization problems. However, after the broad application of GA, many shortcomings of SGA have been exposed constantly, for instance, the processing of single objective function, premature convergence, low efficiency of optimization. To overcome the defects of SGA, an improved self-adaptive multipopulation genetic algorithm (SAMPGA) is introduced to solve the multiobjective optimization design model for cutter ring structural parameters. The steps of SAMPGA are described as follows, where a general scheme is depicted in Figure 2.

- (1) Constructing objective functions: The multiple objective functions and combined objective function are demonstrated in Section 2.3.
- (2) Initialization: Assuming the number of populations is M , the number of individuals in each subpopulation is N . Crossover and mutation are the core operators of GA. According to the characteristics of SAMPGA, each population is given different crossover and mutation probabilities to balance the global and local search capability. The crossover probability P_c and mutation probability P_m are initialized as follows:

$$\begin{aligned} P_c &= 0.7 + (0.9 - 0.7) \times \text{rand}(M, 1), \\ P_m &= 0.01 + (0.1 - 0.01) \times \text{rand}(M, 1). \end{aligned} \quad (27)$$

- (3) Constructing fitness function: To prevent local convergence or divergence owing to the over-small fitness value, the fitness function is constructed according to equation (20) as follows:

$$\text{Fitness} = \frac{2}{1 + \sum_{i=1}^5 w_i (f_i(x)/\chi_i)}. \quad (28)$$

- (4) Selection: A roulette-based nonlinear ranking selection strategy is adopted in this approach.
- (5) Crossover: SGA is not sufficiently flexible to generate offspring by means of a single crossover of different chromosomes. In this paper, the crossover operator is set up by combining the multipoint crossover and uniform crossover.

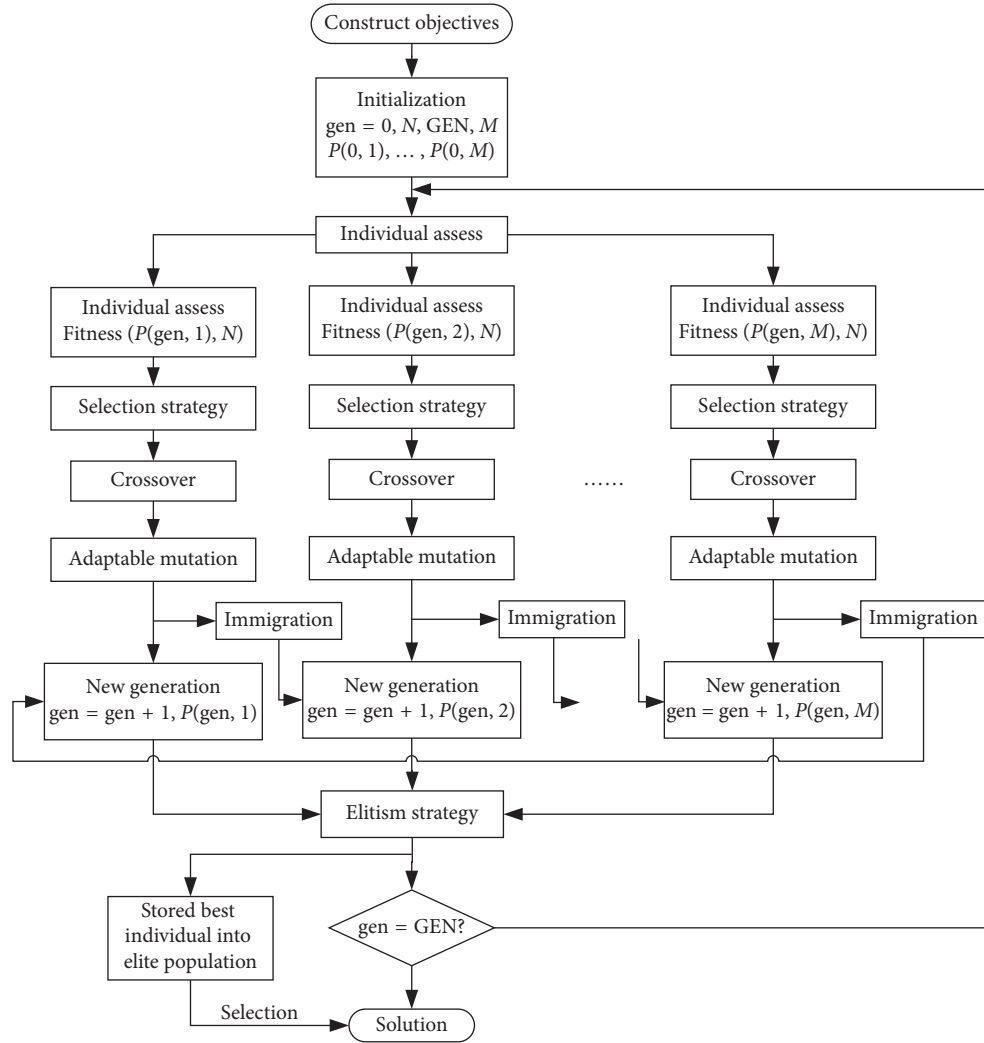


FIGURE 2: Framework of SAMPGA.

(6) Self-adaptable mutation: Mutation is the main factor affecting the convergence and optimal result of GA in the later stage. Mutation of SGA is usually constant and is independent of the number of iterations. In order to improve the global search capability in the early stage, the crossover of SGA is usually set to 0.7–0.9 and the mutation is set to 0.001–0.05, which may lead to premature local convergence and is not conducive to obtaining the optimal result in the later stage. To overcome the aforementioned problem, the self-adaptable mutation operator is adopted in this study. The mutation probability is self-adjusted after each generation of operation and increases gradually with the increase in the number of iterations. The dynamic changing equation is shown as follows:

$$P_m(i+1) = P_m(i) + \left(\frac{\text{gen}}{\text{GEN}}\right)^m \times \left(\frac{P_c}{\zeta} - P_m(i)\right), \quad (29)$$

where gen is the number of iteration, GEN is the total number of iterations, m is the calculation precision

digit of mutation operator, and ζ is the changing coefficient, value of which is set to 7–9 according to the crossover probability.

(7) Immigrant and elitism strategy: At the end of each iteration, immigrant operator is applied to screen out the best and worst individuals of the current population and then substitute the best individual for the worst individual in the population, thus realizing multipopulation coevolution. Through the elitism strategy, the best individuals in each population are recorded and stored into the elite population. The elite population is updated in each iteration. Finally, the optimal individual is found out across all subpopulations.

3.2. Fuzzy Analytical Hierarchy Process. When solving the multiobjective optimization design problem of disc cutter ring, the different assignment of weight coefficients for multiple objective functions will exhibit a significant influence on the design result of cutter ring structure. Meanwhile, setting different weight coefficients for

objectives based on the geological conditions is the core of the cutter ring geological adaptability design. To obtain a suitable coefficient set, the fuzzy analytic hierarchy process (FAHP) is introduced on the basis of the expert investigation. The process of calculating the weight coefficients for cutter ring objective functions by decision makers using the fuzzy AHP can be displayed as follows [42].

Let $O = \{o_1, o_2, \dots, o_n\}$ be an object set and $G = \{g_1, g_2, \dots, g_m\}$ be a goal set. $M_{gi}^1, M_{gi}^2, \dots, M_{gi}^m$ ($i = 1, 2, \dots, n$) are the extent analysis values for each object, where M_{gi}^j ($j = 1, 2, \dots, m$) are triangular fuzzy numbers (TFNs) provided in Table 1.

- (1) The value of fuzzy synthetic extent with respect to i -th object is defined as

$$S_i = \sum_{j=1}^m M_{gi}^j \otimes \left[\sum_{i=1}^n \sum_{j=1}^m M_{gi}^j \right]^{-1}, \quad (30)$$

where

$$\sum_{j=1}^m M_{gi}^j = \left(\sum_{j=1}^m l_i^j, \sum_{j=1}^m m_i^j, \sum_{j=1}^m u_i^j \right),$$

$$\left[\sum_{i=1}^n \sum_{j=1}^m M_{gi}^j \right]^{-1} = \left(\frac{1}{\sum_{i=1}^n \sum_{j=1}^m u_i^j}, \frac{1}{\sum_{i=1}^n \sum_{j=1}^m m_i^j}, \frac{1}{\sum_{i=1}^n \sum_{j=1}^m l_i^j} \right). \quad (31)$$

- (2) The degree of possibility of $M_2 = (l_2, m_2, u_2) \geq M_1 = (l_1, m_1, u_1)$ is defined as

$$V(M_2 \geq M_1) = \text{hgt}(M_1 \cap M_2) = \mu_{M_2}(\text{po})$$

$$= \begin{cases} 1, & m_2 \geq m_1, \\ 0, & l_1 \geq u_2, \\ \frac{l_1 - u_2}{(m_2 - u_2) - (m_1 - l_1)}, & \text{otherwise,} \end{cases} \quad (32)$$

where μ (po) is the largest intersection between two TFNs.

- (3) The degree of possibility for convex fuzzy numbers to be greater than k convex fuzzy numbers M_i is defined as

$$V(M \geq M_1, M_2, \dots, M_k) = V[(M \geq M_1), (M \geq M_2), \dots, (M \geq M_k)]$$

$$= \min V(M \geq M_i), \quad i = 1, 2, \dots, k. \quad (33)$$

Assuming that $d'(A_i) = \min V(S_i \geq S_k)$, $k = 1, 2, \dots, n$ ($k \neq i$), the weight coefficient vector can be determined as

$$W' = \left(d'(A_1), d'(A_2), \dots, d'(A_n) \right)^T, \quad (34)$$

where A_i ($i = 1, 2, \dots, n$) are n elements.

- (4) The final weight coefficient vector is determined as

$$W = (d(A_1), d(A_2), \dots, d(A_n))^T$$

$$= (w_1, w_2, \dots, w_n)^T, \quad (35)$$

where nonfuzzy number W is the normalization of W' .

Based on SAMPGA and FAHP, a new multiobjective optimization method is proposed for the cutter ring structural design, the flow chart of which is depicted in Figure 3.

4. Case Study

4.1. Background. The multiobjective optimization design method is applied to optimize the structural parameters of the cutter ring used in a water conveyance project, located in northeast China. Total length of the TBM construction section in this project is 19.8 km, the main formation across this section is II-III type granite and II-III-IV tuff. The tunnel is excavated using a TBM with a diameter of 8 m, and four double-edged 17-inch (432 mm) center disc cutters and forty-three 19-inch (483 mm) front and edge disc cutters are installed on the TBM cutterhead. A 19-inch front disc cutter is selected as a design object, and two typical construction sections (section A and section B) are selected as the geologic background. The main rock type in section A is granite, and the UCS of the rock reaches to 90–140 MPa. In section B, the main rock type is tuff, and the UCS of the sampled rock is approximately 40–90 MPa. Cutter spacing of this disc cutter is 83 mm, and radius of the cutter ring is 241.3 mm. Cutting depth is 6 mm and average rotational speed of cutterhead is 6.67 r/min in section A, while the average penetration of cutter is 10 mm and average rotational speed of cutterhead is 6.67 r/min in section B. The bearing used for this cutter is Timken H926749/10.

4.2. Comparison of Optimization Results between SAMPGA and GA. To verify the convergence and robustness of the improved SAMPGA, an experiment is performed, in which the rock breaking capability of disc cutter is set as the objective function and section A is chosen as the geological condition. The results are compared with those of SGA. For the two GAs, the evolutionary generation is set to 1000 and the total number of individuals is 500. SGA parameters are set to be 0.8 for crossover probability, 0.05 for mutation

TABLE 1: Linguistic variables and triangular fuzzy numbers.

Linguistic scale	Fuzzy number	Triangular fuzzy number	Triangular fuzzy reciprocal
Equal importance (EI)	$\tilde{1}$	(1, 1, 1)	(1, 1, 1)
Equal to moderate importance (IMI)	$\tilde{2}$	(1, 2, 3)	(1/3, 1/2, 1)
Moderate importance (MI)	$\tilde{3}$	(2, 3, 4)	(1/4, 1/3, 1/2)
Moderate to strong importance (ISI)	$\tilde{4}$	(3, 4, 5)	(1/5, 1/4, 1/3)
Strong importance (SI)	$\tilde{5}$	(4, 5, 6)	(1/6, 1/5, 1/4)
Strong to very strong importance (IVSI)	$\tilde{6}$	(5, 6, 7)	(1/7, 1/6, 1/5)
Very strong importance (VSI)	$\tilde{7}$	(6, 7, 8)	(1/8, 1/7, 1/6)
Very strong to extreme importance (IEXI)	$\tilde{8}$	(7, 8, 9)	(1/9, 1/8, 1/7)
Extreme importance (EXI)	$\tilde{9}$	(8, 9, 10)	(1/10, 1/9, 1/8)

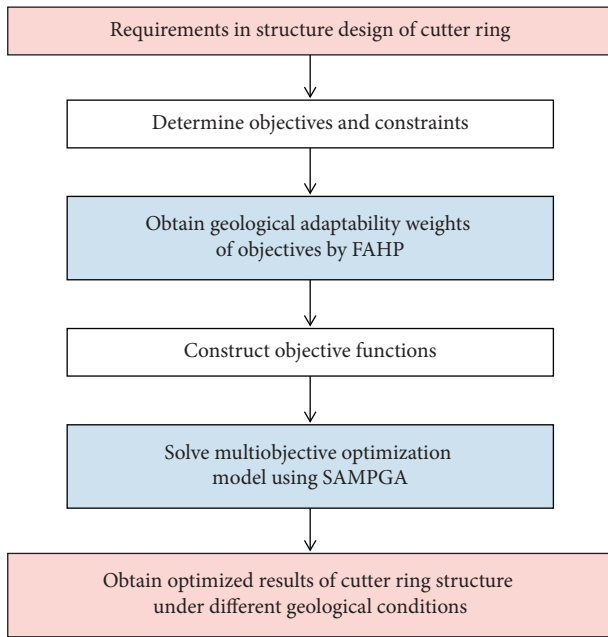


FIGURE 3: Flow chart of cutter ring structural design based on the proposed method.

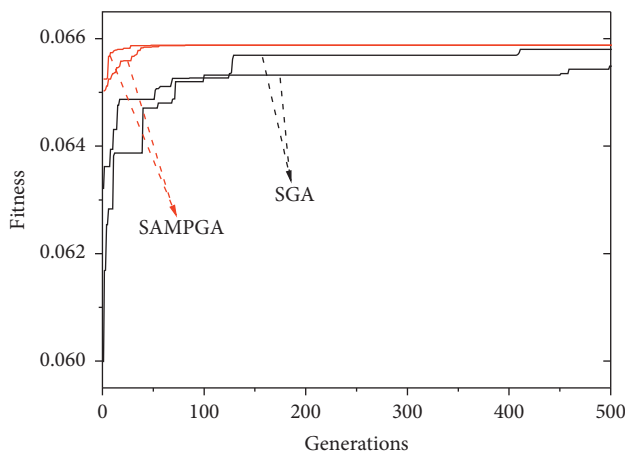


FIGURE 4: Fitness curves of SGA and SAMPGA.

probability [43], along with roulette strategy. SAMPGA parameters are set to 10 for populations and 50 for individuals per population. Initializations of crossover and mutation probabilities vary in different subpopulations.

Specifically, the crossover probability is set to be 0.7–0.9 and mutation probability is set 0.01–0.1 [30, 44], and the mutation probability dynamically increases with the increase of computational generation. The optimization results obtained by SGA and SAMPGA are listed in Tables 2 and 3, where C.G. denotes convergence generation and C.T. denotes convergence time. Figure 3 shows the comparison of fitness curves for SGA and SAMPGA. From Tables 2 and 3 and Figure 3, the following conclusions can be drawn:

- (1) The results of the five operations of SGA are quite different. The minimum value of the optimized objective function is 15.2059 and the maximum value is 15.2742, which indicates the poor stability and premature local convergence in SGA. The results of five experiments of SAMPGA are identical, and the optimal value is 15.1782, indicating SAMPGA performs better than SGA in terms of the three structural parameters in all the tests.
- (2) Figure 3 shows that the two fitness curves obtained by SGA are quite different, and there are still mutations in the later stage of operation. As a contrast, the fitness curves obtained by SAMPGA has little difference and is stable to the same value in the later period, indicating SAMPGA exhibits a better performance in stability and convergence than SGA.
- (3) The average convergence generation of SGA is beyond 400, whereas SAMPGA converges to the optimal results before 150 generations. From Tables 2 and 3, the computation time of SGA is less than that of SAMPGA. However, since the convergence generation of SAMPGA is far less than that of SGA, a smaller evolutionary generation can be set up for SAMPGA to weaken the disadvantage of computing time compared with SGA in practical application.

4.3. Multiobjective Optimization Results of Structural Parameters for Cutter Rings. To solve the multiobjective optimization model, weight coefficients of each objective function need to be determined using FAHP firstly. With the example of computing the weight coefficients of objective functions under the granite condition, the processes of weights determination are demonstrated. Eight experienced decision makers from TBM manufacturer, cutter manufacturer, construction company, and related academic institution are invited to fill in questionnaires using the

TABLE 2: Results obtained by SGA.

Number	T (mm)	θ ($^\circ$)	r (mm)	f_1 (m^{-1})	C.G.	C.T. (s)
1	29.8584	29.7827	9.9687	15.2416	616	9.896
2	29.9205	29.9676	9.9998	15.2059	411	9.726
3	29.9944	28.4154	9.9658	15.2141	595	9.527
4	29.8737	29.3454	9.9903	15.234	383	10.079
5	29.8866	25.6863	9.994	15.2742	409	9.839

TABLE 3: Results obtained by SAMPGA.

Number	T (mm)	θ ($^\circ$)	r (mm)	f_1 (m^{-1})	C.G.	C.T. (s)
1	30	30	10	15.1782	161	19.399
2	30	30	10	15.1782	104	19.303
3	30	30	10	15.1782	94	19.435
4	30	30	10	15.1782	141	19.503
5	30	30	10	15.1782	123	19.372

linguistic variables in Table 1, so as to establish the fuzzy aggregated decision matrix. For a group decision environment with k experts, fuzzy aggregated decision matrix can be obtained using equation (36). Table 4 exhibits the final fuzzy aggregate decision matrix of objectives under the granite condition, where O_1 , O_2 , O_3 , O_4 , and O_5 denote the objectives of rock breaking capability, energy consumption for rock breaking, load-bearing capability, wear life, and wear uniformity, respectively.

$$\left\{ \begin{array}{l} \tilde{x}_{ij} = (Lx_{ij}, Mx_{ij}, Ux_{ij}), \\ Lx_{ij} = \min_k \{Lx_{ijk}\}, \\ Mx_{ij} = \frac{1}{K} \sum_{k=1}^K Mx_{ijk}, \\ Ux_{ij} = \max_k \{Ux_{ijk}\}, \end{array} \right. \quad (36)$$

where \tilde{x}_{ij} is the arithmetic mean of TFNs constructed by k experts.

The fuzzy synthetic extents of the objectives are presented as follows by using equation (30):

$$\begin{aligned} S_1 &= (6, 13, 25) \otimes (0.0136, 0.0273, 0.0601) \\ &= (0.0816, 0.3553, 1.5036), \\ S_2 &= (1.61, 2.905, 4.5) \otimes (0.0136, 0.0273, 0.0601) \\ &= (0.0218, 0.0793, 1.2706), \\ S_3 &= (3.583, 8.472, 17) \otimes (0.0136, 0.0273, 0.0601) \\ &= (0.0487, 0.2315, 1.0224), \\ S_4 &= (2.7, 5.847, 11) \otimes (0.0136, 0.0273, 0.0601) \\ &= (0.0367, 0.1598, 0.6616), \\ S_5 &= (2.733, 6.361, 16) \otimes (0.0136, 0.0273, 0.0601) \\ &= (0.0371, 0.1738, 0.9623). \end{aligned} \quad (37)$$

Computations of the degree of possibility (V value) are depicted in Table 5 by using equation (32).

Using equation (33), the minimum values of degree of possibility are obtained. By using equations (34) and (35), the final normalized weight coefficients under granite geological condition in section A are obtained as: $W_1 = (0.2585, 0.1052, 0.2286, 0.1933, 0.2144)^T$. By using the above-mentioned method, the final weight coefficient set under tuff condition is obtained as $W_2 = (0.2511, 0.1403, 0.1332, 0.2874, 0.188)^T$. Ranking orders of weight coefficients for the five objectives under granite geological condition are $O_1 > O_3 > O_5 > O_4 > O_2$, while those of coefficients under tuff condition become $O_4 > O_1 > O_5 > O_2 > O_3$. By analyzing the weight coefficients under different geological conditions, it is indicated TBM experts and project builder pay more attention to the objectives of rock breaking capability, load-bearing capability, and wear life under the harsh geological conditions with high rock strength (i.e., granite condition), whereas the wear resistance performances (O_4 and O_5) become the topmost objectives and load-bearing capability changes to the low-level one in tuff geological condition. Since the rock is more difficult to break under hard rock conditions (in section A), the bearing life is significantly affected by the strong impact and heavy load during rock breaking and the wear of the cutter ring is more serious due to the high strength rock. Therefore, O_1 , O_3 , and O_5 are selected as the extreme importance objectives in the experts' opinions. However, loads of the cutter ring are relatively small when it breaks rock with low strength (in section B), and the main failure form of the cutter is normal wear; thus, the wear resistance performance objectives (O_4 and O_5) along with rock breaking capability are the most important objectives under tuff condition.

Fitness function is constructed by equation (19) and the weight coefficient of each objective function. SAMPGA is applied to solve the multiobjective optimization model, and the optimized results are obtained and listed in Table 6. Structural parameters of the original disc cutter used in this TBM project are 19.05 mm in cutter tip width, 20° in edge angle, and 5 mm in edge radius.

From Table 6, it can be seen that the values of optimized cutter tip width and edge angle have been reduced while the value of edge radius is slightly increased compared with those of the original cutter ring under the granite condition. After optimization, the optimization objectives are improved except for the wear life of the cutter ring. The values of the objective functions of rock breaking capability, energy consumption, load-bearing capability, and wear uniformity decrease by 13.7%, 5.7%, 12.9%, and 22.1% respectively, while that of wear life increase by 2.6%. Because there are several mutually conflicting objectives in the model and the coupling relationship between objective functions and variables is complex, the improvement of one optimization objective is often accompanied by the degradation of another objective. Thus, it is usually impossible to obtain an optimal individual adapting to all objectives in the optimization process. Due to the relatively low weight of wear life, it is deteriorated in the optimization process, which improves the comprehensive performance of cutter ring.

TABLE 4: Fuzzy aggregated decision matrix.

	O_1	O_2	O_3	O_4	O_5
O_1	(1, 1, 1)	(2, 5.167, 10)	(1, 2, 4)	(1, 2.333, 5)	(1, 2.5, 5)
O_2	(0.1, 0.227, 0.5)	(1, 1, 1)	(0.167, 0.464, 1)	(0.2, 0.486, 1)	(0.143, 0.728, 1)
O_3	(0.25, 0.556, 1)	(1, 2.833, 6)	(1, 1, 1)	(1, 1.833, 4)	(0.333, 2.25, 5)
O_4	(0.2, 0.514, 1)	(1, 2.5, 5)	(0.25, 0.639, 1)	(1, 1, 1)	(0.25, 1.194, 3)
O_5	(0.2, 0.542, 1)	(1, 2.5, 7)	(0.2, 0.736, 3)	(0.333, 1.583, 4)	(1, 1, 1)

TABLE 5: Calculations of degree of possibility (V value).

	S_1	S_2	S_3	S_4	S_5
$V(S_1 \geq \dots)$	—	1	1	1	1
$V(S_2 \geq \dots)$	0.4065	—	0.5931	0.7441	0.7119
$V(S_3 \geq \dots)$	0.8838	1	—	1	1
$V(S_4 \geq \dots)$	0.7478	1	0.8951	—	0.978
$V(S_5 \geq \dots)$	0.8291	1	0.9405	1	—

TABLE 6: Optimization results of structural parameters for the cutter ring.

Geological conditions	Design objective	T (mm)	θ (°)	r (mm)	f_1 (m ⁻¹)	f_2 (MJ·m ³)	f_3 (kN)	f_4 (×10 ⁻³ h ⁻¹)	f_5
<i>Granite</i>	Original cutter ring	19.05	20	5	31.29	79.18	153.25	4.23	6.92
	Optimized cutter ring	16.1	10.61	7.4	26.99	74.61	133.41	4.34	5.39
	Variation (%)				-13.7	-5.7	-12.9	2.6	-22.1
<i>Tuff</i>	Original cutter ring	19.05	20	5	27.38	34.54	98.17	1.81	5.33
	Optimized cutter ring	21.02	15.49	5.77	19.69	35.51	101.4	1.64	4.81
	Variation (%)				-28.1	2.8	3.3	-9.4	-9.8

Under tuff geological condition, the values of optimized cutter tip width and edge radius increase slightly while that of edge angle decreased compared with those of the original cutter. The values of the objective functions of rock breaking capability, wear life, and wear uniformity decrease by 28.1%, 9.4%, and 9.8%, respectively, while those of energy consumption and load-bearing capability increase by 2.8% and 3.3%.

Comparing the optimized results of cutter ring structural parameters under different geological conditions, the cutter tip width under granite condition is smaller than that of original cutter and is contrary under tuff condition. Besides, the cutter edge angle under granite condition is smaller than that of in tuff condition, indicating that it is appropriate to apply the cutter ring with narrow edge and small blade angle in high strength rock condition. When cutting the low-strength rock such as tuff, the cutter tip width should be increased appropriately considering the wear resistance performance. The optimization results of cutter ring structural parameters vary with different geological conditions, which indicate that the geological adaptability should be considered in the design of cutter ring. The proposed design method in this paper determines the weight coefficients of objective functions based on expert knowledge and FAHP under different geological conditions, which realizes the geological adaptability design for cutter ring structure. Additionally, it is revealed in Table 6 that the performance improvement of disc cutter under granite is more significant than that under tuff after optimization and the structural parameters of cutter ring change little under tuff condition compared with the original cutter ring, demonstrating that the original disc cutter is more suitable for the rock with low

strength. The above finding has been verified by practical applications of disc cutters. In the actual construction process, original disc cutters exhibit excellent rock breaking performance and long service life under the tuff geological condition. Daily tunneling progress of TBM can reach to 30 m, and the wear rate of the cutter ring is approximate 0.08–0.12 mm/m. In addition, disc cutters suffer little abnormal failure, and the wear of cutter ring is uniform, which verifies that the original disc cutter is suitable for tuff geology.

5. Conclusions

In this paper, a multiobjective optimization design method for structural parameters of cutter ring is developed by combining a SAMPGA and FAHP, and the conclusions are drawn as follows:

- (1) Based on the complex geological conditions and the corresponding cutter ring structure design requirements, a multiobjective optimization model is established to design the structural parameters of disc cutter ring. The rock breaking capability, energy consumption, load-bearing capability, wear life, and wear uniformity of disc cutter are selected as the objectives, and the geometric structure of cutter ring, ultimate load-bearing capability, and cutterhead drive performance are determined as constraints. An SAMPGA is utilized to deal with the optimization problem, and FAHP is employed to combine the multiple objectives into a single objective function.
- (2) The proposed method is applied to a case study of cutter ring structure design in a TBM project. After

optimization, the rock breaking performance and service life of the disc cutter are improved. For granite condition, the performances of rock breaking capability, energy consumption, load-bearing capability, and wear uniformity are improved by 13.7%, 5.7%, 12.9%, and 22.1% respectively, and the performance of wear life is deteriorated by 2.6%. The performances of rock breaking capability, wear life, and wear uniformity are improved by 28.1%, 9.4%, and 9.8%, respectively, while those of energy consumption and load-bearing capability are deteriorated by 2.8% and 3.3% under tuff geological condition.

- (3) The optimized results obtained by SAMPGA are better than those of SGA in the tests. The convergence generation of SAMPGA is smaller than that of SGA, and the robustness of SAMPGA is better than that of SGA. The utilization of SAMPGA effectively solves the premature and local convergence problems during structural optimization.
- (4) Geological adaptability should be considered in the design of cutter ring. Rock breaking capability, load-bearing capability, and wear uniformity should be considered as the topmost objectives when cutting high-strength rock, while wear life and rock breaking capability should be given priority under low-strength rock condition. It is appropriate to apply the cutter ring with a narrow edge and small blade angle in granite condition, whereas the cutter tip width should be increased appropriately considering the wear resistance performance in tuff condition. The geological adaptability design for cutter ring structure is realized by using the proposed method based on the dynamic weight coefficients.

It should be noted the objective functions of the optimization design model are solved on the premise that the cutter ring can invade the rock smoothly, which is satisfied in the aforementioned TBM project. However, in some TBM project, the UCS of the surrounding rock that TBM encountered will reach to 200 MPa or even more than 300 MPa. It is difficult for disc cutter to penetrate and break rock under such harsh geological conditions. At this time, the TBM builders prefer to replace the conventional cutter ring with heavy narrow-edged cutter ring. Therefore, the penetration capability, as well as stiffness-strength of the disc cutter, should be considered and added to the model in the future work. Moreover, other relevant objectives (e.g., the number of rock cracks) will be taken into account to improve the proposed method.

Data Availability

The data used to support the findings of this study are included within the article.

Conflicts of Interest

The authors declare no conflicts of interest.

Acknowledgments

This work was supported by the National Key R&D Program of China (no. 2018YFB1306700), the National Natural Science Foundation of China (no. 51905550), the Project funded by China Postdoctoral Science Foundation (no. 2019M652795), the National Basic Research Program of China (no. 2013CB035401), and the Project of Key Technology and Integrated Demonstration for Green Remanufacturing of Shield Machines.

References

- [1] N. Afrasiabi, R. Rafiee, and M. Noroozi, "Investigating the effect of discontinuity geometrical parameters on the TBM performance in hard rock," *Tunnelling and Underground Space Technology*, vol. 84, pp. 326–333, 2019.
- [2] J. Huo, H. Wu, W. Sun, Z. Zhang, L. Wang, and J. Dong, "Electromechanical coupling dynamics of TBM main drive system," *Nonlinear Dynamics*, vol. 90, no. 4, pp. 2687–2710, 2017.
- [3] L. Lin, Y. Xia, Q. Mao, and X. Zhang, "Experimental study on wear behaviors of TBM disc cutter ring in hard rock conditions," *Tribology Transactions*, vol. 61, no. 5, pp. 920–929, 2018.
- [4] J. Liu, W. Wan, Y. Chen, and J. Wang, "Dynamic indentation characteristics for various spacings and indentation depths: a study based on laboratory and numerical tests," *Advances in Civil Engineering*, vol. 2018, Article ID 8412165, 12 pages, 2018.
- [5] J. Rostami, "Study of pressure distribution within the crushed zone in the contact area between rock and disc cutters," *International Journal of Rock Mechanics and Mining Sciences*, vol. 57, pp. 172–186, 2013.
- [6] C. Balci and D. Tumac, "Investigation into the effects of different rocks on rock cuttability by a V-type disc cutter," *Tunnelling and Underground Space Technology*, vol. 30, pp. 183–193, 2012.
- [7] D. Tumac and C. Balci, "Investigations into the cutting characteristics of CCS type disc cutters and the comparison between experimental, theoretical and empirical force estimations," *Tunnelling and Underground Space Technology*, vol. 45, pp. 84–98, 2015.
- [8] S. W. Choi, S. H. Chang, Y. T. Park, G. P. Lee, and G. J. Bae, "Experimental evaluation of the effects of cutting ring shape on cutter acting forces in a hard rock," *Journal of Korean Tunnelling and Underground Space Association*, vol. 15, no. 3, pp. 225–235, 2013.
- [9] B. Chiaia, "Fracture mechanisms induced in a brittle material by a hard cutting indenter," *International Journal of Solids and Structures*, vol. 38, no. 44–45, pp. 7747–7768, 2001.
- [10] A. Lislud, *Principles of Mechanical Excavation (No. POS-IVA--97-12)*, Posiva Oy, Eurajoki, Finland, 1997.
- [11] X.-P. Zhang, P.-Q. Ji, Q.-S. Liu, Q. Liu, Q. Zhang, and Z.-H. Peng, "Physical and numerical studies of rock fragmentation subject to wedge cutter indentation in the mixed ground," *Tunnelling and Underground Space Technology*, vol. 71, pp. 354–365, 2018.
- [12] J. Roby, T. Sandell, J. Kocab, and L. Lindbergh, "The current state of disc cutter design and development directions," in *Proceeding of the 2008 North American Tunneling Conference, SME C*, vol. 4, pp. 36–45, San Francisco, CA, USA, 2008.

- [13] B. Maidl, L. Schmid, W. Ritz, and M. Herrenknecht, *Hardrock Tunnel Boring Machines*, John Wiley & Sons, Hoboken, NJ, USA, 2008.
- [14] M. F. Marji, "Simulation of crack coalescence mechanism underneath single and double disc cutters by higher order displacement discontinuity method," *Journal of Central South University*, vol. 22, no. 3, pp. 1045–1054, 2015.
- [15] W. Sun, L. Guo, J. J. Zhou, and J. Z. Huo, "Rock fragmentation simulation under dual TBM disc cutter and design of cutter ring," *Journal of China Coal Society*, vol. 40, no. 6, pp. 1297–1302, 2015.
- [16] J. Li, Y. F. Nie, K. Fu, C. Ma, J. B. Guo, and M. X. Xu, "Experiment and analysis of the rock breaking characteristics of disc cutter ring with small edge angle in high abrasive grounds," *Journal of the Brazilian Society of Mechanical Sciences and Engineering*, vol. 40, no. 10, p. 505, 2018.
- [17] Y. M. Xia, T. Ouyang, L. Chen, D. Z. Luo, and X. M. Zhang, "Study on the influencing factors of the disc cutter performance," *Journal of Basic Science and Engineering*, vol. 20, no. 3, pp. 500–507, 2012.
- [18] J.-H. Yang, X.-P. Zhang, P.-Q. Ji et al., "Analysis of disc cutter damage and consumption of TBM1 section on water conveyance tunnel at Lanzhou water source construction engineering," *Tunnelling and Underground Space Technology*, vol. 85, pp. 67–75, 2019.
- [19] R. V. Rao, D. P. Rai, and J. Balic, "Multi-objective optimization of abrasive waterjet machining process using Jaya algorithm and PROMETHEE Method," *Journal of Intelligent Manufacturing*, vol. 30, no. 5, pp. 2101–2127, 2019.
- [20] M. Kilinc and J. M. Caicedo, "Finding plausible optimal solutions in engineering problems using an adaptive genetic algorithm," *Advances in Civil Engineering*, vol. 2019, Article ID 7475156, 9 pages, 2019.
- [21] M. Aghbashlo, M. Tabatabaei, M. H. Nadian, V. Davoodnia, and S. Soltanian, "Prognostication of lignocellulosic biomass pyrolysis behavior using ANFIS model tuned by PSO algorithm," *Fuel*, vol. 253, pp. 189–198, 2019.
- [22] M. Duma and B. Twala, "Sparseness reduction in collaborative filtering using a nearest neighbour artificial immune system with genetic algorithms," *Expert Systems with Applications*, vol. 132, pp. 110–125, 2019.
- [23] N. D. Hoang, Q. L. Nguyen, and Q. N. Pham, "Optimizing construction project labor utilization using differential evolution: a comparative study of mutation strategies," *Advances in Civil Engineering*, vol. 2015, Article ID 108780, 8 pages, 2015.
- [24] Y. Li, H. Soleimani, and M. Zohal, "An improved ant colony optimization algorithm for the multi-depot green vehicle routing problem with multiple objectives," *Journal of Cleaner Production*, vol. 227, pp. 1161–1172, 2019.
- [25] A. A. Zaidan, B. Atiya, M. R. Abu Bakar, and B. B. Zaidan, "A new hybrid algorithm of simulated annealing and simplex downhill for solving multiple-objective aggregate production planning on fuzzy environment," *Neural Computing and Applications*, vol. 31, no. 6, pp. 1823–1834, 2019.
- [26] T. Muruta and H. Ishibuchi, "MOGA: multi-objective genetic algorithm," in *Proceedings of 1995 IEEE International Conference on Evolutionary Computation*, Perth, WA, Australia, November–December 1995.
- [27] K. Deb, A. Pratap, S. Agarwal, and T. Meyarivan, "A fast and elitist multiobjective genetic algorithm: NSGA-II," *IEEE Transactions on Evolutionary Computation*, vol. 6, no. 2, pp. 182–197, 2002.
- [28] H. A. Leyva, E. Bojórquez, J. Bojórquez et al., "Earthquake design of reinforced concrete buildings using NSGA-II," *Advances in Civil Engineering*, vol. 2018, Article ID 5906279, 11 pages, 2018.
- [29] J. Huo, W. Sun, J. Chen, and X. Zhang, "Disc cutters plane layout design of the full-face rock tunnel boring machine (TBM) based on different layout patterns," *Computers & Industrial Engineering*, vol. 61, no. 4, pp. 1209–1225, 2011.
- [30] A. Shamsavar, A. A. Najafi, and S. T. A. Niaki, "Three self-adaptive multi-objective evolutionary algorithms for a triple-objective project scheduling problem," *Computers & Industrial Engineering*, vol. 87, pp. 4–15, 2015.
- [31] M. Zandieh and N. Karimi, "An adaptive multi-population genetic algorithm to solve the multi-objective group scheduling problem in hybrid flexible flowshop with sequence-dependent setup times," *Journal of Intelligent Manufacturing*, vol. 22, no. 6, pp. 979–989, 2011.
- [32] H. Y. Liu, *Numerical modelling of the rock fragmentation progressive process by mechanical tools*, Ph.D. thesis, Lulea University of Technology, Luleå, Sweden, 2004.
- [33] J. Rostami, "Hard rock TBM cutterhead modeling for design and performance prediction," *Geomechanik und Tunnelbau*, vol. 1, no. 1, pp. 18–28, 2008.
- [34] B. N. Whittaker, R. N. Singh, and G. Sun, *Rock Fracture Mechanics: Principles, Design, and Applications*, Vol. 570, Elsevier, Amsterdam, Netherlands, 1992.
- [35] Z. X. Zhang, "An empirical relation between mode I fracture toughness and the tensile strength of rock," *International Journal of Rock Mechanics and Mining Sciences*, vol. 39, no. 3, pp. 401–406, 2002.
- [36] Y. M. Xia, B. Guo, G. Q. Cong, X. H. Zhang, and G. Y. Zeng, "Numerical simulation of rock fragmentation induced by a single TBM disc cutter close to a side free surface," *International Journal of Rock Mechanics and Mining Sciences*, vol. 91, pp. 40–48, 2017.
- [37] Q. Tan, N. E. Yi, Y. M. Xia, Y. Zhu, X. H. Zhang, and L. K. Lin, "Study of calculation equation of TBM disc cutter optimal spacing," *Rock and Soil Mechanics*, vol. 37, no. 3, pp. 883–892, 2016.
- [38] Z. H. Zhang and D. H. Ye, "The model of the disc cutter's broken-rock and the calculation of its side-force," *Journal of Basic Science and Engineering*, vol. 12, no. 3, pp. 293–298, 2004.
- [39] Z. H. Zhu, "Numerical simulation of disc cutter's wear evolution for tbm," Central South University, Changsha, China, Master Thesis, 2013.
- [40] Y. Zhang, M. Harman, and S. A. Mansouri, "The multi-objective next release problem," in *Proceedings of the 9th Annual Conference on Genetic and Evolutionary Computation*, pp. 1129–1137, ACM, London, UK, July 2007.
- [41] W. Luo, Y. H. Chen, and G. H. Zhang, "Optimization of parameters for planar internal gear primary-enveloping crown worm drive," *Journal of Mechanical Engineering*, vol. 50, no. 7, pp. 1–7, 2014.
- [42] P. Sirisawat and T. Kiatcharoenpol, "Fuzzy AHP-TOPSIS approaches to prioritizing solutions for reverse logistics barriers," *Computers & Industrial Engineering*, vol. 117, pp. 303–318, 2018.
- [43] J.-S. Kim, C.-G. Kim, and C.-S. Hong, "Optimum design of composite structures with ply drop using genetic algorithm and expert system shell," *Composite Structures*, vol. 46, no. 2, pp. 171–187, 1999.
- [44] L. Wang, J.-C. Cai, and M. Li, "An adaptive multi-population genetic algorithm for job-shop scheduling problem," *Advances in Manufacturing*, vol. 4, no. 2, pp. 142–149, 2016.

Research Article

Multiobjective Construction Optimization Model Based on Quantum Genetic Algorithm

Wei He  and Yichao Shi 

College of Civil Engineering and Mechanics, Yanshan University, Qinhuangdao 066004, Hebei, China

Correspondence should be addressed to Wei He; hewei@ysu.edu.cn

Received 16 March 2019; Accepted 23 May 2019; Published 1 July 2019

Academic Editor: Tayfun Dede

Copyright © 2019 Wei He and Yichao Shi. This is an open access article distributed under the Creative Commons Attribution License, which permits unrestricted use, distribution, and reproduction in any medium, provided the original work is properly cited.

It is critical for the construction party to meet the established economic and social demand for the construction project with the shortest construction period and the lowest cost. In this study, the construction characteristics of the project were analyzed. In addition, the multiconstraint and multitarget construction optimization model with minimum period and cost was established based on the quantum genetic algorithm. In order to improve the adaptability of the quantum genetic algorithm for the multiobjective model, the encoding form, quantum revolving door, and genetic flow of the algorithm were reconstructed. MATLAB 2016b was used as the simulation platform, and the implementation of the algorithm was improved according to the characteristics of the variables in the construction project, including period and cost. Finally, the optimization of the algorithm was verified and analyzed by an engineering example. The results showed that using the multiobjective quantum genetic algorithm, the optimal duration/cost can be achieved and the most reasonable and effective control decision scheme for the construction management can be provided through the Pareto solution set.

1. Introduction

With the development of the world economy, more and more attention has been paid to the duration and cost of projects [1]. Large construction projects have large capital investment and long construction cycle [2]. In order to minimize the duration and cost of the project, it is critical to design an effective construction organization plan [3]. The purpose of the construction plan is to obtain a short construction period and a low cost. Researchers have focused on the studies to optimize the period and cost of construction. However, in the optimization algorithm, there is an inevitable conflict between schedule and cost [4]. Therefore, optimization is also known as striking a balance between duration and cost [5]. The optimization balance means that, under the constraints of personnel, machinery, and materials, managers can reasonably allocate resources to achieve the minimum combination of time and cost by appropriately increasing the cost/time of subprojects under the same circumstances [6].

Traditional balance strategy includes the critical path method, integer programming method, and enumeration method. However, due to the expansion of the construction project scale nowadays, the computational complexity has been growing exponentially [7]. Thus, it is difficult for these methods to meet the computing requirements of large-scale construction projects [8]. It is very urgent to find an algorithm that can find a quick, accurate, and effective optimization balance of period and cost, i.e., shortened construction period and reduced cost, without breaking the architectural design and function. In recent years, the heuristic algorithm with global search ability has been used to solve optimization problems, including the Jaya algorithm [9, 10], particle swarm algorithm [11], colony algorithm [12], simulated annealing algorithm [13], harmony search algorithm logic [14], and other hybrid algorithms [15, 16]. In general, the balance between duration and cost, which is the focus of long-term research in project management, can be investigated using these existing methods. Based on the results by Boussad et al. [17], in terms of

design ability and application effect, genetic algorithm was undoubtedly the best solution among many complex heuristic algorithms. Based on the in-depth studies of genetic algorithm, the combination of genetic algorithm and other methods has also been developed. Gulbin [18] considered the influence of environmental factors on the operation of the algorithm and designed the genetic algorithm for nondominant sequencing. Jia et al. [19] applied the fuzzy set theory based on the operation of genetic algorithm, considered the uncertain conditions of construction, and proposed a multiobjective method to optimize the duration, cost, and quality of the construction project. Mungle et al. [20] designed the fuzzy clustering genetic algorithm to solve the problem of multiobjective optimization for highway projects. Xie et al. [21] used the pretreatment method and cost improvement process to the genetic algorithm and established the optimization model of multimode resource-limited projects under variant constraints. However, these methods have inevitable limitations for large-scale projects with the requirements of high precision and high timeliness. Therefore, the computational model and algorithm for the optimization of large-scale construction projects need to be improved.

In theory, the problems which are solvable with genetic algorithm can also be solved by quantum genetic algorithm (QGA) [22, 23]. Thus, the QGA should be feasible in the field of genetic algorithm, such as the multiobjective optimization of both period and cost. In addition, as an alternative calculation method [24], quantum computing has a strong data analysis and processing ability for the large dataset [25–28]. Therefore, in this study, the QGA was used to solve the period/cost trade-off problems and developed an optimization model. In the optimization model, the genetic algorithm was used as the basis, the parallelism of quantum computing was integrated with the genetic algorithm, the quantum vector state expression was introduced into the genetic coding, and the chromosome evolution and renewal were achieved through the quantum revolving door. In this paper, the construction period-cost optimization model with the quantum genetic algorithm was established to improve the search efficiency on the basis of global search and reduce the application error of the Pareto solution. The experimental results proved that the proposed method had a better performance ratio than the traditional genetic algorithm.

2. Problem Description

In the engineering construction management, the period and the cost of the construction project are two main objectives to be controlled. However, there is a restrictive relationship between both objectives; that is, gaining one objective is at the expense of another. For example, the reduction of time leads to an inevitable increase of cost [29, 30]. Thus, the time/cost optimization of the construction project is also considered a multiconstraint hybrid optimization problem [31]. On the contrary, the network plan of a project is composed of several subprocesses which are logically arranged, and there are several alternatives for each of the subprocesses. Different labor and construction

machinery schemes can lead to different time and cost of the process. For instance, the project duration, direct cost, and indirect cost can be affected by different schemes. Thus, the time/cost optimization problem is also considered a multivariable problem. In general, before solving the multiobjective optimization problem [32], functional expressions are needed to show the relationship between each objective. Table 1 lists the symbol interpretation.

2.1. Objective 01: Time. The total time of the project is calculated by summing up the duration of each subprocess. The duration of the subproject is marked with an intermediate variable “ x .” The selected subprocess requires that the work can and must start immediately when the previous work is finished, without restrictions of resources or other processes. The restrictions on the time parameter of each process satisfy the logical relationship between processes. The calculation equation and constraint conditions of the control period of the construction project are defined as follows:

$$T = \sum D_j^i, \quad (1)$$

$$D_i^e \leq D_i^{(j)} \leq D_i^n, \quad (2)$$

$$T \leq T_{\max}. \quad (3)$$

2.2. Objective 02: Cost. The cost includes direct cost and indirect cost. Both costs have different changing rules and need to be calculated separately. Direct cost is the sum of the costs of personnel, construction machinery, and materials, which are directly used in the construction process and the measures of the project. At the same time, the cost is increased in the emergency construction due to the increase in the dispatched resources and the construction difficulty and the extension of working hours of both personnel and machinery. Indirect costs are not directly included in the project. Instead, they refer to other expenses that must be paid for the preparation, organization, and management of construction and production, including enterprise management fees and policy fees. The value of the indirect costs can be estimated by contract documents or experts. The calculation equation and constraint conditions of the control cost of the construction project are defined as follows:

$$C = \min \sum_{i=1}^n \{ \alpha_i^{(j)} C_{(1,i)}^{(j)} + \alpha_i^{(j)} \Delta t C_{(2,i)}^{(j)} \}, \quad (4)$$

$$\sum_{j=1}^m \alpha_i^{(j)} = 1, \quad (5)$$

$$C \leq C_{\max}, \quad (6)$$

$$\{ \alpha_i^{(j)} \} \subseteq \{ 0, 1 \}, \quad (7)$$

where $C_{(1,i)}$ is the sum of the product of the unit price and the work quantity of the process and the measure cost.

TABLE 1: Notations.

Notations	Meanings
D_j^i	Duration of the j th procedure of the i th subitem
$D_i^e (D_i^n)$	Emergency (normal) construction time of available construction plan for the i th subitem
T	Total project time
C	Total project cost
$C_{(1,i)}$	Direct cost of activity i
$C_{(2,i)}$	Indirect cost of activity i
Δt	Duration of alternatives
$\alpha_i^{(j)}$	Probability of selecting plan j in the i th procedure

3. Optimization Model Based on QGA

3.1. QGA. QGA is a new evolutionary optimization algorithm which integrates quantum computation with genetic algorithm. The QGA has obvious performance advantages due to the introduction of quantum concepts such as quantum state, quantum revolving gate, and probability amplitude in quantum computation. The QGA has few iterations, high search efficiency, and wide applicability. Besides, one chromosome can express the superposition of multiple states and thus has a large storage capacity. Even when the population is very small, the global optimization of the algorithm is not affected. Thus, the possibility of the algorithm to fall into a local search is greatly avoided. Compared to the traditional genetic algorithm (GA), the QGA does not rely on the gene updates by genetic operators such as crossover and mutation to achieve the evolution of the population. Although these genetic operators can change the probability amplitude to some extent, the quantum chromosome already exhibits the population diversity due to the use of quantum superposition. Instead, the introduction of genetic operators such as crossover and mutation will reduce the computing speed and performance of the QGA.

3.1.1. Quantum Bits. Bit is the unit of information in binary number. In traditional calculation, there are only two basic states, i.e., “0” and “1.” After the introduction of the quantum concept, the bit state becomes a vector unit in a two-dimensional complex coordinate. Besides 0 and 1, the quantum bit state can also be the linear superposition of the basic states [33], which is called the superposition state of quantum bits:

$$|\phi\rangle = \alpha|0\rangle + \beta|1\rangle. \quad (8)$$

Among them, “ $|\cdot\rangle$ ” is the Dirac notation to indicate the state. The parameters α and β are the probability of the corresponding states, respectively. The probability of $|0\rangle$ is $|\alpha|^2$, while the probability of $|1\rangle$ is $|\beta|^2$. Both probabilities satisfy the normalization condition:

$$|\alpha|^2 + |\beta|^2 = 1. \quad (9)$$

On the basis of binary coding in the genetic algorithm, the quantum bit state $|\phi\rangle$ is used to code the target and the initial value. The coding rules can be expressed as follows: through the expression of the quantum superposition state, a gene can express any quantum bit information. In addition,

the genome sequence can be formed by the composition of chromosomes. The m^{th} chromosome of the scheme can be represented as follows:

$$P_m^n = \left[\begin{array}{c|c|c|c|c} \alpha_1^n & \alpha_2^n & \cdots & \alpha_{j-1}^n & \alpha_j^n \\ \beta_1^n & \beta_2^n & \cdots & \beta_{j-1}^n & \beta_j^n \end{array} \right], \quad (10)$$

where n is the number of iterations and j is the quantum number (length of the chromosome). The complete quantum population containing all the modern chromosomes can be expressed as

$$P(t) = \{P_1^t, P_2^t, \dots, P_m^t, \dots, P_T^t\}. \quad (11)$$

3.1.2. Quantum Gate. The renewal and evolution of the quantum population are conducted through a quantum gate, which is a quantum device that can realize logical transformation within a certain time interval. The quantum gate ACTS is used for the superposition of the quantum and results in the phase change of the gene position in the chromosome. Finally, the probability converges to 0 or 1 within a shortest time and the optimal searching solution is achieved. The only requirement for quantum gates is

$$U^+ * U = I, \quad (12)$$

where U is the matrix representation of the quantum gate, U^+ is the conjugate transpose, and I is the identity matrix. Quantum gates have many forms. In this algorithm design, the method of quantum rotation is defined as follows:

$$U(\theta) = \begin{bmatrix} \cos \theta & -\sin \theta \\ \sin \theta & \cos \theta \end{bmatrix}, \quad (13)$$

where θ is the rotation angle. The chromosome renewal process can be expressed as follows:

$$\begin{bmatrix} \alpha_k^{n+1} \\ \beta_k^{n+1} \end{bmatrix} = \begin{bmatrix} \cos \theta_i & -\sin \theta_i \\ \sin \theta_i & \cos \theta_i \end{bmatrix} \begin{bmatrix} \alpha_k^n \\ \beta_k^n \end{bmatrix}, \quad (14)$$

where $[\alpha_k^n, \beta_k^n]^T$ is the K^{th} quantum bit of the N^{th} generation of the chromosome:

$$\theta_i = \Delta\theta \times \text{sig}, \quad (15)$$

where $\Delta\theta$ determines the convergence speed and the search accuracy of the algorithm. If the amplitude of $\Delta\theta$ is too small, the search time is increased or even “stagnates.” If the amplitude is too large, premature convergence can occur, and it is difficult to obtain the optimal solution. sig is the coefficient sign of the rotation angle, namely, the rotation direction, whose value determines the direction of convergence to the optimal solution. When ibin (current individual quantum bit value) is equal to ibbest (optimal individual quantum bit value), sig is $1/\sqrt{2^m}$; when ibin and ibbest are different, the values of sig are shown in Table 2.

3.2. Optimization Process

3.2.1. Encoding and Population Initialization. There are three encoding methods in the quantum genetic algorithm.

TABLE 2: Values of sig.

ibin	ibbest	$f(\text{fval}) < f(\text{best})$	sig			
			$\alpha_i \beta_i > 0$	$\alpha_i \beta_i < 0$	$\alpha_i = 0$	$\beta_i = 0$
0	1	True	1	0	0	± 1
0	1	False	-1	1	± 1	0
1	0	True	-1	1	± 1	0
1	0	False	1	-1	0	± 1

The initial population encoding is quantum bit encoding, in which N is the length of the encoded quantum bits. The pseudocode is shown in Figure 1.

When the population is first measured, the quantum bit code is converted into the binary code, as shown in Figure 2. The binary is decoded into the decimal in the calculation of the adaptability of the population.

To optimize the construction period and cost of a project, the population can be defined as the set of chromosomes (Figure 3) that stores the duration of all sequential subitems, and the initial population can be expressed as $P(t=0) = \{p_1^0, p_2^0, \dots, p_m^0, \dots, p_T^0\}$, where T is the population size. The probability amplitudes of the population $2jT$ are all $1/\sqrt{2}$, which means that, in the initial state, each chromosome is in a linear superposition state with the same probability of $1/\sqrt{2^m}$.

3.2.2. Evaluation of Adaptability. The individuals in the population can be evaluated by adaptability. Higher adaptability indicates that the individual is better and has greater survival probability. On the contrary, the individuals with lower adaptability are easier to be eliminated. The adaptability evaluation function is generally consistent with the objective function. Since the two opposite subobjectives, i.e., duration and cost, seek for the minimum values in the optimization model, equations (1) and (4) can be changed as follows:

$$\begin{aligned} \text{Value 1} &= \frac{1}{C}, \\ \text{Value 2} &= \frac{1}{T}. \end{aligned} \quad (16)$$

Both the adaptability values in decimal and the non-dominant solution (there was no other solution better than this one) were obtained from the calculation.

3.2.3. Quantum Genetic Operation. In the operation, the $Q(t)$ state of the population is observed and compared with the existing optimal solution, and then the population with the quantum revolving gate is updated to obtain $Q(t+1)$. The adaptability was calculated. If the optimal solution in $Q(t+1)$ is better than the currently stored solution, the stored solution is replaced. In the update process, the population number is always constant and the nondominant solution does not repeat.

3.2.4. Termination Judgment. If the termination condition is satisfied, the set of optimal solutions for the schedule and cost of the subprocess is the output. Otherwise, Steps 2 and 3

```

QGACHrom = zeros(P, N * 2);
for i = 1:P
    for j = 1:N * 2
        QGACHrom(i, j) = 1/sqrt(2);
    end
end

```

FIGURE 1: Code in quantum bit encoding.

```

Chrombin = zeros(P, N);
for i = 1:P
    for j = 1:N
        pick = rand;
        if
            pick > (QGACHrom(i, j)^2)
                Chrombit(i, j) = 1;
            else
                Chrombin(i, j) = 0;
            end
        end
    end
end

```

FIGURE 2: Conversion of the quantum bit code to the binary code.

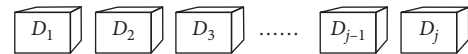


FIGURE 3: Diagram of the single chromosome structure.

are repeated. The flowchart of the optimization process is shown in Figure 4.

3.3. Experimental Results and Analysis

3.3.1. Algorithm Instance. A high-rise building project was selected as the main project for optimization, the construction data (Table 3) were collected, and the feasibility of the experimental model was verified. Before optimization, according to the construction plan, the completion duration of the project was 380 days and the cost was 19.749 million yuan.

The parameters of the quantum genetic algorithm are shown in Table 4. This algorithm was implemented by MATLAB 2016b.

After running the optimization, the results were summarized as follows:

- (1) The period/cost evolution of a project is recorded and shown in Figures 5 and 6. From the figures, it is noted that all the target curves are in a declining trend, which indicates that the evolution of the quantum genetic algorithm is effective. With the increase in the number of iterations, the iteration curve remains flat, which suggests that the algorithm is convergent and can achieve the optimal value in

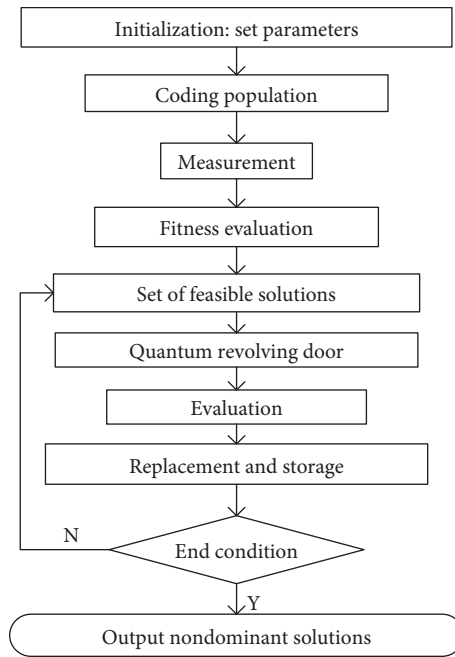


FIGURE 4: Optimization process of the quantum genetic algorithm.

TABLE 3: Construction data.

No.	Activity	Time (days)		Cost (ten thousand yuan)	
		Normal	Emergency	Normal	Emergency
1	Measurement and actinomycetes	3	1	0.1	0.3
2	Precipitation and support	15	10	46	65
3	Earthwork	5	2	9	14
4	Pile foundation	10	6	240	300
5	Earthwork backfilling	5	2	1.8	3
6	Structure of the first layer	12	7	63.5	70
7	Structure of the second or third layer	22	12	58	66
8	Structure of the fourth floor	10	5	56	64
...					
17	Structure of the 13th floor	10	5	56	64
18	Stage acceptance of the main project	3	1	0.5	1.5
19	Wall masonry and secondary structure	50	30	147	196
20	Structure of the 14th floor	10	5	56	64
...					
33	Structure of the 27th floor	10	5	56	64
34	Structure of the 28th floor	12	7	64	70
35	Structure acceptance	3	2	1	2
36	Wall masonry and secondary structure	50	30	147	196

TABLE 4: Parameter values of the QGA.

$\Delta\theta$	Population	Variable dimension	Max. iterations
0.01π	80	36	400

the process of evolution instead of getting into local optimum.

- (2) Figure 7 shows the final solution of the QGA, i.e., the Pareto front under the dual constraints of both time limit and cost. According to the Pareto front of the optimization, the project manager can select a set of

feasible processes with flexible activity arrangement under certain constraints of time or construction period (Table 4) to maximize the economic and social benefits. For example, when the total construction period is 280 days, the total cost is at least 22,882,600 yuan. The corresponding duration of the subprocess is shown in Figure 8, in which the 19th activity is concurrent engineering and does not increase the total construction period. At this time, no other combination method of the subprocesses can be superior to the scheme shown in Figure 8.

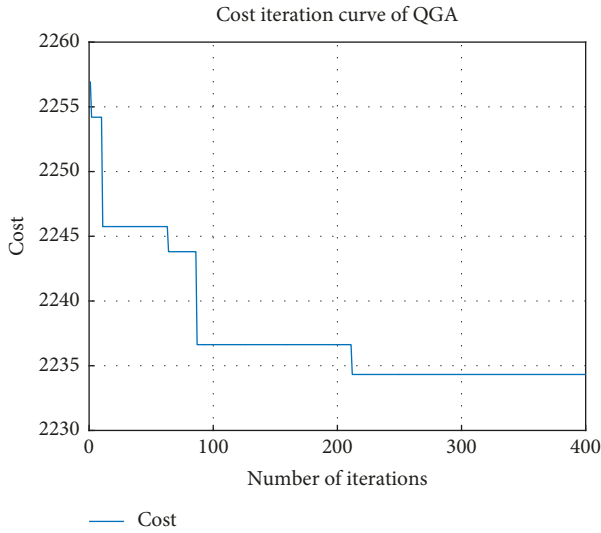


FIGURE 5: Iteration curve of the construction period in the multiobjective quantum genetic algorithm.

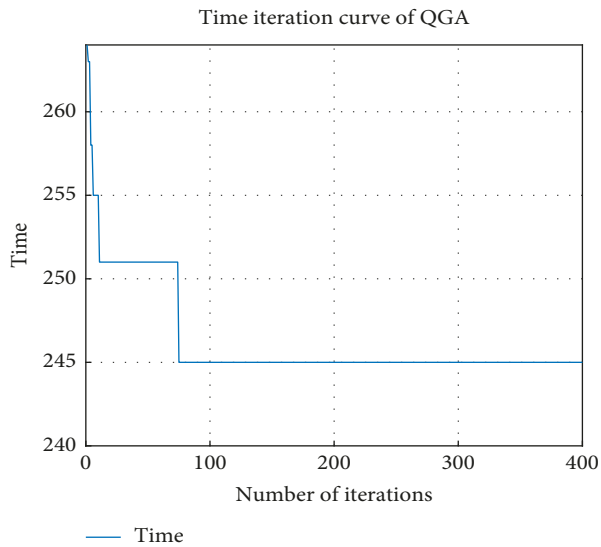


FIGURE 6: Iteration curve of cost in the multiobjective quantum genetic algorithm.

4. Conclusions

The trade-off between period and cost in construction management is a classic problem in the multiobjective optimization with constraints. A new model based on the quantum genetic algorithm (QGA) was proposed in this study. Firstly, in the process of double-objective optimization, the conflict between the construction period and the practical cost was considered, and the direct and complex relationship between the two objectives was analyzed. Two main objective functions were established, which provided a mathematical basis for the application of the algorithm to the construction management. Secondly, a complete optimization concept and process of the quantum genetic algorithm were developed, the quantum coding mode was

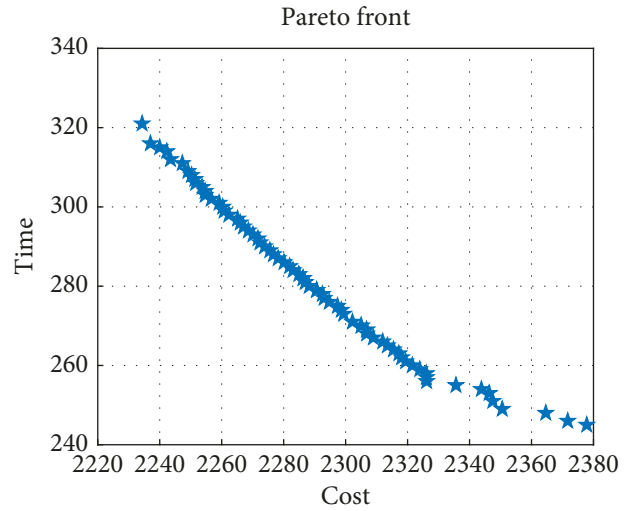


FIGURE 7: Pareto solution set of the multiobjective quantum genetic algorithm.

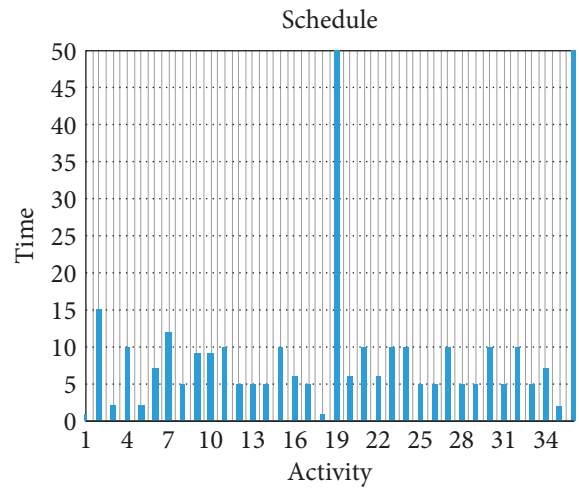


FIGURE 8: Process portfolio for 280 days.

explained, the quantum revolving door was improved, and the computational efficiency of the algorithm was improved in large-scale projects. Through the construction example of a high-rise building project, the quantum genetic algorithm was proved to be able to obtain the optimization results under the condition of small population size and few iteration times. Thus, the quantum genetic algorithm had the advantages of short calculation time and strong global optimization ability. Finally, the developed model was applied to a practical construction project. The experimental results showed that the QGA can perform multiple optimization cycles and find the nonconflicting Pareto solution quickly and accurately to meet the requirements under different constraints in different projects with variant activity arrangements. In addition, the QGA can also provide owners and contractors with more realistic decision-making schemes conveniently and efficiently, which can maximize the economic benefits. In the future, the development of

intelligent algorithms with high efficiency in large-scale engineering optimization will become the research focus.

Data Availability

The data used to support the findings of this study are available from the corresponding author upon request.

Conflicts of Interest

The authors declare that there are no conflicts of interest regarding the publication of this paper.

Acknowledgments

This research was partially supported by the Natural Science Foundation of Hebei Province of China under Grant No. E2016203147. Useful suggestions given by Dr. Dewei Kong of Yanshan University are also acknowledged.

References

- [1] M. J. T. Amiri, F. Haghghi, E. Eshtehardian, and O. Abessi, "Multi-project time-cost optimization in critical chain with resource constraints," *KSCE Journal of Civil Engineering*, vol. 22, no. 10, pp. 3738–3752, 2018.
- [2] Y. Zhong, Z. Chen, and Z. Zhou, "Resource allocation model and strategy research of large-scale construction project: system dynamics modeling and simulation," *Chinese Journal of Management Science*, vol. 24, no. 3, pp. 125–132, 2016.
- [3] J. Zhang, "Discussion on the comprehensive equilibrium optimization scheme of construction period, cost and quality in project management," *Construction & Design for Engineering*, vol. 2, pp. 141–143, 2017.
- [4] S. Monghasemi, M. R. Nikoo, M. A. K. Fasae, and J. Adamowski, "A novel multi criteria decision making model for optimizing time-cost-quality trade-off problems in construction projects," *Expert Systems with Applications*, vol. 42, no. 6, pp. 3089–3104, 2015.
- [5] A. B. Senouci and S. A. Mubarak, "Multiobjective optimization model for scheduling of construction projects under extreme weather," *Journal of Civil Engineering and Management*, vol. 22, no. 3, pp. 373–381, 2016.
- [6] I. Javier, E. P. Karan, and J. Farzad, "Integrating BIM and GIS to improve the visual monitoring of construction supply chain management," *Automation in Construction*, vol. 31, pp. 241–254, 2013.
- [7] D. Agdas, D. Warne, J. Osio-Norgaard, and F. Masters, "Utility of genetic algorithms for solving large-scale construction time-cost trade-off problems," *Journal of Computing in Civil Engineering*, vol. 32, no. 1, 2018.
- [8] J. Wu, M. Chen, K. Ju, and S. Jiang, "Construction period of segmented ship engineering project based on harmonic search algorithm—cost optimization," *Journal of Finance and Accounting*, vol. 6, pp. 68–70, 2015.
- [9] T. Dede, "Jaya algorithm to solve single objective size optimization problem for steel grillage structures," *Steel and Composite Structures*, vol. 26, no. 2, pp. 163–170, 2018.
- [10] M. Grzywnski, T. Dede, and Y. I. Ozdemir, "Optimization of the braced dome structures by using Jaya algorithm with frequency constraints," *Steel and Composite Structures*, vol. 30, pp. 47–55, 2019.
- [11] L. Zhang, Y. Luan, and X. Zou, "Project duration—cost—quality balance optimization," *Systems Engineering*, vol. 3, pp. 85–91, 2012.
- [12] A. M. Adrian, A. Utamima, and K. J. Wang, "A comparative study of GA, PSO and ACO for solving construction site layout optimization," *KSCE Journal of Civil Engineering*, vol. 19, no. 3, pp. 520–527, 2015.
- [13] M. O. Suliman, V. S. S. Kumar, and W. Abdulal, "Optimization of uncertain construction time-cost trade off problem using simulated annealing algorithm," in *Proceedings of the World Congress on Information and Communication Technologies*, IEEE, Trivandrum, India, October–November 2012.
- [14] O. Giran, R. Temur, and G. Bekda, "Resource constrained project scheduling by harmony search algorithm," *KSCE Journal of Civil Engineering*, vol. 21, no. 2, pp. 479–487, 2017.
- [15] D.-H. Tran, M.-Y. Cheng, and M.-T. Cao, "Hybrid multiple objective artificial bee colony with differential evolution for the time-cost-quality tradeoff problem," *Knowledge-Based Systems*, vol. 74, no. 1, pp. 176–186, 2015.
- [16] M. Rogalska, W. Bozejko, and Z. Hejducki, "Time/cost optimization using hybrid evolutionary algorithm in construction project scheduling," *Automation in Construction*, vol. 18, no. 1, pp. 24–31, 2009.
- [17] I. Boussad, J. Lepagnot, and P. Siarry, "A survey on optimization metaheuristics," *Information Sciences*, vol. 237, pp. 82–117, 2013.
- [18] O. D. Gulbin, "Time, Cost, and environmental impact analysis on construction operation optimization using genetic algorithms," *Journal of Management in Engineering*, vol. 28, no. 3, pp. 265–272, 2012.
- [19] J. Liu, Y. Liu, and Y. Shi, "Method of time-cost-quality tradeoff optimization of construction project: A study based on fuzzy set theory," *Journal of Beijing Jiaotong University (Social Sciences Edition)*, vol. 16, no. 3, pp. 30–38, 2017.
- [20] S. Mungle, L. Benyoucef, Y. J. Son, and M. K. Tiwari, "A fuzzy clustering-based genetic algorithm approach for time-cost-quality trade-off problems: a case study of highway construction project," *Engineering Applications of Artificial Intelligence*, vol. 26, no. 8, pp. 1953–1966, 2013.
- [21] F. Xie, Z. Xu, and J. Yu, "Bi-objective optimization for the project scheduling problem with variable resource availability," *Systems Engineering-Theory & Practice*, vol. 36, no. 3, pp. 674–683, 2016.
- [22] J. Yang, G. Xie, Z. Zhang, and L. Guo, "Quantum genetic algorithm and its application in image blind separation," *Journal of computer aided design and graphics*, vol. 20, no. 1, pp. 62–68, 2003.
- [23] Q. Guo and Y. Sun, "Improved quantum genetic algorithm with double chains in image denoising," *Journal of Harbin Institute of Technology*, vol. 48, no. 5, pp. 140–147, 2016.
- [24] N. Sanghvi, A. Shah, and V. Varadan, "The concept and future of quantum computing," *International Journal of Computer Applications*, vol. 106, no. 4, pp. 30–33, 2014.
- [25] S. Wei, T. Wang, R. Dong, and G. Long, "Quantum computing," *Scientia Sinica*, vol. 10, pp. 27–47, 2017.
- [26] T. A. Shaikh and R. Ali, "Quantum computing in big data analytics: a survey," in *Proceedings of the IEEE International Conference on Computer & Information Technology*, Helsinki, Finland, August 2017.
- [27] Y. Tian, W. Hu, D. Bo et al., "IQGA: a route selection method based on quantum genetic algorithm- toward urban traffic management under big data environment," *World Wide Web-Internet & Web Information Systems*, vol. 15, pp. 1–23, 2018.

- [28] L. Zhang, H. Lv, D. Tan et al., "Adaptive quantum genetic algorithm for task sequence planning of complex assembly systems," *Electronics Letters*, vol. 54, no. 14, pp. 870–872, 2018.
- [29] P. Ghoddousi, E. Eshtehardian, S. Jooybanpour, and A. Javanmardi, "Multi-mode resource-constrained discrete time-cost-resource optimization in project scheduling using non-dominated sorting genetic algorithm," *Automation in Construction*, vol. 30, no. 30, pp. 216–227, 2013.
- [30] M.-Y. Cheng and D.-H. Tran, "Opposition-based multiple objective differential evolution (OMODE) for optimizing work shift schedules," *Automation in Construction*, vol. 55, pp. 1–14, 2015.
- [31] D. A. Wood, "Gas and oil project time-cost-quality tradeoff: integrated stochastic and fuzzy multi-objective optimization applying a memetic, nondominated, sorting algorithm," *Journal of Natural Gas Science and Engineering*, vol. 45, pp. 143–164, 2017.
- [32] C. Koo, T. Hong, and S. Kim, "An integrated multi-objective optimization model for solving the construction time-cost trade-off problem," *Journal of Civil Engineering and Management*, vol. 21, no. 3, pp. 323–333, 2015.
- [33] A. V. Kozlovskii, "Fluctuations of the hermitian phase operator of electromagnetic field for quantum phase superpositions of coherent states," *Journal of Modern Optics*, vol. 15, pp. 1–10, 2018.